REVIEW

Stratocumulus Clouds

ROBERT WOOD

University of Washington, Seattle, Washington

(Manuscript received 18 May 2011, in final form 19 January 2012)

ABSTRACT

This paper reviews the current knowledge of the climatological, structural, and organizational aspects of stratocumulus clouds and the physical processes controlling them. More of Earth's surface is covered by stratocumulus clouds than by any other cloud type making them extremely important for Earth's energy balance, primarily through their reflection of solar radiation. They are generally thin clouds, typically occupying the upper few hundred meters of the planetary boundary layer (PBL), and they preferably occur in shallow PBLs that are readily coupled by turbulent mixing to the surface moisture supply. Thus, stratocumuli favor conditions of strong lower-tropospheric stability, large-scale subsidence, and a ready supply of surface moisture; therefore, they are common over the cooler regions of subtropical and midlatitude oceans where their coverage can exceed 50% in the annual mean. Convective instability in stratocumulus clouds is driven primarily by the emission of thermal infrared radiation from near the cloud tops and the resulting turbulence circulations are enhanced by latent heating in updrafts and cooling in downdrafts. Turbulent eddies and evaporative cooling drives entrainment at the top of the stratocumulus-topped boundary layer (STBL), which is stronger than it would be in the absence of cloud, and this tends to result in a deepening of the STBL over time. Many stratocumulus clouds produce some drizzle through the collision–coalescence process, but thicker clouds drizzle more readily, which can lead to changes in the dynamics of the STBL that favor increased mesoscale variability, stratification of the STBL, and in some cases cloud breakup. Feedbacks between radiative cooling, precipitation formation, turbulence, and entrainment help to regulate stratocumulus. Although stratocumulus is arguably the most well-understood cloud type, it continues to challenge understanding. Indeed, recent field studies demonstrate that marine stratocumulus precipitate more strongly, and entrain less, than was previously thought, and display an organizational complexity much larger than previously imagined. Stratocumulus clouds break up as the STBL deepens and it becomes more difficult to maintain buoyant production of turbulence through the entire depth of the STBL.

Stratocumulus cloud properties are sensitive to the concentration of aerosol particles and therefore anthropogenic pollution. For a given cloud thickness, polluted clouds tend to produce more numerous and smaller cloud droplets, greater cloud albedo, and drizzle suppression. In addition, cloud droplet size also affects the time scale for evaporation–entrainment interactions and sedimentation rate, which together with precipitation changes can affect turbulence and entrainment. Aerosols are themselves strongly modified by physical processes in stratocumuli, and these two-way interactions may be a key driver of aerosol concentrations over the remote oceans. Aerosol–stratocumulus interactions are therefore one of the most challenging frontiers in cloud–climate research. Low-cloud feedbacks are also a leading cause of uncertainty in future climate prediction because even small changes in cloud coverage and thickness have a major impact on the radiation budget. Stratocumuli remain challenging to represent in climate models since their controlling processes occur on such small scales. A better understanding of stratocumulus dynamics, particularly entrainment processes and mesoscale variability, will be required to constrain these feedbacks.

CONTENTS

Corresponding author address: Robert Wood, Department of Atmospheric Sciences, University of Washington, Box 351640, Seattle, WA 98195. E-mail: robwood@atmos.washington.edu

DOI: 10.1175/MWR-D-11-00121.1

1. Introduction

Stratocumulus, from the Latin *stratus* meaning "layer," and *cumulus* meaning "heap," is a genus of low clouds composed of an ensemble of individual convective elements that together assume a layered form. The layering is typically achieved through capping by a temperature inversion that is often strong and only tens of meters thick, while the heaping reflects the convective nature of the cloud. Stratocumulus is usefully defined as a low-level cloud system whose dynamics are primarily driven by convective instability caused by cloud-top radiative cooling, a definition that distinguishes stratocumulus from stratus.

Stratocumuli swathe enormous regions of Earth's surface and exhibit a great variety of structure on a wide range of spatial scales (Fig. 1). They cover approximately one-fifth of Earth's surface in the annual mean (23% of the ocean surface and 12% of the land surface), making them the dominant cloud type by area covered (Warren et al. 1986, 1988; Hahn and Warren 2007). Stratocumuli strongly reflect incoming solar radiation (Chen et al. 2000) and exert only a small effect on outgoing longwave radiation, with the result being a strong negative net radiative effect that markedly affects Earth's radiative balance (e.g., Stephens and Greenwald 1991; Hartmann et al. 1992). Only small changes in the coverage and thickness of stratocumulus clouds are required to produce a radiative effect comparable to those associated with increasing greenhouse gases (Hartmann and Short 1980; Randall et al. 1984; Slingo 1990). Understanding why, where, when, and how stratocumuli form, and being able to quantify their properties, therefore constitutes a fundamental problem in the atmospheric sciences.

Stratocumuli tend to form under statically stable lower-tropospheric conditions (Klein and Hartmann 1993). Strong longwave cooling at the cloud top drives convective instability that helps to enhance, maintain, and sharpen the temperature inversion immediately above the cloud top, which can be as strong as 10–20 K in just a few vertical meters (Riehl et al. 1951; Riehl and Malkus 1957; Neiburger et al. 1961; Roach et al. 1982). Longwave cooling is the main driver of the overturning convective circulations that constitute the key dynamical elements of these clouds (Lilly 1968). Turbulence homogenizes the cloud-containing layer, frequently couples this layer to the surface source of moisture that maintains the cloud layer (e.g., Nicholls 1984; Bretherton and Wyant 1997), and controls the development of mesoscale organization (Shao and Randall 1996; Atkinson and Zhang 1996; Jonker et al. 1999; de Roode et al. 2004). Latent heating in the upward branches of the convective elements and evaporation in downdrafts, provides an additional source of turbulence that strengthens the convection (e.g., Moeng et al. 1992). Thus, stratocumulus clouds frequently exert first-order effects upon boundary layer structure and evolution (Atkinson and Zhang 1996; Stevens 2005). Figure 2 shows key processes, to be discussed in this review that operate and interact to determine the properties of the stratocumulus-topped boundary layer.

The strong link between lower-tropospheric stability (typically defined as the difference in potential temperature between 700 and 1000 hPa) and the formation of stratocumuli implies that there are strong large-scale meteorological controls upon these clouds; that is to say they are tightly coupled with the general circulation (Bretherton and Hartmann 2009). As demonstrated in Fig. 3, stratocumuli exist in abundance over the oceans, particularly over the cold parts of the subtropical and tropical oceans (the ocean temperature being the main reason for strong lower-tropospheric stability) and over the midlatitude oceans. They are favored in the downward branches of large-scale atmospheric circulations such as the Hadley and Walker circulations (Schubert 1976; Randall 1980; Klein and Hartmann 1993), in the subsiding regions of midlatitude baroclinic systems (Norris et al. 1998; Norris and Klein 2000; Lau and Crane 1997; Klein and Jakob 1999; Field and Wood 2007), over the undisturbed polar regions (e.g., Hermann and Goody 1976; Warren et al. 1988; Klein and Hartmann 1993; Curry et al. 1996, and references therein), and over the oceans during cold-air outbreaks (Agee 1987; Klein and Hartmann 1993; Atkinson and Zhang 1996). Over continents stratocumuli occur less frequently than over ocean, and tend to be concentrated in postcold-frontal air masses (Lau and Crane 1997; Mechem et al. 2010).

Stratocumulus radiative properties depend not only upon their macrophysical structure, but also upon their microphysical properties (Hansen and Travis 1974). The latter are impacted by variability in atmospheric aerosol, as suggested by Twomey (1974, 1977) and later demonstrated by Brenguier et al. (2000b). The control of stratocumulus radiative properties by processes on scales ranging from the planetary scale to the droplet scale explains why these clouds are such a challenge to understand and to predict (Siebesma et al. 2004; Zhang et al. 2005). Indeed, uncertainties surrounding their behavior thwart accurate prediction of future climate change (e.g., Wyant et al. 2006; Soden and Vecchi 2011).

Our current knowledge of stratocumulus clouds has been built up from an interplay between observational studies (e.g., review by Kloesel 1992), theory (e.g., reviews by Stevens 2005, 2006), and a hierarchy of models. Many studies have focused upon stratocumulus over the ocean as 80% of the world's stratocumulus clouds are located there (Warren et al. 1986, 1988). Increasingly, the focus of both observational and modeling research has centered

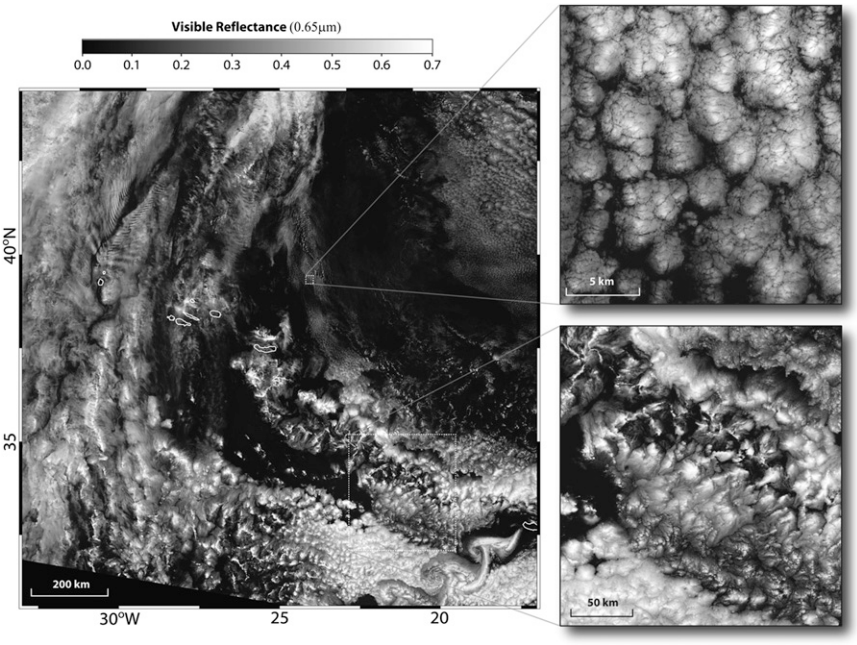

FIG. 1. Satellite imagery demonstrating the tremendous wealth of form for stratocumulus clouds on the mesoscale. (left) A 250-m resolution visible reflectance image ($\lambda = 0.65\ \mu$m) taken at 1235 UTC 7 Apr 2001 using the MODIS over the northeast Atlantic Ocean (note the Azores and Canary Islands). (top-right inset) A higher resolution (15 m) visible image ($\lambda = 0.8\ \mu$m) taken at approximately the same time using the Advanced Spaceborne Thermal Emission and Reflection Radiometer (ASTER). (bottom-right inset) Detail from the main image.

upon how low clouds may change in response to increases in greenhouse gases (e.g., Bony and Dufresne 2005) and changes in the anthropogenic contribution to aerosol loading (see Lohmann and Feichter 2005, for a recent review). This increasingly necessitates observational programs that can couple the small-scale processes critical to cloud formation with the atmospheric general circulation (Brenguier and Wood 2009; Wood et al. 2011b).

This review seeks to summarize our current state of knowledge about stratocumulus clouds with a focus upon what we have learned from observations and process models about their climatological distribution, key elements of their structure and dynamics, and their microphysical properties. Particular emphasis is placed upon the interactions among key processes, in particular the importance of internal feedbacks within the stratocumulus system, and the interactions between microphysics, radiation, turbulence, and entrainment. It may also be useful here to mention what this review does not include. We do not include a detailed discussion of the hierarchy of numerical modeling approaches for understanding stratocumulus clouds, nor do we discuss the way in which these clouds are parameterized in large-scale numerical models. Chemistry–cloud interactions are important and interesting but are not treated here.

This review is organized as follows. Section 2 provides an overview of the climatology of stratocumulus, including

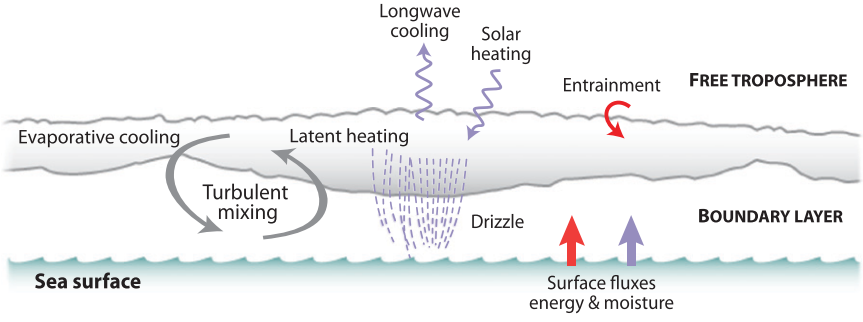

FIG. 2. Schematic showing the key processes occurring in the stratocumulus-topped boundary layer.

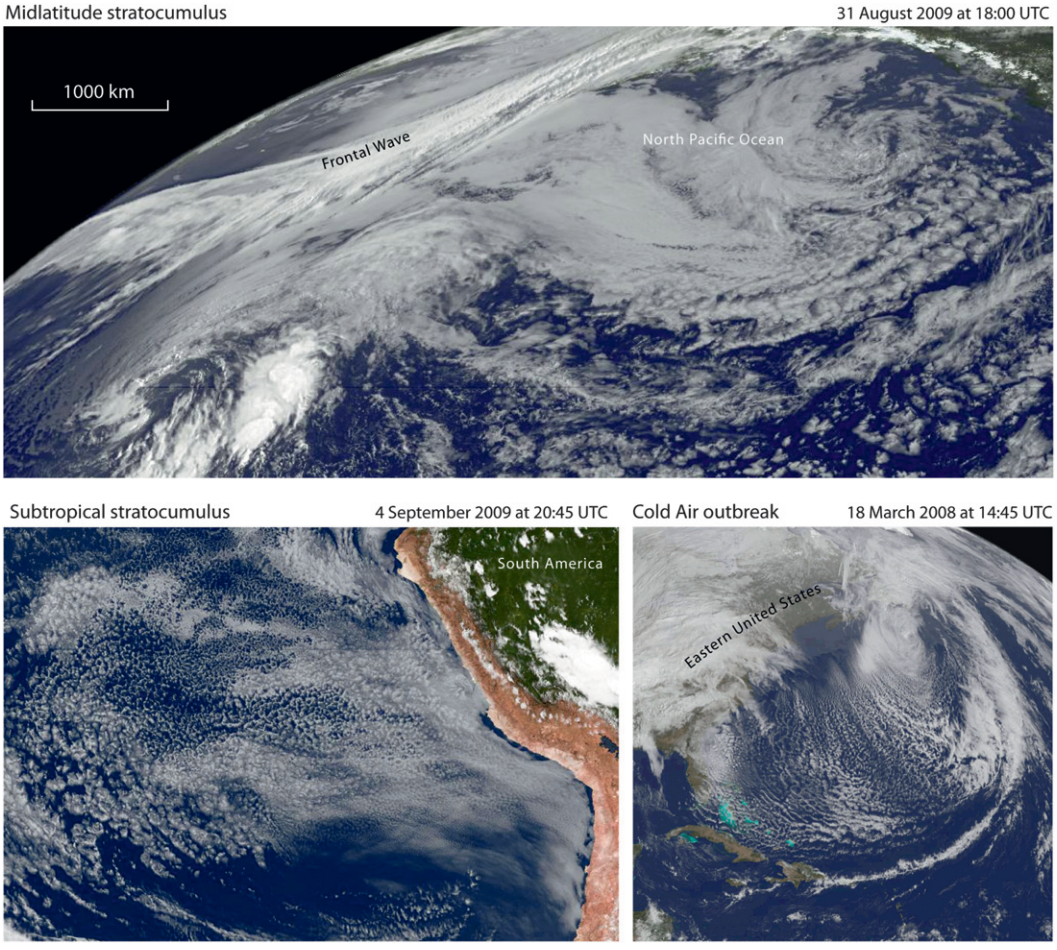

FIG. 3. Visible satellite imagery showing stratocumulus clouds in the midlatitudes, subtropics, and associated with a cold-air outbreak. Data are from the Geostationary Operational Environmental Satellites (GOES), with times shown on the images. The scale is approximately the same in each of the images.

its variability on seasonal, synoptic, interannual and diurnal time scales, and discusses the spatial scales of organization of stratocumulus. Section 3 describes the nature of the stratocumulus-topped boundary layer (STBL), focusing closely upon its vertical structure. Section 4 discusses the key individual processes important for stratocumulus clouds, while section 5 focuses upon microphysical structure and processes. Section 6 then synthesizes our understanding of how the key macrophysical and microphysical processes interact in the maintenance, formation, and dissipation of stratocumulus. Section 7 concludes this review with a summary of the key issues and outstanding problems.

2. Climatology of stratocumulus

Stratocumulus clouds can occur everywhere on Earth, and there are few places where they are not important contributors to the surface radiation budget. However, their climatological distribution is marked by its heterogeneity, with some regions experiencing stratocumulus in excess of 60% of the time and others only a few percent of the time (Warren et al. 1986, 1988; Hahn and Warren 2007). In some regions they occur in vast long-lived sheets, while in others they occur more intermittently. Stratocumulus typically exhibit structure on a broad range of temporal and spatial scales, and this section is organized around these chief variance-containing time and space scales.

a. Annual mean

Figure 4a shows the annual mean coverage of stratocumulus clouds globally. The subtropical eastern oceans are marked by extensive regions, often referred to as the *semipermanent subtropical marine stratocumulus sheets*, in which the stratocumulus cover exceeds 40% and can be as high as 60%. These sheets are approximately latitudinally symmetric about the Atlantic/Pacific ITCZ, and the maxima in stratocumulus cover are not located immediately

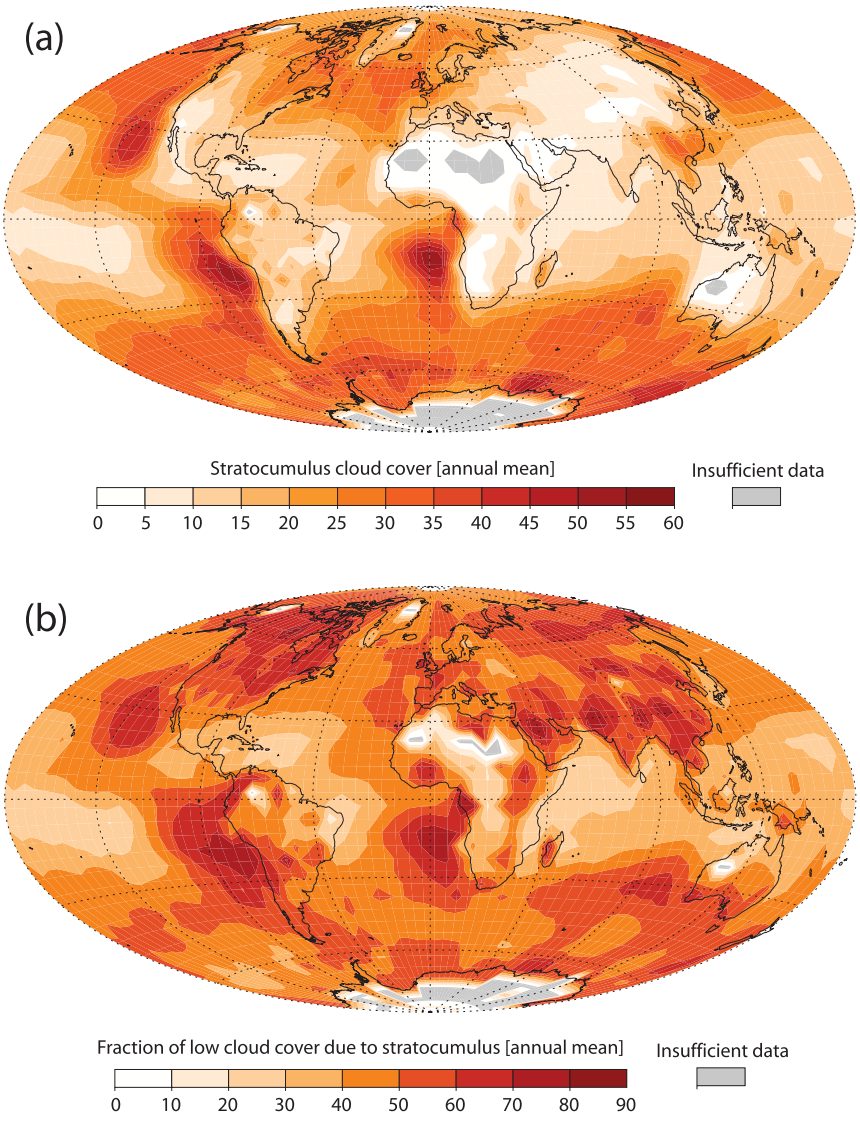

FIG. 4. (a) Annual mean coverage of stratocumulus clouds. (b) Fraction of annual mean low-cloud cover associated with stratocumulus clouds. Locations with no reports of stratocumulus (either because of a lack of stratocumulus or a lack of observations) are shown as gray. Data are from the combined land–ocean cloud atlas database (Hahn and Warren 2007).

adjacent to the coastlines, but are displaced roughly 5°–10° to the west, where the winds are typically stronger and the STBL is deeper than at the coast (Neiburger et al. 1961; Wood and Bretherton 2004). The Southern Hemisphere semipermanent stratocumulus sheets are larger than those in the Northern Hemisphere, a feature likely driven by increased stability and subsidence related to the configuration of elevated terrain to their east (Xu et al. 2004; Richter and Mechoso 2004, 2006).

Stratocumulus also swathe large regions of the midlatitude oceans where their mean coverage is typically 25%–40%. Over land, the regions with the highest stratocumulus cover are chiefly in the midlatitudes and in the coastal hinterlands adjacent to eastern boundary currents. However, the south and east of China is notable for being the only subtropical continental region with a high coverage of stratocumulus.

The western sides of the major ocean basins, the developed trade winds, and the arid continental regions have the lowest coverage of stratocumulus, but Fig. 4b demonstrates that even in these regions, stratocumulus clouds typically constitute over 20% of the overall low-cloud cover. For 97% of Earth's surface, stratocumulus clouds constitute 25% or more of the low-cloud cover. Thus, there are few regions of the planet where stratocumulus clouds are not climatologically important.

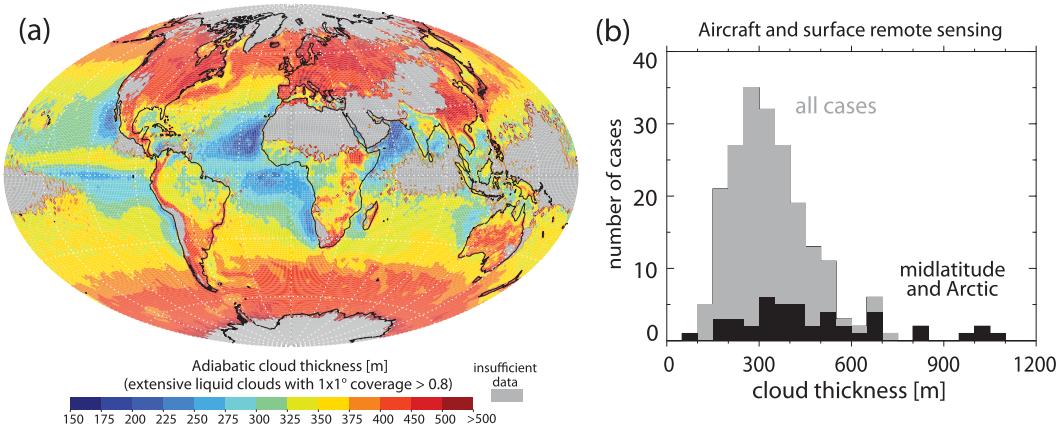

FIG. 5. (a) Annual mean cloud thickness for horizontally extensive liquid cloud (instantaneous coverage exceeding 80% at the $1° \times 1°$ scale). Adiabatic thickness is deduced from MODIS *Terra* liquid water path estimates at ~1030 LT (close to the time where the cloud thickness is close to the mean daily value), and is based on the assumption that the clouds are adiabatic (section 3a). The vertical liquid water gradient is estimated using the MODIS-derived cloud-top temperature. Wood and Bretherton (2004) have additional details. (b) Compilation of measurements of stratocumulus cloud thicknesses from observational case studies using aircraft and ground-based remote sensing, with all cases (gray) and midlatitude and Arctic cases (black) presented separately. Data are from the published literature and available datasets from recent stratocumulus field campaigns (Nicholls and Leighton 1986; Boers and Krummel 1998; Miles et al. 2000; Pawlowska and Brenguier 2003; Comstock et al. 2004; vanZanten et al. 2005; Wood 2005a; Lu et al. 2007; McFarquhar et al. 2007; Lu et al. 2009; Wood et al. 2011b).

Typical climatological mean liquid water paths (LWP, the vertically integrated liquid water content) for regions dominated by marine stratocumulus are 40–150 g m^{-2} (Weng and Grody 1994; Greenwald et al. 1995; Weng et al. 1997; Wood et al. 2002b; O'Dell et al. 2008), but because the cloud cover in these regions is not 100%, the cloud-conditional mean LWP is somewhat higher than this (Greenwald et al. 1995).

Climatological mean stratocumulus geometrical thickness h is difficult to estimate directly. Mean thicknesses estimated indirectly from the LWP climatology and the assumption of an adiabatic cloud are shown in Fig. 5a and range from 200–300 m over most of the cold subtropical eastern oceans to 400 m or more over the midlatitude oceans and continents. A compilation of observed stratocumulus thicknesses from field studies (Fig. 5b) is remarkably consistent with the satellite data, with the majority of cases showing thicknesses from 200–500 m, a median value of 320 m, and a tendency for thicker clouds (median 420 m) in mid- and high latitudes. In a sense, this represents an intriguing *lack* of variability ($200 < h < 400$ m almost everywhere) and hints at important feedbacks that limit the range of thicknesses that stratocumuli can assume (explored further in section 6).

b. *Temporal variability*

Temporal variability of stratocumulus can be broadly separated into four time scales: seasonal, synoptic, and interannual, and diurnal. In most locations, all four of these time scales contribute significantly to the overall temporal variance in stratocumulus cover.

1) SEASONAL CYCLE

In many regions, stratocumulus cloud cover is strongly seasonal. Figure 6 shows the amplitude of the seasonal cycle and the month of maximum stratocumulus cover. The patterns of seasonal stratocumulus variability largely follow the seasonal cycle of lower-tropospheric stability (Klein and Hartmann 1993; Wood and Bretherton 2006; Richter and Mechoso 2004, 2006). For the subtropical marine stratocumulus sheets, especially those in the Southern Hemisphere, the seasonal amplitude of the cover is greatest a few hundred kilometers downwind of the annual mean stratocumulus cover (cf. Fig. 4a). Spring or early summertime maxima are typical for these regions and over the Northern Hemisphere midlatitude oceans, and it is notable that the stratocumulus cover of the two major Southern Hemisphere subtropical marine sheets has a much stronger seasonal cycle and peaks earlier in the season than over the Northern Hemisphere subtropics. The hemispheric asymmetry in seasonality is caused by greater orographic forcing from the elevated continent to the east for the southern sheets (Richter and Mechoso 2004, 2006).

There are major differences in the seasonal phase between the western and the eastern sides of the midlatitude North Atlantic and Pacific Ocean, with a wintertime peak

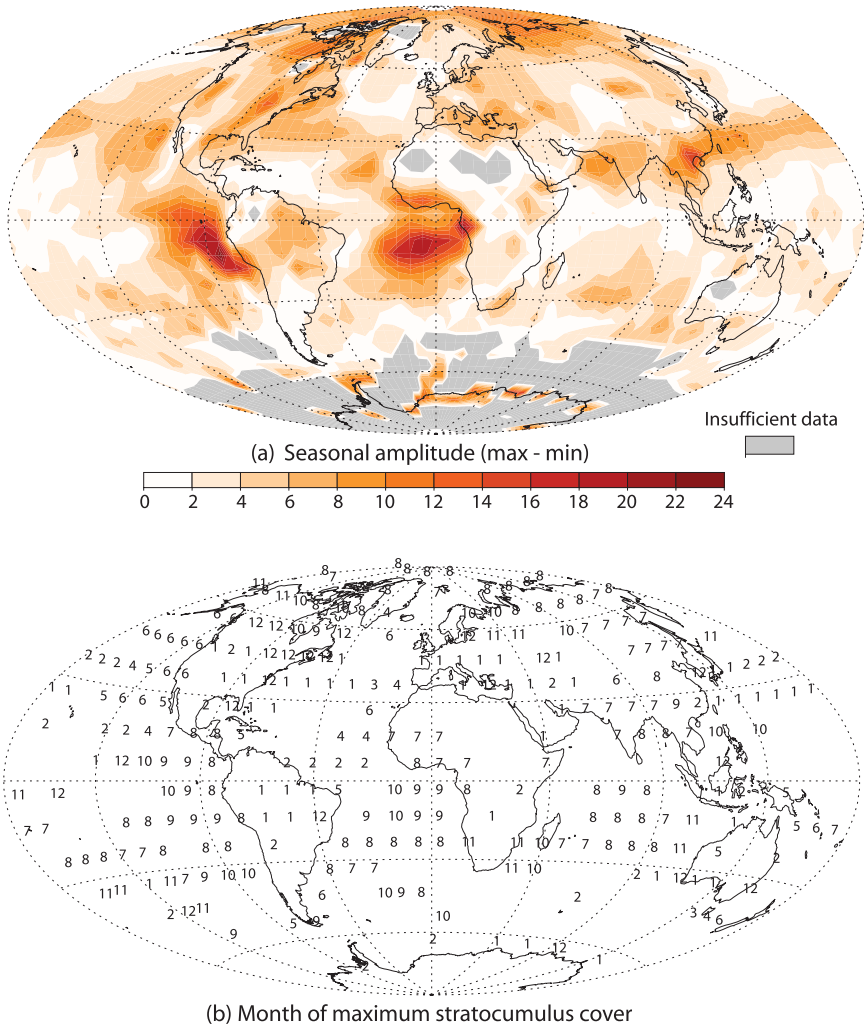

FIG. 6. (a) Seasonal amplitude (maximum − minimum coverage), and (b) month of maximum stratocumulus cover. Locations with no reports, or where the seasonal amplitude of stratocumulus cover is less than 2.5% are not shown. Data are from the combined land–ocean cloud atlas database (Hahn and Warren 2007).

over the western sides and summertime peaks over the eastern sides (Weaver and Ramanathan 1997). This probably reflects the greater importance of surface sensible heat flux (e.g., during wintertime cold-air outbreaks) for stratocumulus on the western side. Over the tropical oceans, there does not appear to be a systematic favored month of maximum stratocumulus cover, apart from over the equatorial eastern oceans where seasonally varying cross-equatorial flow drives SST variability (Mitchell and Wallace 1992), thereby increasing the seasonal variability in lower-tropospheric stability. Over land, especially in the midlatitudes, winter maxima are typical (Fig. 6).

Stratocumulus cover over the Arctic Ocean is strongly seasonal, peaking in late summer (Fig. 6b). Unlike most other regions, this seasonality is not explained by lower-tropospheric stability, which is markedly higher during winter (Klein and Hartmann 1993). The summertime maximum has been attributed to warmer temperatures and therefore greater moisture availability over the melting sea ice (Hermann and Goody 1976), but dissipation of clouds during wintertime through ice formation at colder temperatures has also been hypothesized to contribute to their seasonal cycle (Beesley and Moritz 1999).

2) SYNOPTIC VARIABILITY

The thickness and coverage of stratocumulus clouds are strongly modulated by the changing synoptic setting in which they exist. Although no single meteorological parameter can fully explain the synoptic variability in stratocumulus clouds (Klein 1997), in general, over oceans,

stratocumuli are associated with ridging conditions, with a frequency that is maximal to the east of the midtropospheric ridge line with cold-air advection and large-scale subsidence (Norris and Klein 2000). Thus, the semipermanent subtropical highs nurture semipermanent stratocumulus sheets on their eastern flanks (Fig. 4a), but there is synoptic variability in low-cloud cover and type associated with the strengthening and weakening of the subtropical high (Klein et al. 1995; Klein 1997; George and Wood 2010; Toniazzo et al. 2011) and with changes in its position (Klein et al. 1995; Garreaud et al. 2001). Coastally trapped disturbances also strongly modulate low clouds along the coastlines of the eastern subtropical oceans (Garreaud et al. 2002; Thompson et al. 2005).

At higher latitudes, extensive stratocumulus sheets are more transient, occurring most frequently in equatorward-moving cold sectors of midlatitude cylones (Ciesielski et al. 1999; Norris and Klein 2000; Field and Wood 2007). Baroclinic systems with typical time scales of 20 days or less (Wang et al. 1999; Hakim 2003) are also the primary synoptic modulators of the semipermanent stratocumulus sheets (Garreaud and Rutllant 2003; George and Wood 2010). Stratocumuli associated with cold-air outbreaks occur behind the trailing cold fronts of midlatitude cyclones. Over continents, stratocumuli are typically associated with subsidence and equatorward flow (e.g., Kollias et al. 2007) associated with postcold-frontal air masses (e.g., Mechem et al. 2010).

3) Interannual variability

Interannual variations of low clouds are comparable to synoptic and seasonal variations (Klein and Hartmann 1993; Stevens et al. 2007), but few studies have focused specifically upon stratocumulus. In subtropical marine stratocumulus regions, the interannual variability in low-cloud cover is correlated with lower-tropospheric stability (LTS) where gradients in LTS are aligned with those in mean low-cloud amount (e.g., Klein and Hartmann 1993), but less so in other subtropical regions (Stevens et al. 2007). Because LTS is strongly connected to the sea surface temperature (SST), negative interannual correlations between SST and marine low-cloud cover are observed over much of the ocean (e.g., Hanson 1991; Klein et al. 1995) and are strongest in the regions of transition from stratocumulus to cumulus (Norris and Leovy 1994) during summer. Low-cloud responses to ENSO are due in part to the response to SST anomalies, but also due to midlatitude storm-track teleconnections that affect temperature advection (Park et al. 2004).

Interannual variability in LTS is controlled by both SST and free-tropospheric temperature, and there is evidence suggesting that the free-tropospheric interannual variability is dominant in some regions (Stevens et al. 2007), while in others such as the equatorial eastern Pacific the SST dominates (Klein and Hartmann 1993). Interannual correlations are highest for cloud cover correlated with SST perturbations approximately 24 h upwind (Klein et al. 1995), indicating the importance of the Lagrangian history of the air mass in controlling low clouds.

4) Secular trends

There are no comprehensive trend studies specifically focused on stratocumulus clouds. Using volunteer ship observer reports, Eastman et al. (2011) find systematic decreases in marine stratocumulus cloud cover over the eastern subtropical oceans. It is known that small secular trends in the coverage of low clouds would be sufficient to affect Earth's climate sensitivity (Hartmann and Short 1980). Randall et al. (1984) and Slingo (1990) point out that increases in the absolute area covered by low clouds of 3.5%–5% would be sufficient to offset the warming induced by a doubling of CO_2. As low clouds cover just over 40% of Earth (Warren et al. 1986), this would require 8%–12% *relative* increases in low-cloud cover, or alternatively, a 10%–15% increase in cloud LWP, or a 5%–8% increase in cloud thickness. Identification of long-term secular trends in low-cloud properties is needed but is currently limited because the trends are expected to be small and difficult to distinguish from instrument calibration drifts (Dai et al. 2006; Evan et al. 2007; Norris and Slingo 2009).

5) Diurnal cycle

Stratocumulus clouds exhibit strong diurnal modulation largely due to the diurnal cycle of solar insolation and consequently absorption of solar radiation during the daytime in the upper regions of the cloud (section 4a). This suppresses the total radiative driving, resulting in weaker circulations during daytime than at night (Hignett 1991; Duynkerke and Hignett 1993; Caldwell et al. 2005) and a less efficient coupling of the clouds with the surface moisture supply (Turton and Nicholls 1987; Rogers and Koracin 1992). Because of this, the maximum coverage of stratocumulus tends to be during the early morning hours before sunrise (Rozendaal et al. 1995; Bergman and Salby 1996). This contrasts dramatically with clouds driven by convective heating from below, which tend to exhibit afternoon maxima.

In stratocumulus, diurnal maxima in cloud thickness and LWP also typically occur in the early morning hours (Zuidema and Hartmann 1995; Wood et al. 2002a; Bretherton et al. 2004; Zuidema et al. 2005). The amplitude of the diurnal variation in cloud cover and LWP can exceed 20% of the mean values (Rozendaal et al. 1995; Wood et al. 2002a) over the eastern subtropical oceans. Dedicated studies of the mean diurnal cycle of

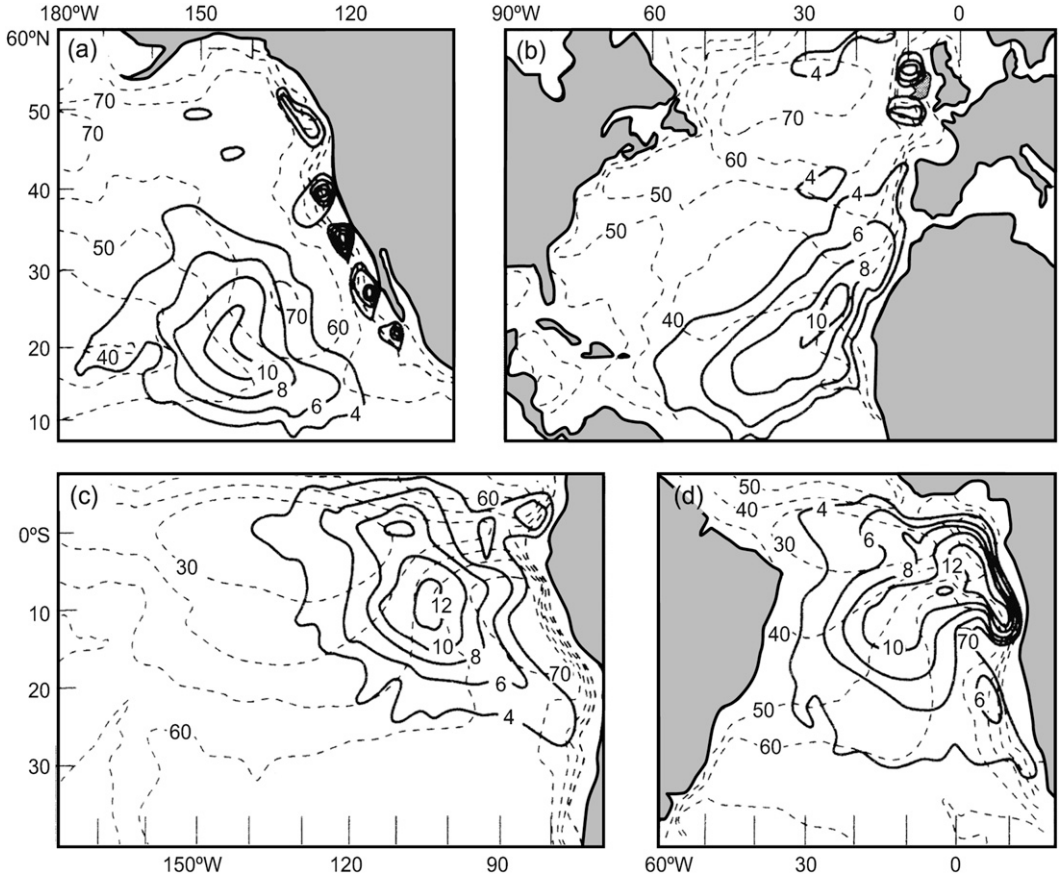

FIG. 7. Amplitude of the first harmonic of the diurnal cycle (solid) and mean low-cloud cover (dashed) for four regions where stratocumulus is a prevalent cloud type. Data from the International Satellite Cloud Climatology Project (ISCCP; Rossow and Garder 1993) for June–July–August 1984–90. From Rozendaal et al. (1995). © American Meteorological Society. Reprinted with permission.

continental stratocumulus cloud properties are lacking, but Hahn and Warren (2007) show that the relative diurnal amplitude of stratocumulus cover (i.e., amplitude expressed as a fraction of the mean coverage) is roughly double that over the ocean.

Strong diurnal variability in cloud cover is observed downwind of the subtropical maxima in cloud cover (Fig. 7) toward the regions of transition from stratocumulus to trade cumulus (Rozendaal et al. 1995; Klein et al. 1995; Miller et al. 1998), where the STBL is deeper than it is closer to the coast. In these regions, the STBL is often decoupled, and the diurnal march consists of an increasing frequency of cumulus clouds during the day from a nocturnal STBL that contains stratocumulus with cumulus below (Fig. 8). There is evidence that the strength of the diurnal cycle in these regions is not controlled by STBL decoupling and recoupling per se (since the STBL is never fully coupled), but by the increased daytime stability of the stable layer atop the surface mixed layer (Klein et al. 1995; Miller et al. 1998; Ciesielski et al. 2001), which results in a more intermittent (albeit locally stronger) cumulus coupling of the STBL. The moisture supply into the overlying stratocumulus layer is thereby limited and diurnal breakup enhanced. Drizzle too has a strong diurnal cycle (Leon et al. 2008; Comstock et al. 2004; Sears-Collins et al. 2006), typically peaking during the early morning hours (although the peak time is more variable over land than over ocean) and approximately in phase with that in cloud thickness and LWP.

In some regions, diurnal variability in the large-scale dynamics (primarily subsidence rate) also contributes to diurnal variability of stratocumulus (Ciesielski et al. 2001; Duynkerke and Teixeira 2001; Garreaud and Muñoz 2004; Bretherton et al. 2004; Caldwell et al. 2005; Wood et al. 2009a). Although this is especially true in near-coastal regions (e.g., Rozendaal et al. 1995), diurnal modulation of surface divergence is also observed in remote oceanic regions (Wood et al. 2009a). This appears to stem from long-range propagation of diurnally forced gravity waves from continents or from regions of

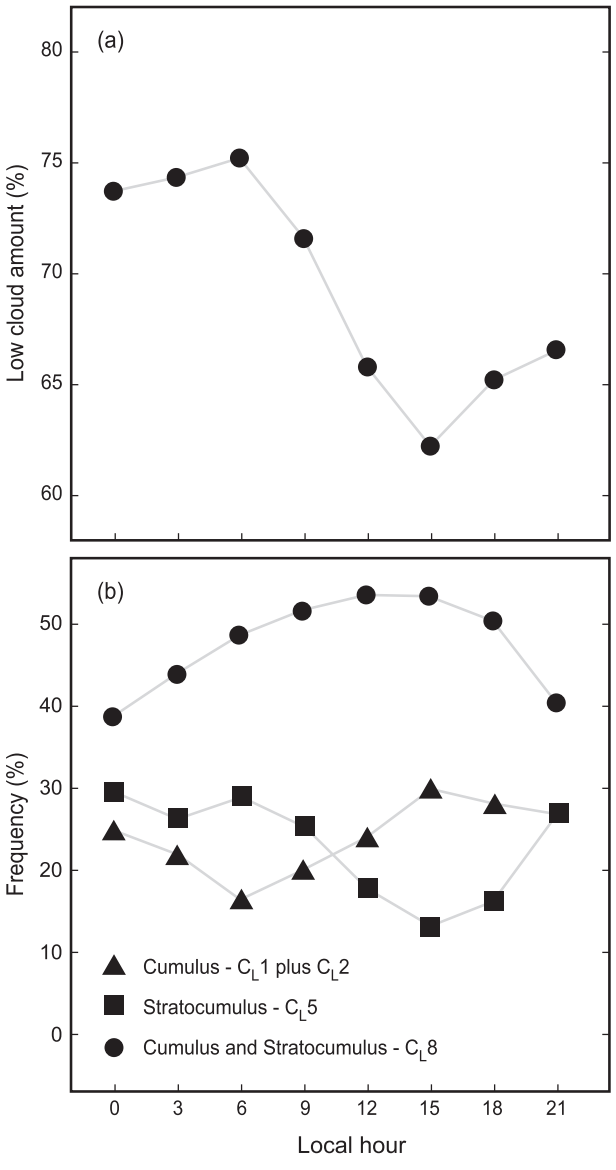

FIG. 8. Mean summertime (June–September) diurnal cycle of (a) low-cloud amount and (b) frequency of occurrence of different WMO low-cloud types for cases of cold advection at 30°N, 140°W, a region of stratocumulus to cumulus transition; from Klein et al. (1995). © American Meteorological Society. Reprinted with permission.

deep convection that can either enhance or decrease cloud diurnal variability depending upon the local phase of the wave with respect to the solar cycle (Wood et al. 2009a).

c. *Spatial scales of organization*

Stratocumulus display a tremendous organizational complexity, as Figs. 1 and 3 clearly show, with the range of spatial scales manifested in stratocumulus fields spanning several orders of magnitude. Variance of scalar fields in the subtropical marine STBL generally increases with spatial scale (e.g., Comstock et al. 2005) from the smallest observable scales out to ~1000 km. For a subset of this range power-law scaling typically extends from the smallest scales (the ''inner'' scale) out to ~5–100 km (the ''outer'' scale) (Nucciarone and Young 1991; Wood et al. 2002b; Davis et al. 1999), or for point observations, out to time scales of several hours or more (Wood and Taylor 2001; Comstock et al. 2005). This scaling regime in the beta and gamma mesoscales is frequently associated with mesoscale cellular convection and is imprinted on the cloud liquid water or cloud optical thickness field (Cahalan and Snider 1989; Cahalan et al. 1994; Davis et al. 1996, 1999; Wood and Taylor 2001; Wood et al. 2002b; Wood and Hartmann 2006). Thus, there is rarely a scale break in STBL scalar fields at the scale of the STBL depth z_i. In contrast, most of the variance in *vertical* motions in stratocumulus is largely restricted to horizontal scales comparable to z_i. This scale is generally referred to as the *large eddy scale*.

1) MESOSCALE STRUCTURE AND ORGANIZATION

Over the mesoscale scaling range typically observed in STBLs, the variance of scalars increases with increasing spatial scale as $\sigma_{\text{scalar}} \approx \alpha L^{\beta}$ with $\beta \approx 1/3$ and α increasing with STBL depth (Wood et al. 2002b). Scaling is not unique to the STBL, but appears to be a general feature of quasi-two-dimensional turbulence (Nastrom and Gage 1985; Vallis 2006) and extends to larger scales than those associated with mesoscale cellular convection. The existence of a clear outer scale in the STBL (e.g., Wood and Hartmann 2006) likely requires a source of turbulent kinetic energy (TKE) in the STBL that adds additional variance to the existing ''background'' field associated with two-dimensional turbulence.

The outer scale is most readily determined using satellite data, but there is evidence from both aircraft and satellite data that the outer scale is greater for deeper boundary layers (Davis et al. 1996; Wood and Hartmann 2006). The outer scale is often associated with a clearly definable mesoscale cellular pattern in the cloud fields (see Wood and Hartmann 2006, for a discussion). For example, the visible radiance power spectrum (not shown) from the bottom-right panel in Fig. 1 has an outer scale of approximately 30 km, and visual inspection shows that this corresponds to the approximate diameters of the mesoscale cellular convective cells. Aspect ratios of these STBL ''closed'' cells are typically 3–40 (Agee et al. 1973; Rothermel and Agee 1980; Agee 1987; Moyer and Young 1994; Atkinson and Zhang 1996).

Stratocumulus over the oceans may be grouped into four general mesoscale morphological types: (i) no cellularity on the mesoscale, (ii) organized closed mesoscale cellular convection, (iii) organized open mesoscale

cellular convection, and (iv) unorganized mesoscale cells. Figure 9 shows examples of these prevailing types. Broadly speaking, these types represent different stages of an airmass transition from shallow marine stratus to trade cumulus over the subtropical–tropical eastern oceans (Agee et al. 1973; Wood and Hartmann 2006). In many cases, the organization of marine stratocumulus may resemble a hybrid of these canonical mesoscale forms (e.g., actinoform clouds; Garay et al. 2004). There are few detailed studies of stratocumulus mesoscale morphology over land, and visual inspection of satellite images suggests that well-defined mesoscale cellularity is not a common feature of terrestrial stratocumulus, most likely because land surface heterogeneities interfere with cell-producing processes.

Stratocumulus may also organize into roll-like structures (Atkinson and Zhang 1996), especially in cold-air outbreaks over lakes and oceans (Agee 1987). Roll formation often occurs prior to the formation of open and closed cellular structures that are more prevalent farther downstream after the boundary layer has deepened (Walter 1980; Agee 1987; Young and Sikora 2003). Rolls are often the dominant form of mesoscale variability in stratocumulus over land (Atkinson and Zhang 1996). Such rolls form in cases with marked wind shear across the STBL (Atkinson and Zhang 1996) and align themselves with the shear vector (e.g., Schultz et al. 2004). STBL rolls or bands in cold-air outbreaks may have aspect ratios larger than those typically found in clear boundary layers (Agee 1987). Rolls are not a common feature of stratocumulus over the remote parts of the ocean other than to the north of the equatorial Pacific cold tongue.

For the marine STBL, the mesoscale variance in cloud thickness is largely caused by fluctuations in cloud-base height, with cloud-top height contributing only weakly (Wood and Taylor 2001, consistent with the visual picture we take away from Fig. 11). For continental stratocumulus, both cloud-top and cloud-base variations have been found to be important at regulating the cloud thickness on the mesoscale (Kim et al. 2005), which may reflect the typically weaker capping inversion in continental cases.

2) LARGE EDDY SCALE

The horizontal wind variance in the STBL often extends to the outer scale seen in the cloud and moisture fields (Nucciarone and Young 1991), whereas there is relatively little variance in the vertical wind component at scales much longer than the STBL depth (Rothermel and Agee 1980; Nucciarone and Young 1991; de Roode et al. 2004).

One might imagine that with weak vertical wind variance in the mesoscale, the vertical transport of energy, moisture, and momentum would also be confined to the large eddy scale, as appears to be the case for the clear convective boundary layer (de Roode et al. 2004). In the STBL, however, some fraction of the vertical transport appears to occur at mesoscales (de Roode et al. 2004; Faloona et al. 2005; Tjernstrom and Rune 2003). Problems with aircraft wind measurement drift and the high-pass filtering (the removal of information on scales longer than around 2–3 km is common) designed to remove these problems may have missed the mesoscale contribution to vertical transports in many observational studies. Clearly more work, and new approaches are needed to assess these contributions.

3. The stratocumulus-topped boundary layer

The vertical and horizontal structure of stratocumulus clouds is very strongly tied to the vertical structure of the boundary layer (Lilly 1968; Albrecht et al. 1995b; Wood and Bretherton 2004; Wood and Hartmann 2006; Bretherton et al. 2010b). This section reviews the vertical structural properties of the STBL, including the profile of cloud liquid water, and the entrainment interfacial layer. This prepares the ground for a discussion of the key controlling processes in section 4.

a. Vertical structure of the STBL

The fractional coverage of low clouds is greatest when the STBL is moderately shallow [$0.5 < z_i < 1$ km, e.g., Albrecht et al. (1995b) and Wood and Hartmann (2006)], and these STBLs are often well mixed. Figure 10 shows an example of the vertical structure of such an STBL with near-constant conserved variables, a near–dry adiabatic lapse rate below cloud, a moist adiabatic layer above cloud base, and a strong capping inversion. Other than very close to the ocean surface, horizontal winds in the well-mixed STBL are often approximately constant with height, and sometimes jumps of several meters per second in wind speed and/or several tens of degrees in wind direction may occur across the inversion (Garratt 1992, chapter 7). Typical mean profiles for the well-mixed STBL over the eastern subtropical oceans paint a very similar picture to that shown in Fig. 10. Figure 11 shows a photograph taken above this type of STBL that demonstrates both the large-scale horizontal homogeneity in the inversion/cloud-top height and also the small-scale convective eddies that are responsible for much of the mixing.

As the STBL deepens beyond 1 km, which often occurs through the entrainment of free-tropospheric air into the STBL, it becomes increasingly difficult for longwave cooling at the top of the cloud to sustain mixing of the positively buoyant entrained air over the entire

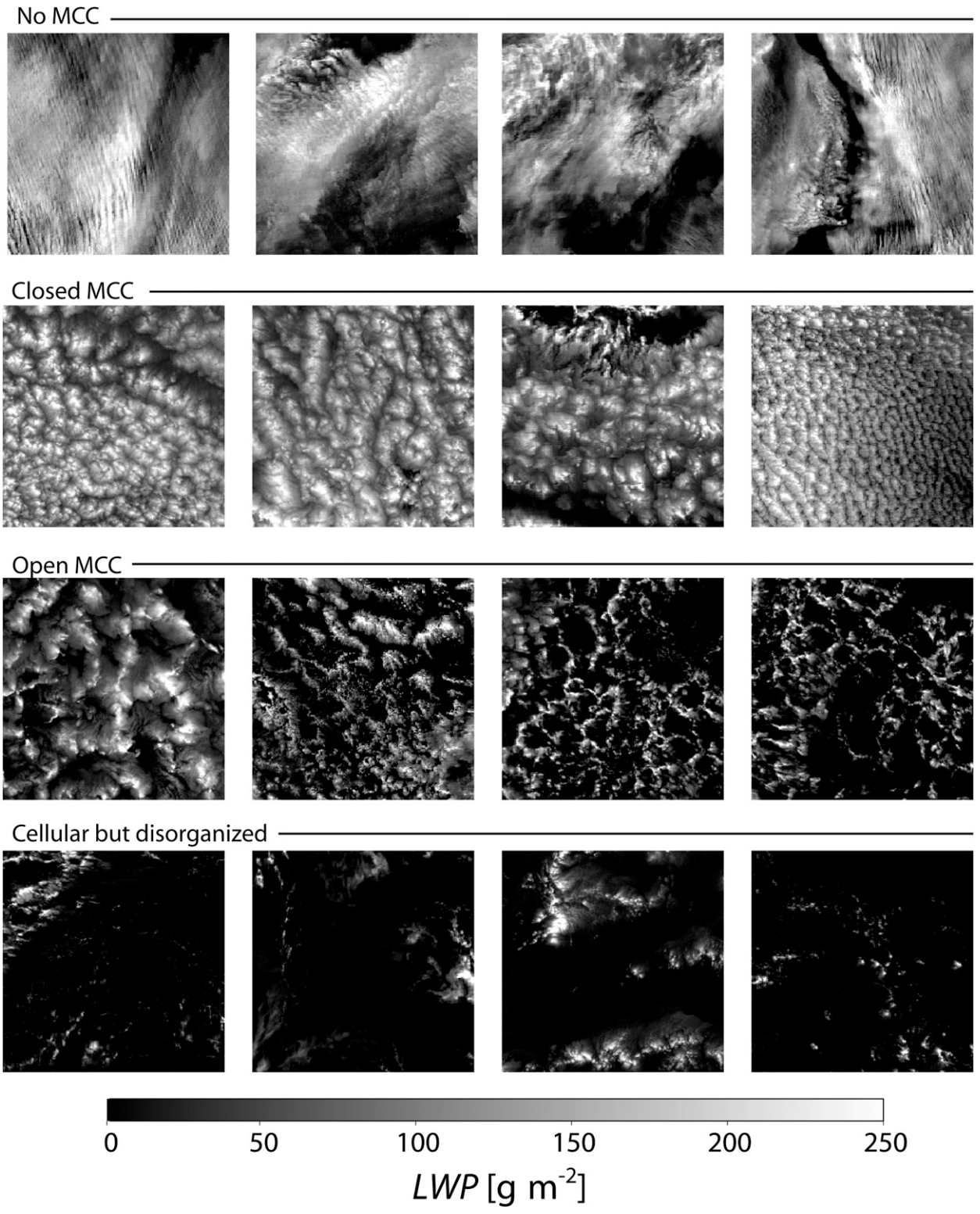

FIG. 9. Examples of different mesoscale structure types occurring in marine stratocumulus. Each image is 256 × 256 km^2 in size and shows liquid water path estimated using MODIS. Note that visible reflectance imagery would look almost identical. Reproduced from Wood and Hartmann (2006). © American Meteorological Society. Reprinted with permission.

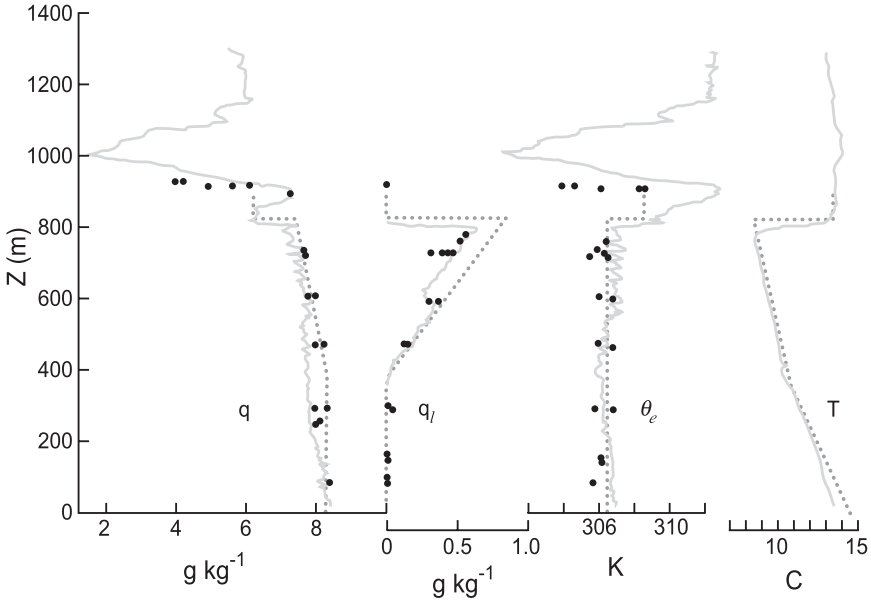

FIG. 10. Vertical profiles of water vapor q and liquid water q_l mixing ratios, equivalent potential temperature θ_e, and temperature T for a summertime shallow and quite well-mixed STBL observed over the North Sea to the east of a ridge. Means from horizontal legs are depicted by dots. The dotted lines in each case show the values expected for a well-mixed layer. Adapted from Nicholls (1984).

depth of the STBL (Bretherton and Wyant 1997). The STBL then begins to separate into two layers (Nicholls and Leighton 1986; Albrecht et al. 1995a; Bretherton and Pincus 1995; Bretherton et al. 1995; Wyant et al. 1997; Miller et al. 1998) with the upper (cloud containing) layer becoming decoupled from the surface moisture supply by a weakly stable interface. An example of a deeper STBL that has undergone decoupling is shown in Fig. 12. Within a decoupled STBL, the stratocumulus layer itself often exists within a mixed layer, but the negatively buoyant eddies generated by longwave cooling are not able to mix through the subcloud layer. Meanwhile, the near-surface layer can be mixed by surface-generated turbulence as in a classic boundary layer. Such a layer is termed the surface mixed layer (SML). Between the SML and the stratocumulus-containing mixed layer there is often a conditionally unstable layer (Fig. 12). Cumulus clouds often form at the top of the SML and act to intermittently and locally couple the stratocumulus layer with the surface (Krueger et al. 1995b). In such situations the stratocumulus deck can show breaks, and there is a greater degree of mesoscale variability, as illustrated in Fig. 13.

Composite vertical profiles from different locations representative of different stages of the transition from a shallow well-mixed STBL to a deep and decoupled STBL, and finally into a cumulus-dominated boundary layer, show increased stratification in conserved variables, and decreased cloud cover, as the boundary layer deepens (Fig. 14). Figure 15 shows schematics for the shallow, well-mixed, and overcast STBL, and for the deep, decoupled STBL containing broken clouds. These can be

FIG. 11. Photograph of the stratocumulus cloud top taken on a research flight over the subtropical northeast Pacific (30.4°N, 122°W) on 20 Jul 2001. The photograph was taken shortly after noon from an altitude of 5 km, with the cloud tops at a height of 800 m. For reference, the horizontal distance across the base of the image is approximately 5 km. Photo courtesy of G. Vali.

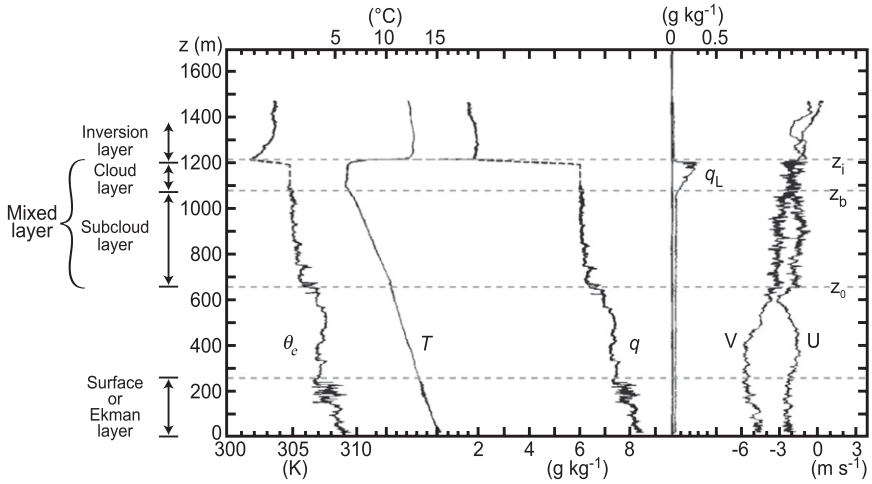

FIG. 12. Vertical profiles of water vapor q and liquid water q_l mixing ratios, equivalent potential temperature θ_e, temperature T, and easterly/northerly wind components (u and v) for a summertime decoupled STBL observed over the North Sea. Adapted from Nicholls and Leighton (1986).

considered the two limiting regimes for STBL structure. Decreased cloud cover is associated with stronger surface forcing, an increased frequency of cumulus clouds, and a decreased frequency of stratocumulus clouds. That said, even for regions with deep, decoupled marine trade wind boundary layers, stratocumulus constitute several tens of percent of the low-cloud cover (Warren et al. 1988, and section 2 above). In this deep STBL limit, the presence of a strong inversion helps to maintain extensive stratiform clouds (Stevens et al. 2001).

Observations from a single aircraft flight through the southeastern Pacific stratocumulus region (Fig. 16) illustrate key characteristics of both the shallow ($z_i \sim 1$ km), well-mixed STBL containing little or no drizzle, just offshore of the northern Chilean coast, and the deeper ($z_i \sim 1.7$ km), decoupled STBL farther offshore. In this case, the shallow STBL has a relatively homogeneous cloud base close to the surface-determined lifting condensation level (LCL). As the STBL deepens, the clouds thicken, produce more drizzle, and become increasingly variable on the mesoscale. Cloud bases become increasingly variable as cumulus clouds form beneath the stratocumulus.

b. Liquid water

Because a cloud's liquid water content is a primary determinant of its optical properties (Stephens 1978a), it is a critical link between the cloud dynamics and radiative effects [Eq. (1) and discussion in section 4a below]. Liquid water mixing ratios q_l typically increase with height in stratocumulus layers at a rate that is frequently quasi-linear and can approach that consistent with well-mixed conserved variables (Fig. 10). The well-mixed rate is often referred to as the *adiabatic* liquid water profile. The adiabatic rate of increase of q_l with height increases primarily with temperature and exhibits a weaker dependence upon pressure (Albrecht et al. 1990, contains the complete expression).

Observations from aircraft (Nicholls and Leighton 1986; Gerber 1996; Miles et al. 2000; Wood 2005a) and surface-based remote sensing (Albrecht et al. 1990; Zuidema et al. 2005) suggest that stratiform boundary layer cloud layers are frequently close to adiabatic. The *adiabaticity* F_{ad} is defined as the ratio of the LWP to that expected for a moist adiabatic layer with the equivalent cloud base and top (Slingo et al. 1982b; Albrecht et al. 1990; Wood 2005a). Given sensitive aircraft and surface remote sensing measurements of liquid water, it is often easier to detect stratification in the vertical thermodynamic profile using measurements of F_{ad} than by examination of temperature or moisture profiles (Nicholls and Leighton 1986).

FIG. 13. Photograph of stratocumulus with cumulus below within a decoupled STBL taken from a research ship over the tropical southeastern Pacific (20°S, 85°W) on 21 Oct 2001. The photograph was taken 2 h after sunrise. Photo courtesy of S. Yuter.

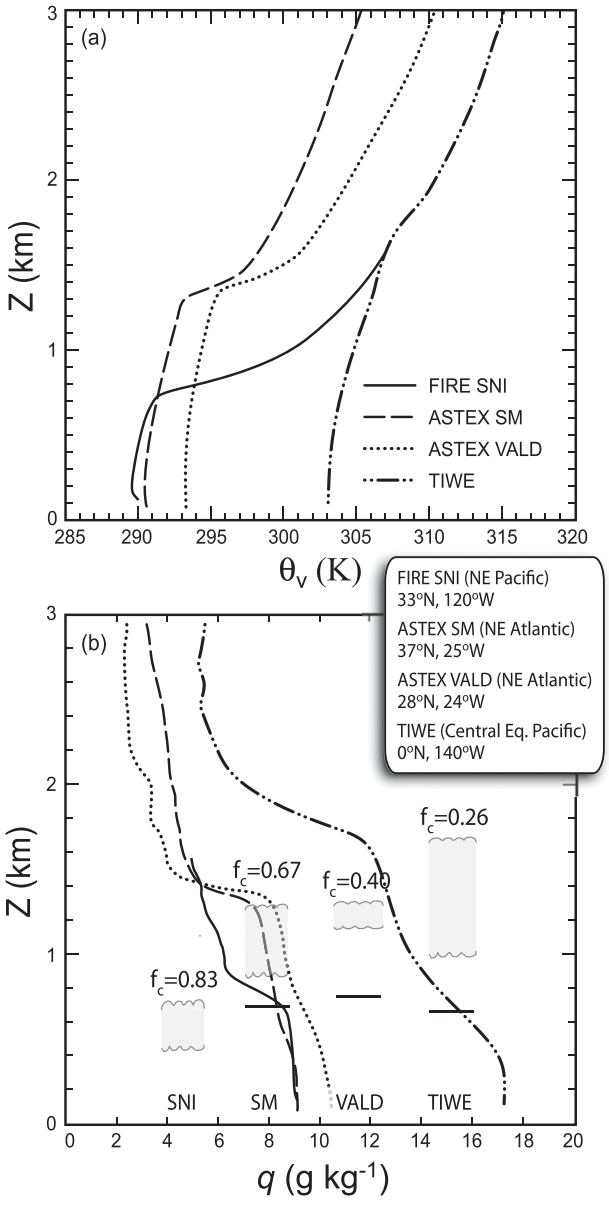

FIG. 14. Composite mean profiles of (a) virtual potential temperature θ_v and (b) water vapor mixing ratio from four marine field studies located in regions with distinctly different marine boundary layer characteristics: just off the California coast [San Nicholas Island (SNI)], the subtropical/midlatitude eastern Atlantic [Santa Maria Island in the Azores (SM)], the subtropical Atlantic [R/V *Valdivia* (VALD)], and the equatorial central Pacific [Tropical Instability and Waves Experiment (TIWE)]. See Albrecht et al. (1995b) for details of the locations. In (b) the mean inversion base heights and cloud bases (indicated with cloud extent), lifting condensation levels (horizontal lines), and cloud cover f_c are indicated. Figure adapted from Fig. 2 and Table 2 of Albrecht et al. (1995b). Reproduced/modified by permission of the American Geophysical Union.

Deviations from the adiabatic liquid water profile are found close to cloud top, where entrainment causes droplet evaporation (e.g., Nicholls and Leighton 1986). The cloud layer can also be subadiabatic when drizzling (Austin et al. 1995; Gerber 1996; Miller et al. 1998; Wood 2005a; Zuidema et al. 2005), and, when the drizzle is heavy, the profile may exhibit no linearity at all (Nicholls and Leighton 1986; Gerber 1996).

The theory to quantify the effects of boundary fluxes (at the cloud base and top) and precipitation on cloud adiabaticity is incomplete; Nicholls and Leighton (1986) adapted a dry surface-driven boundary layer theory (Wyngaard and Brost 1984) to estimate that entrainment might explain the reductions of around 20% from F_{ad} seen in their observations. A more recent study Wood (2005a) finds evidence that substantial departures of F_{ad} from unity appear to scale with the ratio of the time scales for moisture replenishment by turbulent fluxes to that for precipitation removal. Surface-based microwave radiometers also suggest that strongly drizzling stratocumulus is subadiabatic (Zuidema et al. 2005). This adds additional complexity to the factors controlling liquid water path, but is qualitatively consistent with the findings that in strongly precipitating stratocumulus the precipitation flux can exceed the replenishment moisture flux (Austin et al. 1995). Recent evidence suggests that a significant fraction of the condensate in strongly precipitating marine stratocumulus may actually be in the form of drizzle drops (Wood et al. 2011a).

c. *Entrainment interfacial layer*

The STBL is capped by a shallow layer over which there are strong gradients in thermodynamic properties (temperature, humidity, and cloud water), tracers, and radiative cooling rates. This layer has been termed the entrainment interfacial layer (EIL) by Caughey et al. (1982), but is often referred to as the *inversion*, or the *inversion layer*, because the universal and often the defining feature of the EIL is a strong increase in temperature with height that may exceed 1 K m^{-1} in some cases. However, since the EIL represents the layer between the cloud top and the upper limit of mixing influence from the STBL, it is most appropriate to define the EIL using a surface-emitted tracer (e.g., dimethyl sulfide; Faloona et al. 2005). Alternatively, conserved variables such as total water and ozone mixing ratio can be used, but fine layers above the STBL complicate their use.

The structure of the EIL has been documented in a number of observational studies (Caughey et al. 1982; Lenschow et al. 2000; vanZanten and Duynkerke 2002; Gerber et al. 2005; Haman et al. 2007) summarized in Fig. 17. These studies, together with large eddy simulations

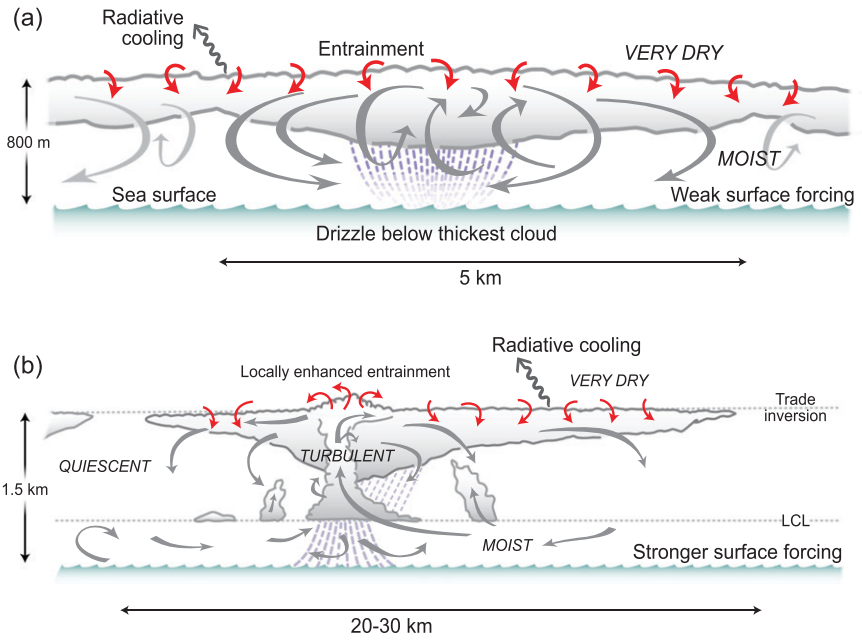

FIG. 15. Schematic showing structure of marine stratocumulus in (a) the shallow, well-mixed boundary layer and (b) deeper, cumulus-coupled boundary layers. Gray arrows indicate the primary motions on the scale of the boundary layer, while smaller red arrows indicate the small-scale entrainment mixing taking place at the inversion atop the layer. Vertical thermodynamic profiles associated with the two schematics are roughly represented by (a) the FIRE SNI and (b) the ASTEX VALD profiles shown in Fig. 14.

(Stevens et al. 1999; Moeng et al. 2005), show that the EIL is typically no more than a few tens of meters thick; but has a highly variable thickness within the same cloud system. The EIL it typically thinned by ascending convective plumes impinging upon it (Stevens et al. 1999). The top of the EIL is less well defined than the base, with weaker vertical gradients relaxing to free-tropospheric values over several meters or tens of meters in some cases. This is in stark contrast with the sharp temperature gradient discontinuity at the base of the EIL (Caughey et al. 1982; Lenschow et al. 2000) that tends to coincide with, or lie above, the local stratocumulus cloud top (Roach et al. 1982; Caughey and Kitchen 1984; Lenschow et al. 2000; Moeng et al. 2005). The sharp temperature gradient at the base of the EIL is maintained by strong radiative cooling of the cloud top. The EIL consists of relatively moist and cool air compared with the free troposphere (Brenguier et al. 2000a; Wang and Albrecht 1994), intermittent turbulence, and can also contain intermittent filaments of cloudy and clear air in different stages of mixing (Haman et al. 2007), particularly near the base of the EIL. The EIL represents a region containing a mixture of STBL and free-tropospheric air such that the cloud top itself does not represent the upper limit of the STBL (Lenschow et al. 2000).

The nature of the EIL, particularly the strength of the gradients in buoyancy and horizontal winds, determines cloud-top entrainment (Wang and Albrecht 1994; Gerber et al. 2005; de Roode and Wang 2007). High temporal resolution and *collocated* measurements of liquid water, temperature, inactive tracers, humidity and turbulence, preferably from a slow-moving or stationary platform [e.g., the Airborne Cloud Turbulence Observation System (ACTOS) helicopter platform; Siebert et al. 2006a], will be required to fully characterize and understand the EIL and how it affects entrainment.

4. Physical processes controlling stratocumulus

As Fig. 2 depicts, stratocumulus clouds are controlled by a tight interplay between radiative driving, turbulence, surface fluxes, latent heat release, and entrainment. In many cases, particularly over the oceans, precipitation also exerts important controls on the STBL. This section describes our state of knowledge of the key controlling processes separately and section 6 focuses on the critical interplay between these processes.

a. Radiative driving of stratocumulus

Longwave radiative cooling at the cloud top is the primary cause of convection in stratocumulus (Lilly

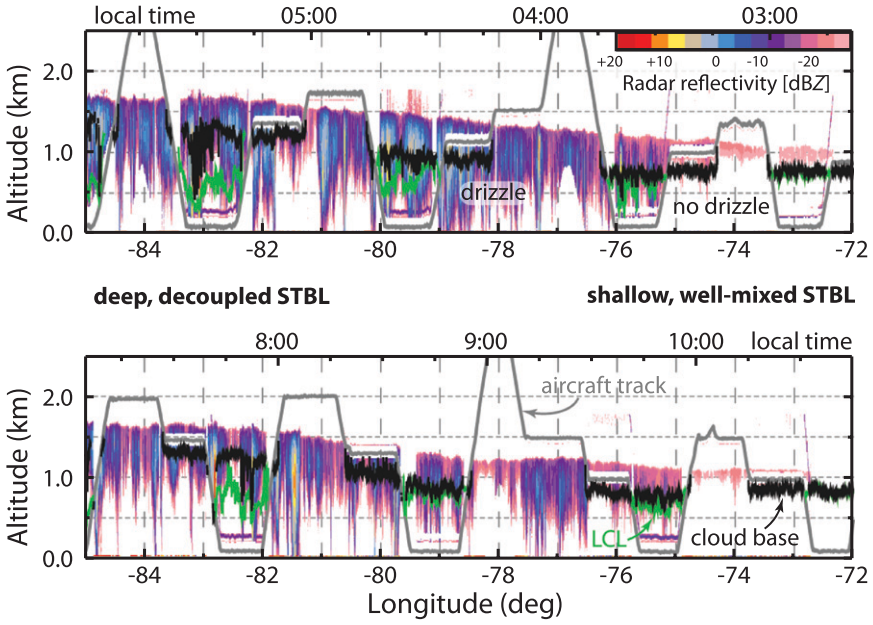

FIG. 16. Observed spatial transition from (right) a shallow, well-mixed STBL to (left) a deeper, decoupled STBL. Longitude–height plot of radar reflectivity (color scale at top right) measured using an up/down-pointing millimeter radar on a research aircraft flying along 20°S latitude line from the coast of northern Chile (70°W, right) to the remote southeastern Pacific Ocean (85°W, left) on 21 Oct 2008 during the VOCALS Regional Experiment (Wood et al. 2011). The (top) outbound and (bottom) return portions of the flight are shown. The aircraft track is indicated by the gray line. During flight legs below cloud, the in situ lifting condensation level (green) and the upward-pointing lidar cloud base (black) are superimposed. During cloud legs, the black line shows the cloud base adiabatically derived from in situ liquid water content measurements. The top axis labels show local time. Adapted from Fig. 2 of Bretherton et al. (2010a). Reproduced/modified with the author's permission.

1968; Nicholls 1984, 1989; Moeng et al. 1996). During the day, absorption of solar radiation warms the cloud layer and partially offsets longwave driving. On longer time scales, stratocumulus clouds also impact the radiative budget at the top of the atmosphere and the surface. The latter helps maintain a cool ocean surface and may help explain the persistence of stratocumulus over the eastern tropical and subtropical oceans (Park et al. 2005).

Liquid droplets scatter and absorb radiation to a degree that depends primarily upon wavelength, but also upon the cloud droplet size. They also emit efficiently in the longwave (thermal infrared $4 < \lambda < 50$ μm). Scattering is important at all wavelengths across the visible and infrared, but absorption dominates in the thermal infrared and is important for some bands in the near-infrared ($0.8 < \lambda < 4$ μm). For visible wavelengths ($\lambda < 0.8$ μm), there is very little absorption by liquid water.

1) LONGWAVE RADIATION

Besides driving convective instability in stratocumulus clouds, longwave cooling is typically the leading term in the STBL energy budget (e.g., Caldwell et al. 2005). Most stratocumulus contain liquid water in sufficient abundance that they are largely opaque to longwave radiation (Paltridge 1974; Platt 1976). The volume absorption coefficient in the longwave increases approximately linearly with liquid water mixing ratio q_l (Platt 1976; Pinnick et al. 1979) and can be expressed as $\beta_\lambda = \kappa_\lambda \rho q_l$, where ρ is the air density, and κ_λ is a spectrally dependent mass absorption coefficient.

The mass absorption coefficient in the thermal infrared is virtually independent of cloud droplet size for droplet effective radius[1] r_e smaller than the wavelength (Stephens 1978a; Chylek et al. 1992), but depends upon effective radius when a significant fraction of the mass is contained in droplets larger than the wavelength [see

[1] The droplet effective radius is the ratio of the third to the second moment of the droplet size distribution $n(r)$, so $r_e = \int_0^\infty r^3 n(r)\,dr / \int_0^\infty r^2 n(r)\,dr$ and thus relates the total surface area of the droplets to their combined mass (Hansen and Travis 1974). Calculations show that r_e is sufficient to encapsulate information about the droplet size distribution in radiative transfer calculations (Hu and Stamnes 1993).

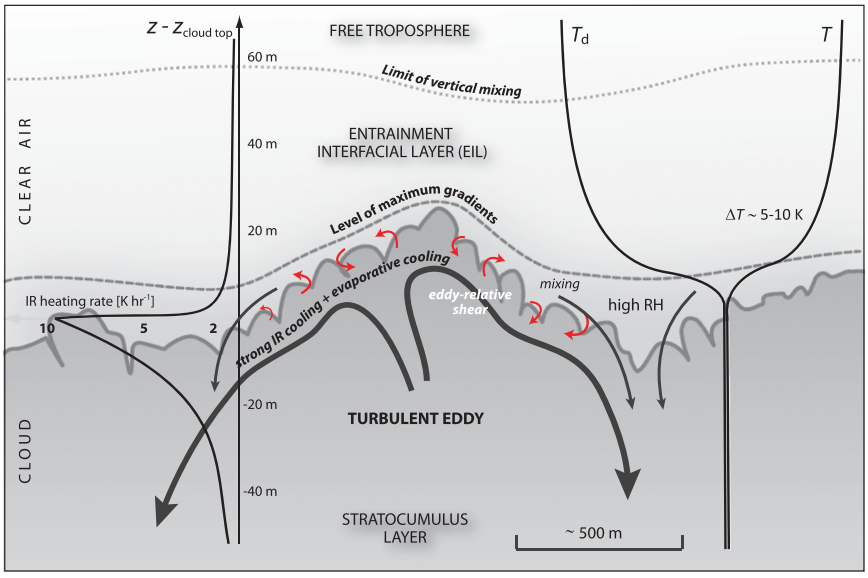

FIG. 17. Schematic of the entrainment interfacial layer (EIL) atop a layer of marine stratocumulus. A similar schematic appears in Stevens et al. (1999).

review by Stewart and Essenwanger (1982) and papers by Chylek et al. (1992); Garrett et al. (2002)]. Appropriate single values of κ_λ for the entire longwave spectrum are in the range 100–160 m^2 kg^{-1} (e.g., Larson et al. 2007, for a discussion), with κ_λ decreasing with increasing r_e.

Most stratocumuli with q_l in excess of ~0.2 g kg^{-1} have longwave cloud-top penetration depths (the inverse of the volume absorption coefficient, β^{-1}) of only a few meters to tens of meters. Since values of q_l are often several times greater than this (e.g., Stevens et al. 2003a; Wood 2005a), much of the cloud-top longwave cooling is concentrated in the upper few meters of the cloud and is practically independent of droplet size. However, for clouds with low-cloud droplet concentrations or low liquid water contents such as those commonly found in the Arctic, or in very clean regions of the subtropics, the droplet size must be taken into account when considering the infrared emissivity, which leads to the potential for such clouds to exhibit indirect aerosol effects in the infrared (Garrett et al. 2002).

Stratocumuli typically occur under a dry free troposphere so that the downwelling longwave radiative flux just above the cloud top is several tens to >100 W m^{-2} less than the upwelling flux. By no more than a few tens of meters below the cloud top (e.g., Fig. 18), downwelling and upwelling fluxes are almost equal, and thus the upper few meters of the cloud experience strong cooling. The flux divergence across this layer is typically 50–90 W m^{-2} (e.g., Nicholls and Leighton 1986; Wood 2005a; Caldwell et al. 2005) with the greatest values occurring under a dry free troposphere (Siems et al. 1993).

Besides there being strong longwave cooling *within* the upper reaches of the cloud, there can in some cases be cooling in the layer above the cloud top (Deardorff 1981; Nieuwstadt and Businger 1984; Siems et al. 1993). Although not evident in the example shown in Fig. 18, this cooling has been observed in other cases (e.g., Fig. 3 in Slingo et al. 1982a). The presence of highly emissive cloud below increases the free-tropospheric cooling up to a height that is dependent upon the atmospheric emissivity, but that can be several kilometers above the cloud top (Stevens et al. 2005b; Caldwell and Bretherton 2009). Peak above-cloud cooling rates are found immediately adjacent to the cloud top (vanZanten and Duynkerke 2002), but because this cooling extends over a layer deeper than the turbulent interface itself, it primarily acts to reduce the strength of the buoyancy jump atop the boundary layer and thereby facilitates entrainment (Nieuwstadt and Businger 1984). However, a fraction of the cooling serves to enhance the subsidence rate above the cloud top rather than directly cool the layer, with the partitioning between the two outcomes dependent upon the ability of the atmosphere to sustain large-scale horizontal gradients in temperature (Caldwell and Bretherton 2009). Indeed, there is a lack of definitive research on the factors controlling the fraction of total longwave flux divergence that occurs above the cloud. Both the free-tropospheric moisture and the temperature jump at the inversion are likely to be important (Nieuwstadt and Businger 1984).

Above the base of the cloud there is also a net longwave flux convergence causing heating that can enhance

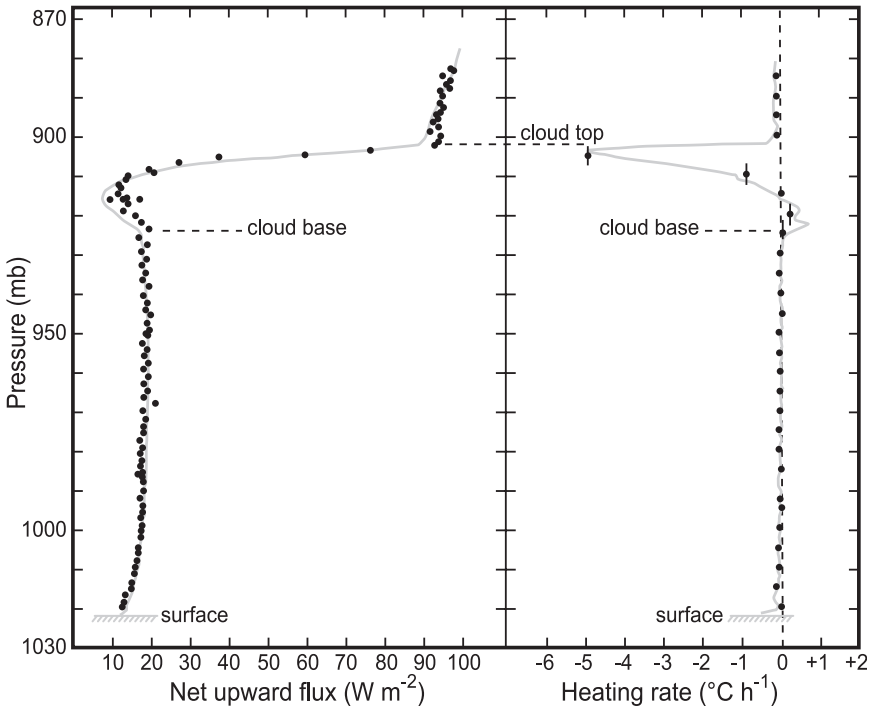

FIG. 18. Profiles of observed (dots) and theoretical (solid lines) (left) net upward infrared flux and (right) associated heating rates for a nocturnal stratocumulus layer. From Slingo et al. (1982a).

the circulation within the cloud layer. Because the liquid water contents near the cloud base tend to be much less than at the cloud top, the flux divergence is spread over a deeper layer (Roach and Slingo 1979) that is typically of order 100 m thick (e.g., Fig. 18). The net flux divergence across the base increases with cloud-base height and can be several watts per meters squared to around 20 W m^{-2} (Slingo et al. 1982a; also Fig. 18). Away from the cloud boundaries and below the cloud, the longwave flux divergence is quite small and does not contribute significantly to the net heating/cooling of the STBL.

2) SOLAR ABSORPTION

Solar absorption is a major component of the STBL energy budget (e.g., Caldwell et al. 2005), and is the primary driver of its diurnal cycle (Turton and Nicholls 1987; Rogers and Koracin 1992; Duynkerke and Hignett 1993, and section 2b above). For cloud droplets formed on nonabsorbing aerosol, practically all of the solar absorption occurs in the near-infrared, primarily for the absorption bands between 1.2 and 4 μm (Ramaswamy and Freidenreich 1991; O'Hirok and Gautier 1998).

The fraction of incident solar radiation absorbed by a particular stratocumulus layer is of the order of a few percent up to around 15% (Stephens 1978a; Slingo and Schrecker 1982; Slingo 1989; Taylor et al. 1996). The fractional absorption decreases with the solar zenith angle (Stephens 1978a) and increases with cloud optical depth τ, up to a limit that depends upon droplet size and solar zenith angle. The fractional absorption can reach 15% or more in clouds with $\tau > 100$ (Stephens 1978b; Twomey and Bohren 1980). For clouds of lower optical depth, the fractional absorption increases approximately logarithmically with cloud liquid water path (Stephens 1978b; Stephens et al. 1984) and has a weak dependence upon droplet effective radius (Stephens 1978a).

Close to half of the absorption of solar radiation in the cloud layer is by water vapor (Stephens 1978a; Twomey and Bohren 1980), which increases with the temperature and thickness of the cloud layer. A doubling of the water vapor path in the cloud layer increases the fractional absorption by roughly 0.01 (Stephens 1978a). Droplets containing nonsoluble absorbing material also absorb in the visible portion of the solar spectrum (Danielson et al. 1969; Chylek et al. 1996), and visible absorption by interstitial aerosols within the cloud layer can also increase solar heating rates (Ackerman and Baker 1977; Haywood and Shine 1997; Ackerman et al. 2000). There is still some uncertainty regarding the contribution of absorbing aerosols in cloud droplets to the overall solar heating rate for the cloud (e.g., Erlick and Schlesinger 2008), but values are unlikely to exceed about 10%–15% even in heavily polluted conditions (Chylek et al. 1996).

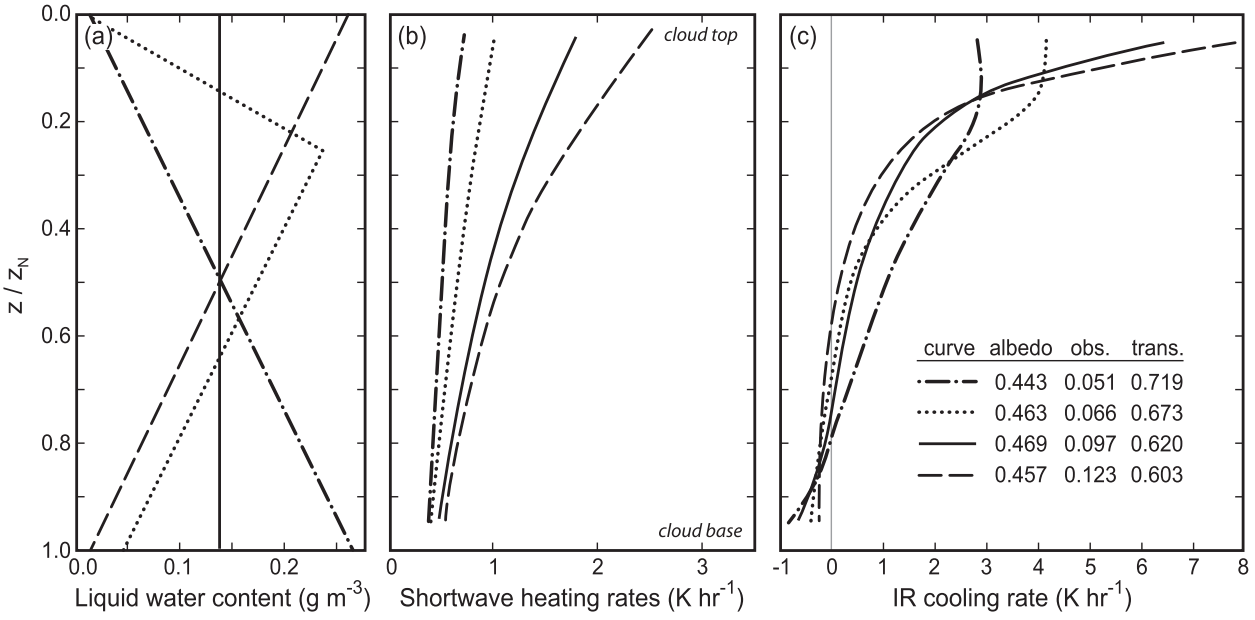

FIG. 19. Comparison of (b) shortwave heating rates and (c) longwave cooling rates in a stratocumulus-like idealized cloud layer (320 m thick, LWP = 44 g m^{-2}) for (a) different vertical profiles of liquid water content. From Stephens (1978a). © American Meteorological Society. Reprinted with permission. The meteorological conditions are described in Stephens et al. (1978), with a downwelling solar irradiance at the top of the cloud of 880 W m^{-2} typical for the subtropics around noon.

For all solar zenith angles and cloud optical depths, solar heating in a cloud layer is largest at the cloud top (Fig. 19), even in clouds in which the liquid water content decreases with height (Stephens 1978a). This is chiefly because the strong scattering of solar radiation at the top of the cloud limits absorption lower down. For most stratocumulus clouds, in which liquid water content increases upward, absorption is greater than it would be for a vertically homogeneous cloud of the same optical thickness (Li et al. 1994), and the shortwave absorption decreases much more slowly downward through the cloud layer (with an effective *e*-folding distance of 100–300 m compared to only a few tens of meters for thermal infrared; cf. Figs. 19b,c) than does the longwave cooling. Even with strong daytime solar insolation the net effect of radiation is, in most cases, to destabilize the stratocumulus layer.

3) SCATTERING OF SOLAR RADIATION

Stratocumulus clouds reflect a markedly greater fraction of the incident solar radiation than they absorb (e.g., Stephens 1978a), hence their large albedo (Stephens et al. 1978). Cloud albedo is governed by the cloud optical thickness τ, the single-scattering albedo ω, the asymmetry parameter g, and the solar zenith angle θ_0 (Liou 1992). In the visible and nonabsorbing parts of the near infrared $\omega = 1$ and $g = 0.82$–0.86 (Liou 1992), so that τ and θ_0 alone determine the cloud albedo (Fig. 20). Because much of the incoming solar irradiance is at wavelengths with negligible absorption (Slingo and Schrecker 1982), conservative scattering approximations can be made to the radiative transfer equation (King and Harshvardhan 1986 has a comparison of approaches), which yields useful analytical expressions that are quite accurate [e.g., albedo $\alpha = \tau/(\tau + 7)$; Seinfeld and Pandis 1997].

Stratocumulus optical thicknesses vary tremendously even for completely overcast stratocumulus fields (e.g., Roach 1961), ranging from less than 1 to more than 20 (Hahn et al. 2001), and locally can be as high as 50 or more (Nakajima et al. 1991; Szczodrak et al. 2001). For a solar zenith angle of 30°, this represents a range of visible albedos from less than 10% to over 70% (Fig. 20).

The concavity of the albedo–optical thickness relationship ($d\alpha/d\tau$ decreases with τ) means that the area-mean albedo of a spatially variable cloud field is lower than for the equivalent homogeneous field with the same mean τ (Cahalan et al. 1994), such that the effective optical thickness is lower than that for a homogeneous cloud. However, for regions of the oceans dominated by marine stratocumulus clouds the correction to τ is generally 10% or less (Rossow et al. 2002).

For stratocumulus, in which most droplets are much larger than the wavelength of solar radiation, cloud optical thickness τ depends upon the vertical integral of the ratio of cloud liquid water content ρq_l to the effective radius r_e:

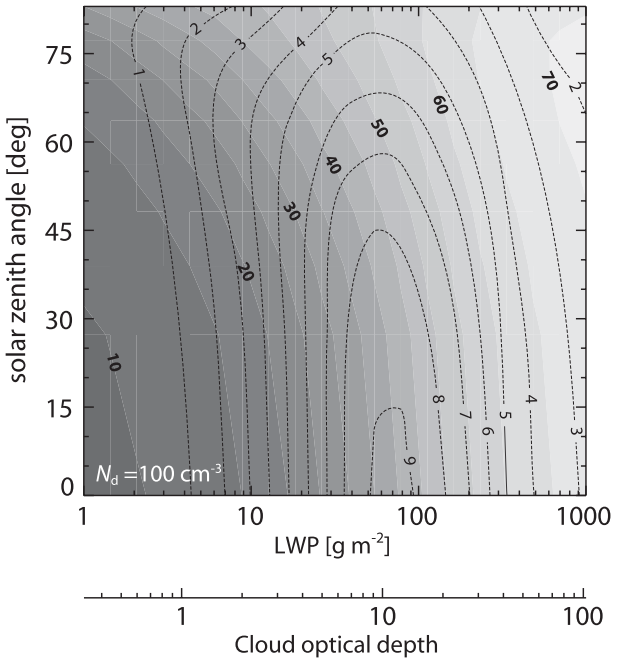

FIG. 20. Broadband solar albedo (at the top of the atmosphere) for an adiabatic plane–parallel liquid water cloud with a cloud droplet concentration of $N_d = 100$ cm^{-3} as a function of the cloud LWP and the solar zenith angle (shaded contours). Dashed lines show the increase in albedo (upon increasing N_d from 100 to 300 cm^{-3}). Calculations use the Fu–Liou two-stream radiative transfer code. The tropical dry thermodynamic profile used is described in Caldwell et al. (2005).

$$\tau = \frac{3}{2\rho_w}\int_0^h \frac{\rho q_l}{r_e}dz, \tag{1}$$

where ρ_w is the density of liquid water, ρ is the air density, q_l is the liquid water mixing ratio, and h is the cloud thickness ($z = 0$ at the cloud base). Because q_l typically increases approximately linearly with height (section 3a), and there is little vertical stratification in cloud droplet concentration (Wood 2005a), r_e increases as $z^{1/3}$ (Brenguier et al. 2000b; Szczodrak et al. 2001; Bennartz 2007), and τ is given by

$$\tau = \frac{9L}{5\rho_w r_e(h)}, \tag{2}$$

where $L = \int_0^h \rho q_l\, dz$ is the liquid water path. Expressed in terms of the droplet number concentration N_d:

$$\tau = A_v \frac{(N_d k)^{1/3} L^{5/6}}{\rho_w^{2/3}\Gamma^{1/6}}, \tag{3}$$

where $A_v = (9/5)(8\pi^2/9)^{1/6} = 2.585$, and k is the ratio of the cubes of the mean volume radius and the effective radius (Martin et al. 1994).

Because N_d is primarily determined by the availability of cloud condensation nuclei (CCN), Eq. (3) neatly expresses the impacts of microphysical variability on the cloud optical thickness. Figure 20 also shows the increase in albedo upon tripling N_d from 100 to 300 cm^{-3} at constant L, in keeping with Twomey's findings (Twomey 1974, 1977) that there is sensitivity of the cloud albedo to changes in cloud droplet concentration. The microphysical *susceptibility* $d\alpha/dN_d$ is largest for $\alpha \approx 50\%$ (Platnick and Twomey 1994). This corresponds to LWP in the range 50–200 g m^{-2} (Fig. 20), making stratocumulus, which have LWP in this range (e.g., Wood 2005a; Zuidema et al. 2005; O'Dell et al. 2008), particularly sensitive to increases in cloud droplet concentration caused by increased anthropogenic aerosol concentrations. Figure 20 also shows heightened microphysical susceptibility for high sun because α depends more strongly upon τ at low solar zenith angle (King and Harshvardhan 1986).

b. Turbulence

The mean state of the STBL is determined by fluxes of energy, water (both vapor and liquid), and, more indirectly by other atmospheric constituents (e.g., aerosols). These fluxes are predominantly turbulent. The amount of energy associated with the turbulent components of the wind field, particularly the vertical component, influences the rate at which free-tropospheric air is entrained into the STBL. An accessible primer on the general properties of turbulent flows is found in Tennekes and Lumley (1972), and useful reviews of STBL turbulent structure are found in Driedonks and Duynkerke (1989) and Moeng et al. (1992).

For clear convective boundary layers similarity theory provides well-characterized scaling relations for TKE and fluxes as a function of the mean state. This is not the case for the STBL (Garratt 1992; Nieuwstadt and Duynkerke 1996) because of the complexity of the diabatic processes that shape it, and its often intermittently coupled nature. Thus, the existence of simple nondimensional scaling relationships for fluxes and variances within the STBL is not guaranteed in general (Nieuwstadt and Duynkerke 1996). Nevertheless, progress has been made toward understanding some of the most important statistical properties of the turbulent vertical motion field, and some approximate scaling relationships and normalizing variables have been found to be useful for relatively well-mixed stratocumulus layers (e.g., Nicholls 1989).

1) TURBULENT FLUXES

Profiles of the vertical turbulent fluxes of energy and moisture are important for determining stratocumulus cloud properties (e.g., Schubert et al. 1979a; Bretherton

and Wyant 1997). An elegant description of these fluxes is termed *mixed layer theory* (Lilly 1968), which describes the vertical structure of the fluxes necessary to maintain a well-mixed layer given the various forcings applied to it. Mixed layer theory can be used to understand many aspects of stratocumulus behavior (e.g., Lilly 1968; Schubert et al. 1979a,b; Nicholls 1984; Bretherton and Wyant 1997; Caldwell et al. 2005; Stevens 2005; Wood 2007).

For a layer to remain well mixed, the vertical energy and moisture fluxes must be linear functions of height. For nonprecipitating mixed layers, the vertical turbulent flux of total water must be linear with height. Since entrainment fluxes of dry air are often comparable to the surface moisture flux, the turbulent moisture flux can either increase or decrease with height. However, precipitation and cloud droplet sedimentation can also contribute to moisture transport (Brost et al. 1982b; Nicholls 1984; Duynkerke et al. 1995; de Roode and Duynkerke 1997; Wood 2005a), especially in thick stratocumulus. In the cloud layer the vertical turbulent flux of liquid water is an important contributor to the total water flux (Nicholls 1984; Duynkerke et al. 1995). Total water flux estimates are challenging but can be made using aircraft measurements (e.g., Nicholls 1989; Stevens et al. 2003b). Difficulties arise because of large horizontal length scales for moisture in convective boundary layers (Lenschow and Stankov 1986), a problem that is particularly acute for the STBL (de Roode et al. 2004).

Under most circumstances, the buoyancy flux[2] is the primary generator of TKE in the STBL (Moeng et al. 1992; Bretherton and Wyant 1997) and nearly always has a maximum in the cloud layer (Nicholls and Leighton 1986; Garratt 1992; Duynkerke et al. 1995), with smaller values in the subcloud layer. Large buoyancy fluxes are caused mainly by radiative cooling and are additionally enhanced by latent heating effects. For mixed layers, there is a sharp increase in the buoyancy flux above the cloud base due to latent heat release (Lilly 1968; Schubert et al. 1979a; Moeng et al. 1992; Bretherton and Wyant 1997). This can be illustrated rather elegantly in "Schubert" circuit diagrams (Schubert et al. 1979a), the most useful of which (Bretherton 1997) are reproduced in Fig. 21. In stratocumulus layers, updrafts are usually warmer, and more positively buoyant, than the cooler downdrafts (Fig. 21), which constitutes the source of buoyant turbulence production. The asymmetry, which is reflected in differences in the cloud base for upward- and downward-moving branches of the circulation, is primarily driven by differences in total water between upward- and downward-moving eddies such that, at a given height in cloud, the upward-moving parcel has a higher liquid water content (Fig. 21a). Thus, the buoyancy flux is strongly related to the vertical flux of liquid water by the eddies (Bretherton and Wyant 1997). At the top of the circuit, radiative cooling makes the rising parcel negatively buoyant and entrainment evaporates some of the liquid water from it making the resulting downdrafts drier than the updrafts (Figs. 21a,b). With small supersaturations ($<1\%$) in the cloud layer, the liquid water flux in the cloud layer is thus primarily governed by the vertical flux of water vapor into the cloud layer (Bretherton and Wyant 1997).

During the daytime (when solar radiation reduces the overall cloud-top cooling), or when cloud-top entrainment warming and drying is sufficiently strong to elevate the LCL for downward-moving parcels, the LCL may be reached in the downward branch with a virtual potential temperature that is warmer than that of the subcloud layer air. In this case, the buoyancy flux is negative just below the stratocumulus cloud base (Nicholls and Leighton 1986). Subzero buoyancy fluxes are a sink of turbulence and lead to layer decoupling (Turton and Nicholls 1987; Bretherton and Wyant 1997; Stevens 2000; Lewellen and Lewellen 2002).

In cumulus-coupled STBLs, most of the convective updrafts in the subcloud layer have insufficient inertia to penetrate the weakly stable layer near cloud base (section 3a). The trajectory circuit diagram in this case consists of two circuits (Figs. 21d–f). The strongest updrafts from the subcloud layer gain positive buoyancy through condensation warming and then rise as cumulus clouds into the stratocumulus aloft. The cumulus updrafts can become quite strong and penetrate into the STBL inversion more efficiently than in the case of updrafts in well-mixed STBLs, which results in locally strong entrainment of free-tropospheric air. The parcel cools by radiative cooling until it begins to subside, but the strong penetrative entrainment dries the parcel strongly so that the LCL for the downdraft that is much higher than that for the updraft. As in the well-mixed STBL the largest buoyancy fluxes are found in the upper part of the STBL (Figs. 21c,f) and minimize near the top of the subcloud layer, but the buoyancy flux profile is more complicated by the presence of the stable layer. Bretherton (1997) provides a more complete discussion of the trajectory circuits.

Vertical momentum transport in the STBL also affects the surface fluxes of moisture and temperature by changing near-surface wind speed (Stevens et al. 2002). There are some observations of the STBL (e.g., Brost et al. 1982b) that are consistent with those expected under near-neutral conditions.

[2] The buoyancy flux is defined as $\overline{w'b'} = (g/\theta_v)\overline{w'\theta_v'}$, where g is the gravitational acceleration, θ_v is the virtual potential temperature, and w' is the vertical velocity fluctuation.

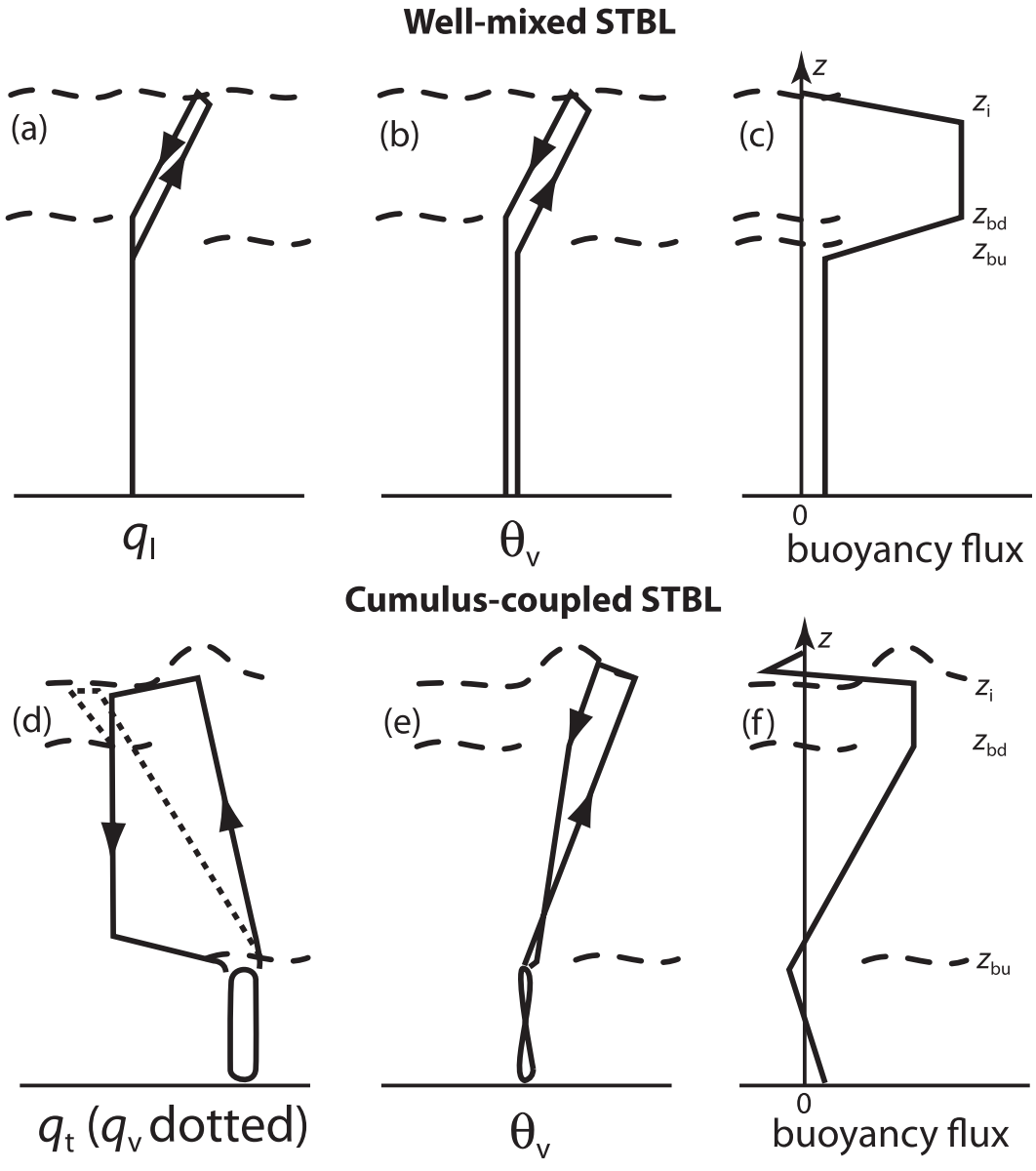

FIG. 21. "Schubert" diagrams indicating (a),(b),(d),(e) air typical air parcel circuits and (c),(f) buoyancy flux profiles through STBLs that are (a)–(c) well mixed and (d)–(f) cumulus coupled. For the well-mixed case, (a) liquid water mixing ratio q_l and (b) virtual potential temperature θ_v circuits are shown, while the cumulus-coupled case shows (d) total water q_t and vapor q_v mixing ratios and (e) θ_v. Wavy dashed lines indicate heights of updraft and downdraft condensation levels z_{bu} and z_{bd}, respectively, and inversion height z_i. Reproduced from Bretherton (1997) with the author's permission.

2) VERTICAL AND HORIZONTAL WIND FLUCTUATIONS

Vertical and horizontal turbulent wind fluctuations are important for transporting energy, moisture, and mass within the STBL. Vertical wind fluctuations near the inversion atop the STBL are responsible for mixing within the EIL, while horizontal wind fluctuations can set up local wind shear near the top of the STBL even when the mean shear is close to zero, thus influencing cloud-top mixing indirectly.

Measurements of the vertical structure of the vertical wind variance $\overline{w'^2}$ (Fig. 22) indicate that both during the day and night the strongest updrafts and downdrafts are found away from the boundaries and particularly in the upper half of the STBL consistent with in-cloud buoyancy production being the primary driver of convection. The eddies are more vigorous during the night; buoyancy

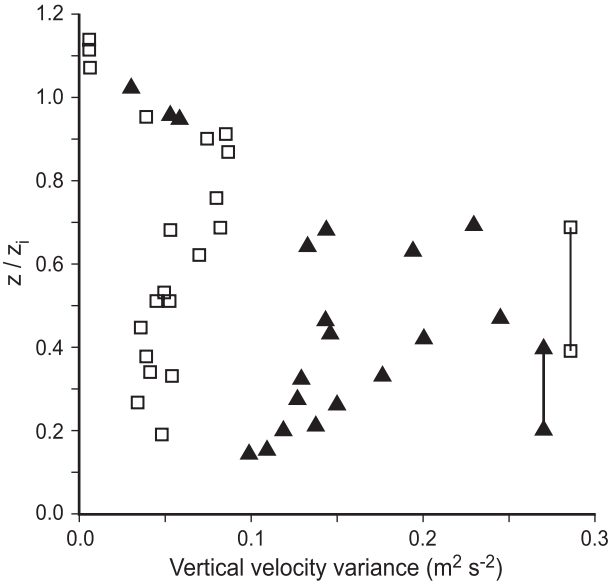

FIG. 22. Variance of the vertical wind against height normalized by the STBL depth around local noon (open squares) and for 2130–2400 (filled triangles). Measurements were made from a tethered balloon at San Nicholas Island in unbroken Californian marine stratocumulus sheet during July 1987. The range of cloud-base height for the two periods is depicted by the vertical lines. Reproduced from Hignett (1991). © American Meteorological Society. Reprinted with permission.

production is greatest at this time because the stabilizing effect of shortwave absorption is absent (Hignett 1991). In well-mixed STBLs, the horizontal size of the convective eddies is of the order of the STBL depth, but downdrafts are smaller and stronger than updrafts, which manifests itself as a negatively skewed vertical wind distribution through most of the cloud layer (Nicholls 1989; Kollias and Albrecht 2000), and below (Hogan et al. 2009). Positive vertical wind skewness can be found in cumulus-coupled STBLs (de Roode and Duynkerke 1996).

For shallow, relatively well-mixed STBLs, and for mixed layers forming part of a more decoupled STBL, the magnitude and vertical profile of $\overline{w'^2}$ scales fairly well with a convective velocity scale w_* defined using the vertical integral over the mixed layer depth h of the buoyancy flux (Deardorff 1980b):

$$w_*^3 = 2.5\int_0^h (g/\theta_v)\overline{w'\theta_v'}\,dz. \quad (4)$$

Observations show that $\overline{w'^2}/w_*^2$ tends to maximize at values of 0.3–0.5 in the upper quarter of the mixed layer (Nicholls and Leighton 1986; Nicholls 1989; Garratt 1992; Nieuwstadt and Duynkerke 1996; de Roode and Duynkerke 1997), decreases sharply toward the cloud top, and more gradually toward the mixed layer base. The magnitude of w_* is controlled by the key buoyancy-influencing processes in the mixed layer, most importantly the radiative cooling/warming at cloud top, latent cooling/warming in convective downdrafts/updrafts, the mixing down of stable entrained air, and precipitation. However, in some cases, particularly in regions with strong horizontal gradients in boundary layer depth, vertical shear in the horizontal winds can also influence $\overline{w'^2}$ (Brost et al. 1982a,b; Nicholls and Leighton 1986; Wang et al. 2008). Values of w_* in the range 0.25–1.25 m s^{-1} are typical in the STBL (e.g., numerous case studies summarized in Nicholls and Leighton 1986; de Roode and Duynkerke 1997; Wood 2005a; Faloona et al. 2005).

The structure of the horizontal wind fluctuations is more complex than the vertical wind fluctuations because the energy-containing horizontal scales of these components are not constrained by the STBL depth (de Roode et al. 2004). Continuity requires that vertical wind damping below the inversion leads to stronger horizontal wind fluctuations (as observed in Nicholls 1989). This allows energy to build up in the horizontal components so that for deeper STBLs these components may become increasingly important in the TKE budget (e.g., de Roode and Duynkerke 1997). Horizontal wind variances do not scale as well with w_* as do the vertical wind variances (Nicholls 1989).

c. *Surface fluxes*

The surface latent heat flux (LHF) provides the main source of moisture in most STBLs. Exceptions include some Arctic STBLs in which free-tropospheric moisture sources are important (Solomon et al. 2011). The surface LHF is determined by the surface relative humidity (RH), the surface temperature, and the wind speed (e.g., Hartmann 1994, chapter 4). The surface RH is dependent upon processes controlling the STBL moisture and temperature budgets, primarily entrainment and also surface precipitation. As such, the surface RH and LHF should be considered internal parameters of the STBL system. The same is true of the surface sensible heat flux (SHF), although in most marine STBLs the SHF is a much weaker source of turbulence compared with longwave cooling. Over land, and in cold-air outbreaks, the surface SHF can rival turbulence production from radiation (Atkinson and Zhang 1996). In well-mixed STBLs, particularly over warm oceans, the surface LHF is an important source of buoyant TKE production (Bretherton and Wyant 1997), and so LHF cannot simply be thought of as important for the moisture budget, but as a key process affecting the internal STBL dynamics, to which we will return in section 6.

d. Entrainment

A major unresolved question in stratocumulus dynamics is how the entrainment rate w_e at the top of the STBL relates to STBL turbulent dynamics (e.g., Driedonks and Duynkerke 1989; Stevens 2002). The extent to which entrainment is controlled by the large eddies (those dominating convection in the MBL) as opposed to small-scale mixing processes and direct nonturbulent radiative/evaporative cooling of the EIL is not fully understood. The nonturbulent processes depend sensitively upon the details of very small-scale cloud and thermodynamic structure near the inversion (Lewellen and Lewellen 1998). So to what extent do physical models of entrainment need to account for the detailed small-scale structure of the cloud–EIL interface?

Broadly speaking, there are two classes of formulations for w_e: (i) *flux-partitioning closures* assume that w_e adjusts to maintain a constant ratio of some measure of TKE-destroying (negative) buoyancy fluxes to the TKE-producing (positive) buoyancy fluxes (e.g., vanZanten et al. 1999, for a review); (ii) w_* *closures* assume that w_e scales with the vertical integral of the buoyancy flux irrespective of how the TKE is produced (Deardorff 1976).

Flux-partitioning closures are very effective for the clear convective boundary layer but observations of the STBL violate this class of closure's basic assumptions. Specifically, shallow STBLs are observed for which the buoyancy flux is positive throughout the subcloud layer. Thus, most modern entrainment formulations are of the w_* closure form, and can be written, following Stevens (2002), as

$$w_e = A\left(\frac{W}{\Delta b}\right) + w_{\mathrm{dir}}, \tag{5}$$

where W is an appropriate measure of the rate of turbulent production in the STBL, Δb is a measure of the buoyancy jump atop the STBL (which in some closures includes diabatic effects), and A is a state-dependent efficiency. The first term on the rhs of Eq. (5) represents *turbulent* entrainment, while the second term w_{dir} is the direct, nonturbulent deepening of the STBL (Deardorff 1980a). As discussed at length in Stevens (2002), the difficulty has been to determine how W, A, w_{dir}, and Δb depend upon the STBL mean state and turbulence. The following are all factors that hinder progress:

1) Making sufficiently accurate measurements of the entrainment rate in STBLs to cleanly distinguish between different entrainment formulations is challenging (e.g., Faloona et al. 2005; Gerber et al. 2005).
2) The strong, sharp inversion atop the cloud makes it difficult to measure (and resolve in numerical models) the radiative cooling profile, thermodynamic structure, and dynamics of the entrainment interfacial layer sufficiently well to separate the turbulent from the nonturbulent entrainment (e.g., Kawa and Pearson 1989; Lewellen and Lewellen 1998).
3) Turbulence-generating processes such as radiative and evaporative cooling occur close to the interface itself, unlike the situation in the dry convective boundary layer where the inversion region is solely a sink of TKE.

The question of how to determine the appropriate rate of turbulent production W is still open. A number of entrainment formulations set W [Eq. (5)] as proportional to the mean rate of TKE production by buoyancy, which is the mean buoyancy flux over the mixed layer [Eq. (4)], $W = w_*^3/h$. Doing this, and setting $w_{\mathrm{dir}} = 0$, leads to an expression for the dimensionless entrainment rate w_e/w_* that is inversely proportional to a Richardson number (Ri) representing the ratio of the stability (potential energy) to the TKE in the STBL:

$$\frac{w_e}{w_*} = A\left(\frac{w_*^2}{h\Delta b}\right) = \frac{E}{\mathrm{Ri}}. \tag{6}$$

Formulating entrainment in this way works well for the dry surface-driven convective boundary layer (Driedonks 1982), for which an efficiency $A \approx 0.2$ is appropriate. Efficiencies for the STBL are found to be much greater than 0.2, with values greater than unity implied from observations (Nicholls and Turton 1986; de Roode and Duynkerke 1997; Faloona et al. 2005; Caldwell et al. 2005). However, there is a large spread in implied efficiencies derived from different observational cases (e.g., Caldwell et al. 2005), which has been used to argue that the efficiency is dependent on some other aspect of the STBL state.

Buoyancy fluctuations near the inversion driven by evaporative cooling enhance the entrainment efficiency (Lilly 1968; Deardorff 1980a; Randall 1980; Nicholls and Turton 1986). The process of mixing dry free-tropospheric air into the cloud can in some cases create mixtures that are negatively buoyant with respect to the unmixed cloudy air (e.g., Nicholls and Turton 1986; Stevens 2002, see illustrations). This occurs when the negative buoyancy perturbation from evaporative cooling of liquid water in the mixture exceeds the positive buoyancy perturbation from mixing in the lower density air from aloft. The term *buoyancy reversal* is used to describe the case where negatively buoyant mixtures are possible. Negatively buoyant mixtures can enhance mixing near

cloud top and in some cases through the entire depth of the mixed layer. It was originally thought that buoyancy reversal would lead to rapid runaway entrainment (Kraus 1963; Lilly 1968; Deardorff 1980a; Randall 1980) in a process known as cloud-top entrainment instability (CTEI), but conditions under which destructive CTEI occurs are now known to be less common than originally thought. A more complete discussion of CTEI is presented in section 6e below. Nevertheless, buoyancy reversal appears to be important for driving small-scale turbulent enhancement near cloud top, which enhances entrainment, and this has been used to propose new or modified w_* entrainment closures [Eq. (5)]. These include modifications to the buoyancy jump term Δb (e.g., Nicholls and Turton 1986) and the turbulence production term W (Lock 1998) rather than the entrainment efficiency term A per se.

Other factors affecting cloud-top entrainment in stratocumulus are the specifics of whether the TKE is primarily generated nearer the cloud top or the surface (Lewellen and Lewellen 1998; Lilly 2002; Lilly and Stevens 2008). Stronger weighting of buoyancy flux near the cloud top is appropriate for a weak turbulent diffusion to dissipation ratio (Lilly and Stevens 2008). This is consistent with arguments made in earlier work (Stage and Businger 1981; Lewellen and Lewellen 1998) that it is the characteristics of the energy-containing (large) eddies when they impinge upon the inversion that ultimately determine their ability to entrain air from above.

The spread in A also partly reflects uncertainties in making reliable observational entrainment estimates (Faloona et al. 2005; Gerber et al. 2005). There is also evidence from large eddy models suggesting that it is unrealistic to assume $w_{\mathrm{dir}} = 0$. In fact, direct radiative cooling of the inversion may constitute a large fraction (perhaps as much as 30%–60%) of the total entrainment rate (Lewellen and Lewellen 1998; Lock 1998), although observationally constrained estimates of the importance of above-cloud radiative cooling differ (Nicholls and Leighton 1986; vanZanten and Duynkerke 2002) primarily due to uncertainty over what cooling-layer thickness is relevant. In reality, it is likely that a number of different processes increase the entrainment efficiency of the STBL compared with that for the dry CBL (Lewellen and Lewellen 1998). Another connected question is whether it is appropriate to include the nonturbulent entrainment rate in the efficiency term A.

e. Precipitation

Stratocumulus clouds, especially those in marine air masses, frequently produce light precipitation, mostly in the form of drizzle (Ohtake 1963; Nicholls and Leighton 1986; Petty 1995; Austin et al. 1995; Pawlowska and Brenguier 2003; Wood 2005a; vanZanten et al. 2005; Leon et al. 2008). Drizzle (using a definition of low clouds with radar reflectivity exceeding -17 dBZ, equivalent to precipitation rates of $\sim$0.2 mm day^{-1}) is found 20%–40% of the time in the regions of persistent marine stratocumulus (Leon et al. 2008; Wood et al. 2009a).

Drizzle begins to exert an influence on STBL dynamics when rates reach a few tenths of a millimeter per day. A surface precipitation rate of 1 mm day^{-1} equates to a warming of the drizzle-producing cloud layer of 29 W m^{-2}, a magnitude comparable to the radiative driving. Precipitation rates in stratocumulus peak close to the cloud base and decrease toward the top of the cloud (Wood 2005a; vanZanten et al. 2005), and so drizzle is often characterized by its rate at cloud base R_{cb}. Values of R_{cb} can be usefully classified as light ($R_{\mathrm{cb}} <$ 0.5 mm day^{-1}), moderate ($0.5 < R_{\mathrm{cb}} < 2$ mm day^{-1}), and heavy ($R_{\mathrm{cb}} > 2$ mm day^{-1}).

Drizzle effects on the STBL are complex. First, drizzle warms the cloud layer and thereby stabilizes the STBL, which reduces turbulent mixing and induces stratification. Second, drizzle evaporates readily below cloud base owing to the small size of drizzle drops. Mean volume radii $r_{v,D}$ of drizzle drops are typically in the range 30–100 μm at cloud base (Wood 2005a; Wood et al. 2011a). The evaporation scale height (e-folding distance below cloud base over which precipitation rate decreases due to evaporation) increases rapidly with $r_{v,D}$, from only 100 m for $r_{v,D} = 30$ μm to 400 m for $r_{v,D} = 50$ μm, to over 2 km for $r_{v,D} = 100$ μm (assuming a well-mixed subcloud layer). Thus, the profile of drizzle evaporative cooling is sensitive to the microphysics of drizzle formation, which is discussed in section 5. Interactions between drizzle and STBL dynamics are discussed in section 6 below.

Liquid precipitation has also been observed to fall from supercooled stratocumulus even with tops as cold as -10°C (Huffman and Norman 1988), or even colder (Kajikawa et al. 2000), but snow is also common for stratocumulus with tops colder than approximately -5°C (Henrion et al. 1978; McFarquhar et al. 2007). Drizzle drops are frequently present in Arctic stratocumulus clouds (Hobbs and Rangno 1998; Lawson et al. 2001), although much of the precipitation falling from the cloud base appears to be in the form of ice (McFarquhar et al. 2007). There is evidence that glaciation in supercooled liquid clouds tends to occur simultaneously with the production of drizzle drops (Rangno and Hobbs 1991). Artificial seeding of supercooled stratocumulus can create precipitation (Locatelli et al. 1983). Modeling studies show that depletion of ice nuclei is necessary for supercooled drizzle to form (Rasmussen et al. 2002). However, the process of ice formation in supercooled

stratocumulus is still poorly understood (Cantrell and Heymsfield 2005; Fridlind et al. 2007) and is not considered further in this review.

Over both land and ocean the frequency of occurrence of drizzle maximizes in the early morning hours (Kraus 1963; Dai 2001; Bretherton et al. 2004; Stevens et al. 2005a; Sears-Collins et al. 2006; Leon et al. 2008; Serpetzoglou et al. 2008) when cloud thickness and LWP tend to be at their greatest (section 2b above). For decoupled STBLs, cumulus rising into stratocumulus appear to produce heavier drizzle during the late afternoon (Miller et al. 1998). This may help to explain why there are *daytime* maxima in the precipitation observed by the Tropical Rainfall Measuring Mission (TRMM) in regions of persistent tropical and subtropical marine stratocumulus, particularly downwind of the maxima in cloud cover (Yang and Smith 2006), since TRMM can detect only the heaviest drizzle events (radar reflectivity >17 dBZ).

5. Microphysics

The microphysical properties of stratocumuli help determine their albedo (section 4a above) and their ability to form precipitation (e.g., see Wood 2005a for a discussion). Microphysical processes in stratocumulus are therefore critical for understanding the aerosol indirect effects on climate, and so we devote this section to their discussion. Of all microphysical parameters, the mean cloud droplet size is most directly influential. The droplet radius influences the cloud optical thickness [Eq. (2)]. Because both fall speed and collection efficiency depends strongly upon droplet size (e.g., Long 1974; Liu and Daum 2004; Wood 2006), it also impacts precipitation. In addition, latent heating/cooling rates also depend somewhat upon the mean droplet size (e.g., Pruppacher and Klett 1997), which hints at possible links between cloud droplet size and cloud dynamics (Arnason and Greenfield 1972), even without consideration of precipitation.

For a given cloud liquid water content the droplet radius is determined primarily by the cloud droplet concentration N_d, which is the key variable linking aerosol and cloud microphysical properties. In this section we focus primarily upon the factors controlling N_d, and upon the microphysical controls on precipitation formation. Section 6b assesses interactions between microphysical and macrophysical processes.

a. *Cloud droplet concentration and controlling factors*

1) GEOGRAPHICAL DISTRIBUTION

Cloud droplet concentrations N_d in stratocumulus range from fewer than 10 cm^{-3} in extremely aerosol-rare conditions (mostly over the oceans) to over 500 cm^{-3} in air masses with high aerosol concentrations (e.g., Martin et al. 1994). Global estimates of N_d (Fig. 23) reveal remarkably rich spatial variability in N_d, with the single most striking feature being one of great ocean–continent contrasts. This picture is corroborated by in situ studies, collations of which are provided in Martin et al. (1994), Miles et al. (2000), Yum and Hudson (2002), vanZanten et al. (2005), Wood (2005a), and Fountoukis et al. (2007).

Over the oceans high concentrations ($N_d > 200$ cm^{-3}) are typically found downwind of continental regions (e.g., off the Southern California coast, off the coast of Chile, off the eastern seaboard of the United States, the East China Sea and the Sea of Japan, and in the North Sea). Low values are found over the remote oceans, especially those in the subtropics and tropics, where concentrations of 50 cm^{-3} or less are common. There is some in situ observational support for modest increases in N_d toward the Southern Ocean and Antarctica (Yum and Hudson 2004), which has been attributed to the highly productive oceans there (e.g., Boers et al. 1994). However, the values of 300 cm^{-3} or more close to the Antarctic peninsula seen in Fig. 23 probably reflect problems with the Moderate Resolution Imaging Spectroradiometer (MODIS) retrievals at high solar zenith angle and/or over ice surfaces, and the few in situ measurements of aerosols and CCN do not support such high values of N_d (O'Dowd et al. 1997; Koponen et al. 2003). Continental regions of the Northern Hemisphere show the greatest concentrations (Fig. 23), with mean values of N_d exceeding 200 cm^{-3} over and downwind of heavily industrialized areas, in accordance with in situ measurements in these regions. But there are also continental regions (e.g., northern Amazonia and central Africa) with low concentrations.

2) FACTORS CONTROLLING CLOUD DROPLET CONCENTRATION

The cloud droplet concentration in stratocumulus is limited by the availability of CCN (Martin et al. 1994), but is also sensitive to the updraft strength. Based upon a well-developed understanding of the condensational growth process, Twomey (1959), reproduced in Pruppacher and Klett (1997), derived an approximate analytical formulation for the number of droplets activated in an adiabatic parcel as a function of the CCN spectrum and the updraft speed. Extensions to Twomey's formulation have been derived that account for more realistic variability in aerosol size distributions, kinetic effects, and more accurate treatments of the condensation rate integral (Cohard et al. 1998; Abdul-Razzak et al. 1998; Abdul-Razzak and Ghan 2000; Nenes and Seinfeld 2003),

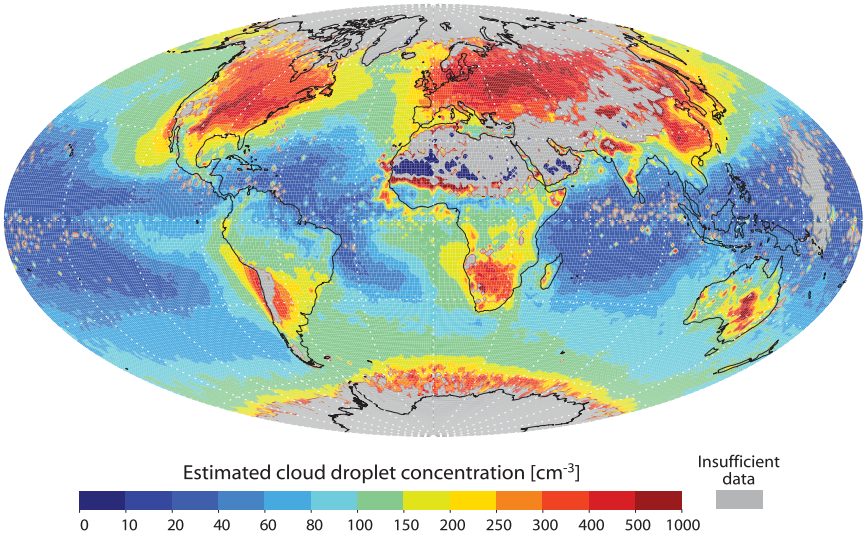

FIG. 23. Global mean cloud droplet concentration N_d for horizontally extensive liquid clouds estimated using visible/near-infrared retrievals of cloud-top effective radius and optical thickness (King et al. 1997) from the MODIS. Four years (2001–04) of level-3 daily aggregated MODIS data at $1° \times 1°$ resolution are used to create the plot. Data are screened to include only liquid clouds (cloud-top temperature warmer than 270 K) and only those days for which at least 80% of the $1° \times 1°$ available pixels in each box are cloudy. Those regions for which fewer than 10 days from the possible 1461 days satisfy the selection criteria are colored gray. Droplet concentration is estimated from the MODIS retrievals using the method described in Bennartz (2007) assuming an adiabatic cloud layer.

and this general approach forms the basis for aerosol activation parameterizations used in large-scale models (Khain et al. 2000; Cohard and Pinty 2000). A recent summary of progress and outstanding questions in this area can be found in McFiggans et al. (2006).

Both theoretical treatments and observational attempts to constrain the droplet activation process (Snider et al. 2003; Fountoukis et al. 2007) demonstrate the importance of the aerosol size and the vertical wind speed w as primary variables determining the fraction of aerosols that activate, f_{act}. Aerosols composed of soluble salts activate at a critical supersaturation $S_* \propto r_{dry}^{-3/2}$ (Junge and McLaren 1971; Pruppacher and Klett 1997), where r_{dry} is the dry radius of the salt particle. Observations of atmospheric aerosols generally support such a relationship (McFiggans et al. 2006; Dusek et al. 2006), although some deviations are found, mostly because of incomplete aerosol solubility (Hudson 2007; Conant et al. 2004).

(i) Dependence of N_d upon vertical wind speed

For a given aerosol population, stronger ascent raises the peak supersaturation and therefore reduces the minimum size of CCN activated, resulting in a higher f_{act} (Twomey 1959). The sensitivity to w weakens for high values of f_{act} (Abdul-Razzak et al. 1998; McFiggans et al. 2006), which most typically occurs in clean conditions (Glantz et al. 2003; Snider et al. 2003). Variations in w are unlikely to explain much of the climatological variability in N_d (Fig. 23) because the typical vertical wind speed scales as only the 1/3 power of the buoyancy flux [Eq. (4)].

(ii) Dependence of N_d upon aerosol properties

With a monomodal aerosol distribution, for a given w and aerosol concentration, f_{act} increases with the mean radius of the aerosols (Abdul-Razzak et al. 1998; McFiggans et al. 2006). This is expected despite lower peak supersaturations for larger and more rapidly supersaturation-depleting particles. The sensitivity to mean radius is expected to be greatest at low w (e.g., Snider et al. 2003) characteristic of stratocumulus, but observations to support this appear to be lacking, presumably for want of sufficient data to control for both aerosol concentration and w.

For $w < 1$ m s^{-1} that is typical of most stratocumulus uprafts (e.g., Nicholls 1989), f_{act} is not strongly dependent upon the aerosol concentration unless the concentration is very high (~300 cm^{-3} or higher), or if the mean aerosol radius is very small. Thus, in clean conditions the number of activated droplets in stratocumuli approaches the accumulation mode aerosol concentration N_a, and observations generally support this (Martin et al. 1994; Leaitch et al. 1996; Gultepe and Isaac 2004; Twohy et al. 2005; Lu et al. 2007). As N_a increases beyond ~200 cm^{-3},

N_d increases sublinearly with N_a, but observations still show a good case-to-case correlation between N_a and N_d (Martin et al. 1994). The accumulation mode aerosol concentration is therefore the primary determinant of N_d in stratocumulus. Within a particular stratocumulus cloud system where N_a does not strongly vary, there is evidence that variability in N_d is primarily controlled by variability in updraft speed (e.g., Lu et al. 2007).

Increasing the breadth of the aerosol size distribution, either through broadening of a single mode (Abdul-Razzak et al. 1998), or the introduction of a coarse aerosol mode (Ghan et al. 1998; O'Dowd et al. 1999b), also leads to a reduced f_{act} due to increased competition for vapor from larger particles. When broadening is related to sea-salt particles as is the case at wind speeds over the ocean in excess of ~7 m s^{-1} (O'Dowd et al. 1999a), the reduction tends to be greatest at high wind speed and high N_a and is estimated to reduce the total N_d by ~20% for surface wind speeds of 15 m s^{-1} (Ghan et al. 1998).

Under most circumstances in which stratocumulus clouds form, chemical effects have a more limited impact upon N_d than do N_a, the aerosol size, and w (Dusek et al. 2006; Feingold 2003), but there can be situations in which reduced solubility (Fountoukis et al. 2007; Hudson 2007), surface-tension changes (Facchini et al. 1999; Nenes et al. 2002), reductions in the mass accommodation coefficient due to film-forming compounds (Feingold and Chuang 2002), and the presence of additional condensible vapors (Kulmala et al. 1993) may have important impacts upon N_d, especially in highly polluted conditions (Nenes et al. 2002). An excellent review of these effects is provided in McFiggans et al. (2006).

b. *Microphysics of precipitation formation*

The initial formation of drizzle requires coalescence of cloud droplets because growth by condensation to sizes larger than ~20 μm takes too long to explain observed precipitation growth in warm clouds (Jonas 1996). The initial formation of drizzle begins with small embryonic drizzle drops produced by the coalescence of droplets grown by condensation. Coalescence growth of such drops is hindered for two reasons: (i) collisions have a low efficiency (e.g., Hall 1980; Pruppacher and Klett 1997) and (ii) droplet size distributions (DSDs) become narrower with time under condensational growth conditions because the deposition process is surface area limited (Howell 1949; Mordy 1959).

Collision efficiencies $E(R, r)$ between small ($R, r <$ 30 μm) water drops of radii R and r falling in still air are well known (e.g., Pinsky et al. 2001). Recent measurements (Vohl et al. 2007) have filled in important gaps missed in earlier laboratory studies and generally confirm earlier theoretical treatments. Current uncertainties in collision efficiencies are those stemming from the effects of microscale turbulence (Jonas 1996; Vaillancourt and Yau 2000; Pinsky and Khain 1997; Xue et al. 2008b; Seifert et al. 2010). Recent attempts to use theory and direct numerical simulation to quantify the effects of small-scale turbulence suggest that turbulent dissipation rates ϵ required for droplet inertial effects to cause 10%–20% increases in the rapidity of precipitation initiation are of the order 10–100 cm^2 s^{-1} (Xue et al. 2008b). Although there are certainly local regions within some stratocumulus clouds in which ϵ can reach these values (Siebert et al. 2006b), we should note that 10%–20% increases in the rapidity of precipitation formation can also be achieved with relatively modest increases in the liquid water content in typical stratocumuli (Table 5 in Xue et al. 2008b) or by small increases in the mean radius of the droplets (e.g., Gerber 1996). Thus, while small-scale turbulence may help initiate precipitation in stratocumulus, its effects are likely to be quite modest and difficult to isolate from those related to cloud spatiotemporal variability.

1) AUTOCONVERSION

The gravitational collection kernel $K(R, r)$ is the probability that a drop of radius R will collect another with radius r in a unit time if both drop sizes exist in unit concentration. This forms the heart of the stochastic collection equation (SCE) from which we can express the *autoconversion rate* A_c, the rate at which mass crosses a particular radius threshold through coalescence between droplets smaller than the threshold (Beheng and Doms 1986; Wood and Blossey 2005).

As demonstrated by Long (1974), $K(R, r)$ is well represented by the square of the collector drop mass for $R < 50$ μm [i.e., $K(R, r) \propto R^6$], and this can be used to provide an analytical approximation for A_c. Following Liu and Daum (2004), if one allows all coalescence events between cloud droplets to contribute to A_c, then the autoconversion rate is proportional to the product of the cloud liquid water content L and the sixth moment of the cloud DSD. Thus, a strong dependence of the autoconversion rate upon the droplet size is clearly evident.

In stratocumulus, the DSD moments are generally well correlated with one another (e.g., Martin et al. 1994), so that $A_c \propto L^3/N_d$. Despite overestimating the true A_c by as much as an order of magnitude in very weakly precipitating clouds (e.g., Wood 2005a; Wood and Blossey 2005), the approximate dependencies of A_c on L and N_d are consistent with observational data (see Fig. 24a and Wood 2005b) and large eddy simulations with explicit microphysics (Khairoutdinov and Kogan 2000). Given that the greatest values of L usually occur toward the top of stratocumulus layers (section 3a), autoconversion rates tend to maximize near cloud top (Fig. 24).

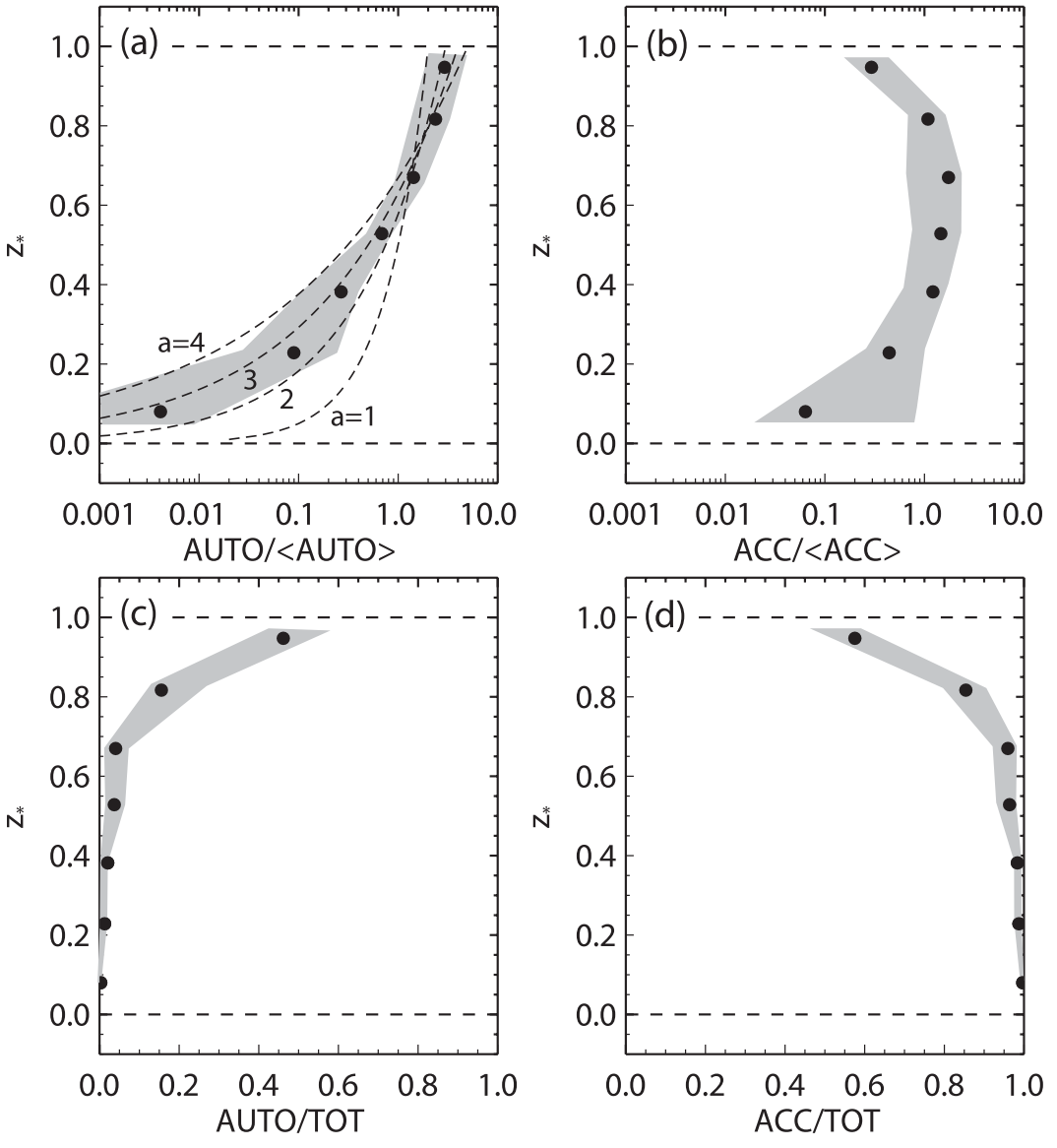

FIG. 24. Composite profiles from 12 cases of weakly to moderately drizzling stratocumulus of (a) autoconversion and (b) accretion rate normalized with the case mean in each case. The normalized height z_* is 0 at the cloud base and 1 at the cloud top. The process rates were derived by applying the SCE to observed drop size distributions. The fraction of total drizzle liquid water content production rate (autoconversion + accretion) contributed by (c) autoconversion and (d) accretion. In (a)–(d) solid circles are median values for each height bin; gray area encompass 25th and 75th percentiles. The dashed curves in (a) show the autoconversion rate expected for a cloud with a linear increase in cloud liquid water content with height and where autoconversion depends upon liquid water content to the power a, with $a = 1, 2, 3, 4$. From Wood (2005b). © American Meteorological Society. Reprinted with permission.

The approximate inverse dependence of A_c on cloud droplet concentration N_d is a pathway through which aerosols can influence precipitation. This dependency is poorly represented, or is not represented at all, in some autoconversion expressions used widely in models (e.g., Kessler 1969; Tripoli and Cotton 1980). A summary of existing parameterizations for A_d is provided in Liu and Daum (2004), and a comparison with observationally derived rates in stratocumulus can be found in (Wood 2005b).

2) ACCRETION

Much of the precipitation liquid water content L_D in drizzling stratocumulus is ultimately produced by

the accretion (collection) of cloud droplets by falling drizzle drops rather than by autoconversion (Fig. 24). Even near cloud top, where autoconversion is maximal, accretion tends to contribute around 50% to the mass transfer from cloud to precipitation. Maximum production of L_D by accretion occurs in the mid- to upper levels of the cloud (Wood 2005b).

Differences between the various bulk formulations in the literature for the mass accretion rate K_c are much smaller than those for the autoconversion rate (Wood 2005b), primarily because the collision efficiency does not vary strongly for collector drops with radii greater than 50–100 μm and cloud droplets larger than 5 μm. Because of this, and because the terminal velocity of drops with $r > 40$ μm depends linearly upon r (Pruppacher and Klett 1997), for most bulk formulations, K_c approximately scales with the product of the cloud and rainwater mass (Kessler 1969; Tripoli and Cotton 1980; Beheng 1994; Khairoutdinov and Kogan 2000).

3) MICROPHYSICAL IMPACTS ON PRECIPITATION RATE

Recent field studies have shone new light on the importance of cloud droplet concentration in driving variability in precipitation in stratocumulus. Bretherton et al. (2004) shows observations from the southeast Pacific stratocumulus region suggesting that drizzle rates in stratocumulus are reduced in periods when N_d increases. A survey of in situ observations in the literature (Wood 2005a) indicates that precipitation rates at cloud base decrease as N_d increases, and other recent studies in marine stratocumulus are consistent with this (Lu et al. 2007), as are observations from ship tracks embedded in these clouds (Ferek et al. 2000; Lu et al. 2007). Recent spaceborne radar measurements are also consistent with drizzle suppression with increasing N_d (for fixed LWP) in marine stratocumulus regions (Leon et al. 2008). Large eddy simulations of stratocumulus with explicit representation of microphysics show similar suppression of precipitation as N_d is increased (Ackerman et al. 1995; Jiang et al. 2002).

Several recent observational studies of marine stratocumulus have found that the precipitation rate at cloud base R_{cb} decreases with N_d, but increases strongly with the cloud thickness h (Pawlowska and Brenguier 2003; vanZanten et al. 2005), or liquid water path (Comstock et al. 2004; Kubar et al. 2009; Wood et al. 2009b). Some of these results are summarized in Fig. 25 taken from Brenguier and Wood (2009). There remain discrepancies between the observationally derived scalings, which are likely attributable in part to differences

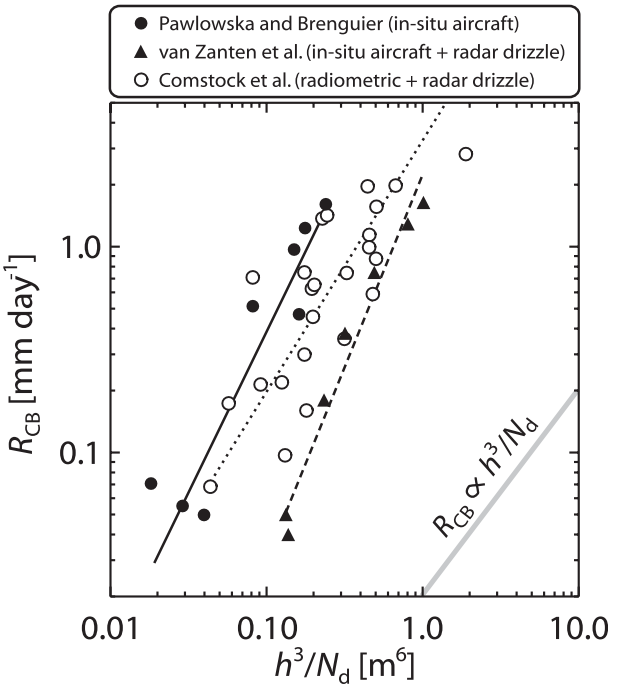

FIG. 25. Cloud-base precipitation rates R_{cb} from observational case studies in subtropical marine stratocumulus, plotted against the ratio of the cube of the cloud thickness h to the cloud droplet concentration N_d. The lines represent linear least-distance regressions to the case studies for each field campaign. From Brenguier and Wood (2009).

in the strategies used to determine the R_{cb}, h, and N_d (e.g., Geoffroy et al. 2008). However, other factors such as turbulence (e.g., Nicholls 1987; Baker 1993; Austin et al. 1995) also influence precipitation rate. Furthermore, recent observational and modeling results suggest that the sensitivity of precipitation rate to N_d [termed the *precipitation susceptibility* in recent papers by Feingold and Siebert (2009) and Sorooshian et al. (2009)] varies with LWP, so that it is unlikely that a simple scaling of R_{cb} with N_d (and cloud thickness or LWP) will be sufficient. There is still considerable discrepancy between different modeling and observational approaches to estimating the precipitation susceptibility, with large eddy simulation, parcel model results, and some observational studies (Feingold and Siebert 2009; Sorooshian et al. 2009; Jiang et al. 2010) suggesting that susceptibility increases with LWP up to some threshold LWP value ($\sim$1000 g m^{-2}), but with other observational studies (L'Ecuyer et al. 2009) and simple steady-state bulk modeling (Wood et al. 2009b), suggesting that the susceptibility decreases monotonically with LWP. Further work is required to untangle these differences, which are likely to be particularly important given that climate models indicate such strong second indirect effects (Lohmann and Feichter 2005; Isaksen et al. 2009).

6. Interactions between physical processes

Stratocumulus is fundamentally a convective cloud system, and as such, its maintenance is critically dependent upon the generation of convective instability by radiative cooling (section 4a) at the top of the cloud. The release of this instability drives turbulent convective overturning (section 4b), which helps mix the STBL and sets its temperature and humidity profiles, causes cloud-top entrainment (section 4d), and therefore controls surface fluxes (section 4c). These in turn determine cloud thickness, its liquid water content, the tendency of the STBL to decouple in some cases, and the ability of the cloud to precipitate, all of which modify the turbulent structure and dynamics.

The great variety of morphological forms and dynamical structures that stratocumulus clouds adopt ultimately results from the wide range of possibilities for interplay between the different physical processes discussed in sections 4 and 5. Maintenance of stratocumulus is achieved by strong internal regulation of interacting processes. The STBL responses to the different processes are often complicated by the wide range of time scales over which different processes affect STBL moisture and temperature budgets. For example, the development of cloud-top height and mesoscale structure in stratocumulus can take many hours (Shao and Randall 1996; de Roode et al. 2004; Bretherton et al. 2010b), while changes in cloud-base height tend to occur on time scales of only a few hours (Schubert et al. 1979b). Interplay between processes is also critically modulated by time-dependent large-scale meteorology. This section begins with a discussion of how processes interact to maintain stratocumulus clouds. We follow this by a discussion of microphysical–macrophysical interactions, interactions between the STBL and large-scale meteorology, stratocumulus formation processes, and finally discuss how processes interact to dissipate or break up stratocumulus.

a. Maintenance and regulating feedbacks

Turbulent mixing within STBLs is frequently sufficient to maintain a well-mixed state (e.g., Nicholls and Leighton 1986; Stevens et al. 2003a; Wood 2005a; Caldwell et al. 2005). For well-mixed layers the existence of a saturated sublayer at the top of the PBL requires that the inversion base height z_i is higher than the surface-based LCL. Processes that moisten and/or cool the mixed layer will lower the LCL, and, assuming that z_i does not change, this will thicken the cloud (Randall 1984). Large-scale subsidence and entrainment lead to z_i changes, and entrainment also leads to changes in the LCL (Randall 1984; Wood 2007). Thus, for a mixed layer, both thermodynamic and dynamic processes are responsible for the maintenance of saturation.

Approximately 1 K of PBL cooling, or 0.2–0.6 g kg^{-1} of moistening, is required to lower the LCL by 100 m (e.g., Wood 2007, see his appendix). From this perspective, given typical stratocumulus cloud thicknesses of a few hundred meters, it would appear that the maintenance of stratocumulus clouds is sensitively dependent upon small changes in the surface or entrainment fluxes, or in the radiative cooling. And yet, in many regions the persistence of stratocumulus sheets is remarkable. This persistence is due to strong feedbacks that help to regulate cloud thickness. Figure 26 provides a conceptual diagram detailing the important internal feedbacks that influence the STBL.

Stratocumuli can also persist in decoupled STBLs, where the coupling of the stratocumulus layer to the surface is intermittent and localized (Betts et al. 1995; Albrecht et al. 1995b), and is achieved by cumulus convection with roots in the subcloud layer that loft and then vent moisture into the stratocumulus deck above (Martin et al. 1995; Miller and Albrecht 1995; Wang and Lenschow 1995).

A major regulating feedback that helps to maintain stratocumulus clouds and likely explains why their thickness variability is quite limited (Fig. 5) has been termed the cloud–radiation–turbulent–entrainment feedback (Zhu et al. 2005), and this is depicted by thick arrows in Fig. 26. Under most circumstances, especially for relatively shallow STBLs under a dry free troposphere, increased entrainment (section 4d) thins stratocumulus by incorporating warm, dry air that lifts the LCL faster than it lifts the STBL top (Randall 1984). The cloud-top entrainment rate is strongly enhanced by evaporative cooling (section 4d) and so the entrainment rate increases for thicker clouds that have greater condensate amounts (section 3b). Thick clouds also generate more buoyant turbulence production by virtue of a larger liquid water flux (Bretherton and Wyant 1997). Therefore, a thickening cloud drives stronger entrainment, which results in cloud thinning, while a thinning cloud suppresses entrainment, which allows the cloud to thicken. Thus the cloud–radiation–turbulent–entrainment feedback represents an extremely strong negative feedback to changes in large-scale meteorological variables, and will operate in both continental and marine regimes.

The cloud–radiation–turbulent–entrainment feedback may also help explain why stratocumulus clouds tend to be geometrically thicker at higher latitudes (Fig. 5). For a given cloud thickness h, the adiabatic cloud-top liquid water content increases with temperature (section 3b), and so the evaporative enhancement of entrainment is

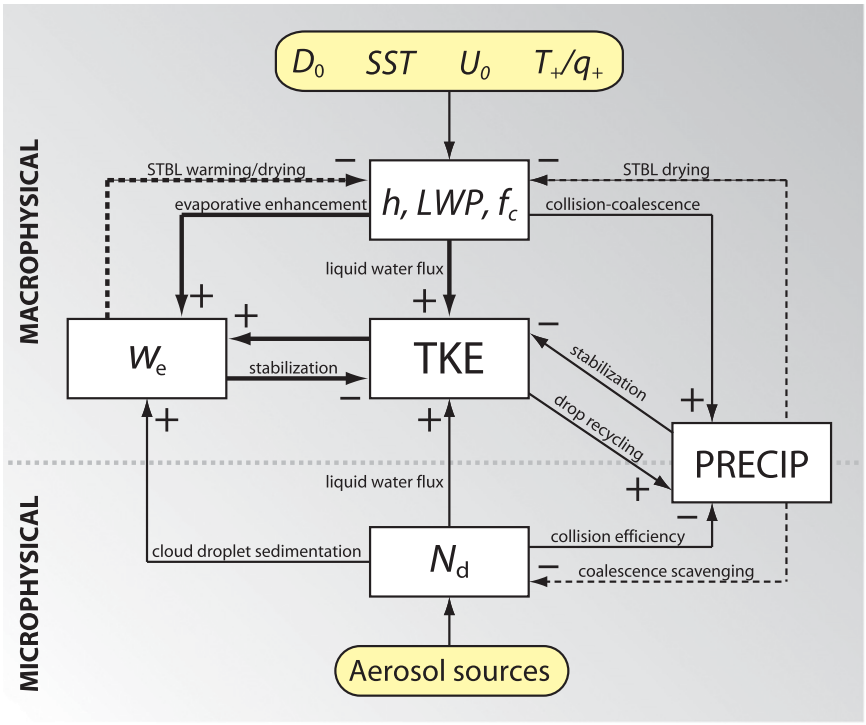

FIG. 26. Conceptual system dynamics diagram illustrating important feedbacks that serve to regulate the thickness h, liquid water path LWP, and cloud cover f_c of stratocumulus clouds. Yellow rounded rectangles show external meteorological and aerosol parameters: surface divergence D_0, surface temperature SST, surface wind speed U_0, free-tropospheric temperature T_+ and humidity q_+, and aerosol sources. White boxes show key internal variables: TKE represents a measure of the strength of the TKE within the STBL; w_e is the cloud-top entrainment rate; PRECIP is a measure of the precipitation rate; and N_d is the cloud droplet concentration, which is the key microphysical variable that can influence macrophysical processes. Plus and minus signs indicate positive and negative impacts of one variable on another, with the key physical processes accompanying the arrows where necessary. Thick arrows indicate the cloud–radiation–turbulent–entrainment feedback system that constitutes a dominant negative feedback system regulating stratocumulus thickness and cover. Solid lines indicate feedbacks that operate on time scales comparable with the eddy turnover time scale (typically an hour or less), while dashed lines indicate feedbacks that operate on markedly longer time scales. The thick dotted gray line is used to separate the chart into (top) macrophysical and (bottom) microphysical variables, with precipitation straddling the boundary between the macrophysical and microphysical realms.

greater in warmer clouds. In addition, the liquid water flux will be larger and the entrainment will be further increased via enhanced TKE. All else being equal, a larger ratio of entrainment to h favors thinner clouds, but there are other factors that may be important in controlling h such as differences in external meteorological parameters.

Precipitation (section 4e) can also serve as an important regulator of stratocumulus cloud properties, but feedbacks involving precipitation are not all negative (Fig. 26), and these feedbacks do not operate in all STBLs. For clouds thick enough for collision–coalescence to be active, the formation of precipitation can serve to limit cloud thickness by STBL drying (Lenderink and Siebesma 2004). Precipitation also serves to reduce TKE in the STBL by stabilization (section 4e), which can reduce the entrainment rate (Ackerman et al. 2004; Wood 2007) and this effect will counteract the thickness reductions associated with moisture loss. That said, recycling of precipitation drops by turbulent eddies within the STBL is important for the growth of drizzle drops (Nicholls 1987; Baker 1993; Austin et al. 1995; Vali et al. 1998). The spreading Taylor plume drizzle growth model of Baker (1993) suggests that precipitation rates might increase severalfold for a doubling of the vertical velocity variance. Large eddy simulations also show that turbulence enhances drizzle production by increasing the in-cloud residence time for drizzle drops, thereby facilitating their growth by collision–coalescence (Feingold et al. 1996).

Strongly turbulent STBLs thus promote the formation of drizzle, which then limits the turbulence, and so this represents an additional negative feedback that serves to limit cloud thickness.

b. Microphysical–macrophysical interactions

Figure 26 includes interactions between microphysics (here denoted by the cloud droplet concentration N_d) and the macrophysical realm. It is quite well understood that changes in N_d can impact precipitation, but less well understood and quantified are the direct impacts that N_d can have on TKE and entrainment other than those mediated through precipitation.

Stratocumulus precipitation can be suppressed by increasing aerosol concentration, which increases N_d (section 5b). Such suppression can reduce moisture loss from the STBL, which leads to thicker clouds, but would also invigorate buoyant TKE production and drive increases in cloud-top entrainment (Ackerman et al. 2004; Wood 2007), which would typically result in cloud thinning akin to the cloud–radiation–turbulent–entrainment interaction discussed above [see also Stevens et al. (1998), which discusses how drizzle may sustain shallower STBLs with more extensive cloud cover]. Together, model results suggest that these opposing effects can result in increases in cloud liquid water path (Ackerman et al. 2009) and cloud cover (Savic-Jovcic and Stevens 2008; Xue et al. 2008a) in some cases, and decreased cloud thickness in others (Ackerman et al. 2004; Wood 2007). Support for both increases and decreases in liquid water path in polluted clouds is provided by studies of ship tracks (Coakley and Walsh 2002). Increased TKE caused by external aerosol-induced precipitation suppression (section 5b) would serve to weaken the suppression by promoting drizzle growth, an example of the buffering effects discussed in Stevens and Feingold (2009). Given the strong sensitivity of drizzle production to turbulent mixing, it is remarkable that this sensitivity is not accounted for in any parameterization of precipitation production used in climate models.

Although drizzle reduces the overall TKE in the STBL, evaporating drizzle can actually *destabilize* the subcloud layer, which can initiate penetrating cumulus (Feingold et al. 1996; Jiang et al. 2002), cause cold pool formation (Jensen et al. 2000; Xue et al. 2008a), and enhance mesoscale variability and dynamics (Comstock et al. 2005, 2007; Savic-Jovcic and Stevens 2008; Xue et al. 2008a). Whether the drizzle evaporates or not, both one-dimensional and large eddy modeling studies show that drizzle promotes STBL stratification by warming the upper STBL (Nicholls 1984; Wang and Albrecht 1986; Stevens et al. 1998; Mechem and Kogan 2003; Ackerman et al. 2009) and by reductions in vertical wind variance (Stevens et al. 1998; Ackerman et al. 2009). Precipitation can also exert control over the STBL system on daily time scales by modulating the cloud-forming aerosols and therefore the cloud microphysics, which then feeds back into the cloud macrophysical processes (Fig. 26).

In addition to precipitation-mediated turbulence changes associated with increasing aerosols, an increase in N_d caused by increased external aerosol sources can also decrease the condensation time scale (by increasing the overall droplet surface area), which increases TKE by increasing the liquid water flux (Wang et al. 2003; and Fig. 26). This *microphysically limited condensation* is more acute for low droplet concentration N_d because the equilibrium supersaturation is inversely proportional to N_d (Squires 1952; Kogan et al. 1995). For example, Kogan and Martin (1994) find that condensation rates are only a few percent lower than those assuming saturation adjustment (no supersaturation) in a stratocumulus case with $N_d = 400\ \text{cm}^{-3}$, but are almost 50% lower when $N_d = 25\ \text{cm}^{-3}$. Increasing N_d would thus be expected to increase the cloud-top entrainment rate. Modeling studies demonstrate that microphysically limited condensation indeed has effects upon the mean fields, most importantly the cloud liquid water path (Kogan and Martin 1994; Wang et al. 2003; Lee et al. 2009) and may constitute an important aerosol indirect effect on radiative fluxes that has yet to be represented in climate models.

Increasing N_d also decreases the sedimentation rate of cloud droplets. Although this does not have a major impact throughout the body of the cloud because the sedimentation rates of clouds droplets are so low (few centimeters per second) compared with the vertical motions ($\sim$1 m s^{-1}), there may be a greater impact near the sharp liquid water gradient at cloud top where vertical motions are suppressed. Large eddy simulation indicates that the reduced removal of liquid water from the entrainment interface associated with increased N_d may result in a marked increase in the entrainment rate (Bretherton et al. 2007) without a large impact on the TKE in the STBL (Fig. 26). Whether this effect constitutes an important aerosol indirect effect is currently unknown.

Because the responses of stratocumulus macrophysical properties to external aerosol changes all involve changes in the nature of the turbulence (either in the bulk of the STBL or at the entrainment interface), representing these effects in climate models represents a formidable challenge. Currently, climate models that account for aerosol indirect effects other than the Twomey effect tend not to represent the STBL, and particularly its turbulent structure, explicitly. Thus, the interplay between microphysical and turbulent processes is handled

only through the mean state, which is not how the system works in reality.

c. Interactions between the STBL and large-scale meteorology

1) LARGE-SCALE DIVERGENCE

By continuity, the large-scale divergence profile $D(z)$ determines the subsidence rate profile $w_s(z)$, and hence the rate at which the boundary layer would become shallower in the absence of entrainment. Over the oceans, $D(z)$ is approximately independent of height in the lower troposphere where stratocumuli reside. Given an entrainment rate w_e, the equilibrium boundary layer depth is $z_i^{eq} = w_e/D$. Since the STBL depth strongly influences many of its key structural and dynamical properties, D has an important influence upon stratocumulus (Randall and Suarez 1984; Zhang et al. 2009). This response is nonlinear because low divergence rates permit the MBL to grow sufficiently deep so that it decouples and can no longer support stratocumulus, while strong divergence can lower the MBL top below the LCL resulting in no clouds (Randall and Suarez 1984; Weaver and Pearson 1990; Zhang et al. 2009).

For the semipermanent subtropical marine stratocumulus sheets, the mean low-level divergence is ~2–4 $\times$ 10^{-6} s^{-1} (Zhang et al. 2009), leading to mean subsidence rates at the STBL inversion of 2–4 mm s^{-1} (Wood and Bretherton 2004). The low-level divergence then provides a time scale $\tau_{top} = D^{-1} \sim$ 3–6 days, which is the relaxation time scale over which the STBL inversion height (cloud-top height) responds to changes in entrainment rate (Schubert et al. 1979b). This time scale is quite slow compared with typically more rapidly changing meteorological changes (e.g., in SST) along airmass trajectories and implies that the STBL depth is rarely in equilibrium with its local meteorological forcing.

Reduction in surface divergence, in addition to the more well-studied impact of increasing SST (e.g., Krueger et al. 1995a; Wyant et al. 1997), can also hasten the transition from shallow to deep MBL over the subtropical oceans (Norris and Klein 2000; Wood and Bretherton 2004), although recent research suggests that the Lagrangian transition from overcast stratocumulus to more broken clouds downstream occurs upstream of the decrease in divergence (Sandu et al. 2010).

2) FREE-TROPOSPHERIC TEMPERATURE AND LOWER-TROPOSPHERIC STABILITY

Much research has focused upon the influence of lower-tropospheric stability (LTS) in controlling the coverage of low clouds, particularly over the oceans (Slingo 1987; Klein and Hartmann 1993; Wood and Bretherton 2006). Conventionally, LTS is defined as the difference in potential temperature between 700 and 1000 hPa (Klein and Hartmann 1993), but one can also use surface air temperature, or even SST, in place of the temperature at 1000 hPa (e.g., Norris 1998). There is a remarkably good correlation between seasonal mean LTS and low-cloud amounts over the major regions of tropical/subtropical stratocumulus (Klein and Hartmann 1993), and such a correlation works equally well over the midlatitude oceans if one accounts for the temperature-dependent (and therefore latitude dependent) stability of the free troposphere above the STBL (Wood and Bretherton 2006). Strong LTS favors a strong inversion that inhibits entrainment (section 4d), favoring a shallower and therefore more well-mixed boundary layer (Wood and Bretherton 2004; Wood and Hartmann 2006). In such boundary layers the cloud layer is strongly coupled to the ocean moisture source and the strong capping inversion results in horizontally extensive, albeit thin, saturated layers. Despite this physical explanation, it is interesting that low-cloud amounts over oceans seem to be well explained by the temperature structure alone. Because LTS is strongly correlated with free-tropospheric moisture and large-scale ascent over the subtropical oceans, as a metric it likely captures a variety of covarying influences on marine low-cloud cover.

3) FREE-TROPOSPHERIC MOISTURE

Mixed layer theory and large eddy simulations indicate that the free-tropospheric moisture q_+ should also influence cloud thickness and height. All else being equal, dry free-tropospheric (FT) air favors a more elevated cloud base since the entrainment of said air into the STBL causes a lifting of the LCL (Betts and Ridgway 1989). Taken in isolation this would lead to cloud thickness decreasing as FT moisture decreases. However, the evaporative enhancement of entrainment increases, and the longwave cooling increases, as q_+ decreases. These both drive stronger entrainment (section 4d) under conditions of low q_+, and therefore higher cloud tops, compared with the case with a moister free troposphere. Within a mixed layer construct, equilibrium cloud thickness is actually a *decreasing* function of q_+ (also Betts and Ridgway 1989). However, strong entrainment favors a greater likelihood of a transition to cumulus (section 6e). Therefore, exactly how free-tropospheric moisture determines stratocumulus properties remains rather uncertain. Furthermore, because the free-tropospheric humidity, radiatively driven large-scale subsidence, and stability are closely connected, it is very difficult to isolate impacts of free-tropospheric moisture from other meteorological controls (Klein et al. 1995).

d. Formation

There are few studies that investigate the formation of stratocumulus, while many exist detailing its maintenance and evolution. In general, stratocumulus forms in response to large-scale cooling or moistening of the boundary layer, driven by radiative processes, by buoyancy- or shear-driven mixing, or by a mixture of these processes. Cooling can also be driven by low-level large-scale ascent or by the entrainment deepening of a clear convective boundary layer.

Under clear skies, the lower atmosphere can cool by several kelvin per day by the emission of longwave radiation (e.g., Garratt and Brost 1981; Tjemkes and Duynkerke 1989), with a weaker diurnal mean solar absorption by water vapor (e.g., Barker et al. 1998). Thus, radiation alone tends to drive the atmosphere toward saturation. However, turbulent mixing also acts to change the moisture and temperature structure of the boundary layer and under many circumstances may be a more efficient means for generating large-scale saturation. Under clear skies the primary source of this turbulence is either vertical shear of the horizontal wind (Garratt 1992) or buoyancy generated by exchange with the surface.

The effect of exchange with the surface upon vertical mixing is critically dependent upon the buoyancy of the air immediately adjacent to the surface that has been modified by the exchange (Paluch and Lenschow 1991). A parcel's virtual potential temperature T_v perturbation from the mean at a level is approximately expressed as

$$T_v' \approx T' + (\epsilon^{-1} - 1)\overline{T}q', \tag{7}$$

where ϵ (=0.622) is the ratio of the molar masses of water vapor and dry air, and $\overline{T}$ is the mean temperature of the layer. For a parcel modified by exchange with the surface the relative changes in T' and q' are critical to determining if the modified parcel will be positively buoyant. For an unsaturated near-surface layer, q' is always positive because evaporation will occur, and so the sign of the resulting parcel buoyancy is determined by T', which critically depends upon the surface–air temperature difference.

Consider the case of clear skies over the ocean. If the SST is warmer than the air temperature, then parcels of air moistened by surface evaporation are also warmed and will thus always be positively buoyant. This can even occur when the SST is cooler than the air temperature provided that $T_v' > 0$. These parcels rise and result in mixing and temperature profiles that are near neutral. Such layers are the precursors of stratus and stratocumulus formation (Paluch and Lenschow 1991). In contrast, when $T_v' < 0$, the modified parcels remain close to the ocean surface. This leads to mixing ratio increases near the surface and stratified boundary layers that eventually favor either the formation of shallow cumulus convection, or, if the temperature stratification is very strong, sea fog. Over land the physical processes are essentially the same, but the moisture supply is sensitive to the nature of the underlying surface, and shear within the developing boundary layer can also drive turbulent mixing (Zhu et al. 2001).

The formation of stratus occurs when the upper parts of the near-neutral layer reach saturation. At this point the inversion is not strongly defined because the turbulent eddies are fairly weak and reach varying altitudes. Once the saturated layer becomes thicker than a few tens of meters, it becomes strongly radiatively active (section 4a) and infrared emission from the upper parts of the cloud cools the cloud layer (e.g., Paluch and Lenschow 1991). This sharpens the inversion and, if sufficiently strong generates convective instability that helps mix the layer (section 4b), which has now become a stratocumulus layer.

A number of studies have used numerical and analytical modeling to determine whether a given set of meteorological forcings will result in the formation of stratocumulus (e.g., Randall and Suarez 1984; Chlond 1992). Over the ocean, the key requirements are heating from below (as discussed above) coupled with relatively strong lower-tropospheric stability to prevent deep cloud development, and subsidence rates that are not so strong as to prevent the PBL to deepen to the point where the surface-based LCL is below the inversion (Randall and Suarez 1984).

e. Dissipation and transition to other cloud types

Stratocumulus clouds dissipate in three ways: they can become thinner and disappear altogether in a somewhat spatially uniform manner; they can become horizontally heterogeneous, thickening in places and thinning/dissipating in others; and they can transition into a completely different cloud type. These modes may also occur in concert (e.g., stratocumulus-to-cumulus transition).

1) DISSIPATION BY CLOUD THINNING

The primary factors that reduce the thickness of the saturated layer in which stratocumuli reside include the following: strong subsidence that can lower the inversion (Randall and Suarez 1984), especially in coastal regions affected by land–sea interactions (Sundararajan and Tjernstrom 2000); an increase in the temperature of the PBL by increased heat fluxes or especially solar radiation (Turton and Nicholls 1987; Rogers and Koracin 1992); removal of moisture by drizzle (Wang and Wang 1994; Ackerman et al. 1993); precipitation falling through

the layer from aloft (e.g., Rutledge and Hobbs 1983); or entrainment of warm, dry air from aloft (Randall 1984). Although cloud thinning can occur on its own, the processes driving it often also cause changes in the STBL that lead to horizontal heterogeneity and/or transitions to different cloud types.

2) CLOUD-TOP ENTRAINMENT INSTABILITY

An additional mechanism for the breakup of stratocumulus clouds was first presented by Kraus (1963), and then examined further by Lilly (1968), Deardorff (1980a) and Randall (1980). Known as CTEI,[3] this mechanism is based on the idea that evaporation in mixtures of saturated STBL air, and dry air from above the STBL can under certain circumstances generate negatively buoyant downdrafts that are hypothesized to increase the TKE in the STBL, leading to further entrainment and thus serving as a positive feedback that can rapidly dry the STBL and dissipate cloud. This is in contrast to dry entrainment in which the buoyancy force associated with mixing warm air into the STBL destroys TKE.

The Randall–Deardorff criterion for CTEI, which is derived assuming that the parcel containing a mixture of cloudy and free-tropospheric air remains just saturated, can be defined simply as a function of the jumps in equivalent potential temperature θ_e and total water mixing ratio q_t across the cloud-top inversion (Δ indicates a difference between the free-tropospheric value and the value in the top of the STBL):

$$\Delta\theta_e < \kappa\frac{L_v}{c_p}\Delta q_t, \tag{8}$$

where L_v is the latent heat of condensation of water, c_p is the heat capacity of air at constant pressure, and κ is a thermodynamic constant that depends on temperature and pressure ($\kappa = 0.20$ at a temperature of 280 K and a pressure of 900 hPa and increases with temperature). Equivalently, the criterion can be expressed in terms of the inversion jump in liquid potential temperature $\theta_l \approx \theta - L_v q_l/c_p$, where q_l is the liquid water mixing ratio:

$$\Delta\theta_l < -\Delta q_t\frac{L_v}{c_p}(1 - \kappa). \tag{9}$$

Since the jump $\Delta\theta_l$ is close to the inversion strength ΔT, this latter form of the Randall–Deardorff CTEI criterion is a little more intuitive and essentially states that the combination of weak inversions and/or strong hydrolapses (stronger evaporative potential) would lead to CTEI.

Numerous field measurements show that persistent stratocumulus layers can exist even when the criterion for CTEI as defined by Eqs. (8) and (9) is met (e.g., Kuo and Schubert 1988; Weaver and Pearson 1990; de Roode and Duynkerke 1997; Stevens et al. 2003b), and controlled laboratory analog experiments led to the same conclusions (Siems et al. 1990). This finding drove a search for extensions of the original theoretical arguments and modified criteria. The primary concern with the Randall–Deardorff criterion is that it assumes the entrained parcel remains saturated by having liquid continuously evaporate into it, such that there is no limit to the availability of liquid water. Thus, the Randall–Deardorff criterion can be seen to represent the maximum cooling potential that could be gained. This potential is not often reached, however, and parcels entering and mixing with STBL air can in many cases become subsaturated before their cooling potential is realized. Adjustments to the CTEI criterion that take this consideration into account were conceived by MacVean and Mason (1990), Siems et al. (1990), and Duynkerke (1993). For relatively small moisture jumps Δq_t, the criterion of Duynkerke (1993) relaxes to that of Randall–Deardorff for realistic liquid water contents found in stratocumulus clouds, and, for zero cloud liquid water, it relaxes to the dry adiabatic stability criterion ($\Delta\theta_v > 0$). For strong hydrolapses typical of most STBLs, the condition for instability in Duynkerke (1993) is more stringent than that from Randall–Deardorff. Numerical simulations of well-mixed STBLs suggest κ values closer to 0.7 are required for CTEI (MacVean 1993), which agrees with the modified criterion of MacVean and Mason (1990). Although the exact formulations used by MacVean and Mason (1990) and Siems et al. (1990) differ somewhat from Duynkerke (1993), the stability criteria emanating from all three studies share the common element of requiring a weaker inversion than Randall–Deardorff, for a given moisture jump, to generate instability.

The modified CTEI criteria are less inconsistent with the observations of unbroken stratocumulus cloud decks than is the Randall–Deardorff criterion (e.g., Duynkerke 1993; de Roode and Duynkerke 1997), in that the stratocumulus cases tend to exist in stable CTEI conditions. Taken alone, this might hint that some form of CTEI may still be relevant for understanding the breakup of stratocumulus clouds in nature. More recent research, however, suggests that the cloud-dessicating effects of CTEI may be masked by cloud-maintaining processes such as cloud-top radiative cooling (Yamaguchi and Randall 2008). Other recent research using extremely high-resolution numerical simulation (Stevens 2010;

[3] Deardorff (1980a) proposed the term CTEI and Randall (1980) proposed the term conditional instability of the first kind upside-down (CIFKUD).

Mellado 2010) suggests that buoyancy reversal is not a sufficient condition for the rapid breakup of stratocumulus layers. Instead, while negatively buoyant evaporatively driven thermals do increase the transport of entrained mass away from the inversion (i.e., they enhance the entrainment rate), they do not feed back onto the interfacial dynamics in such a way as to drive a runaway positive feedback on the entrainment rate (i.e., CTEI). We therefore choose to display the influence of entrainment on STBL TKE in Fig. 26 as universally suppressive. In decoupled boundary layers, numerical simulations show that cloud cover scales strongly with κ (Lock 2009), with major decreases in cloud cover occurring as κ increases from 0.2 to 0.4. However, observational evidence does not support such a strong scaling relationship (Jones et al. 2011), but some decoupled STBLs do show decreased cloud cover for $\kappa > 0.3$. There little evidence that CTEI is decisive, and more evidence that it plays at most a minor role in the life of stratocumulus cloud systems, particularly those in well-mixed boundary layers. However, the parameter κ may prove a useful one for understanding cloud-cover changes in already decoupled STBLs.

3) Transition to cumulus

In addition to consideration of the dissipation mechanisms for stratocumuli in boundary layers that remain relatively well mixed, mechanisms by which stratocumulus clouds dissipate and/or break up involve the transition to a stratified and intermittently coupled boundary layer (Garratt 1992; Paluch et al. 1994). Often, but not always, this transition is accompanied by increased horizontal heterogeneity (Wang and Lenschow 1995; Wood and Hartmann 2006). The transition from overcast stratocumulus to trade cumulus clouds is an important example of this type of stratocumulus breakup (Albrecht et al. 1995a,b; Bretherton and Wyant 1997), and this is critical for setting the distribution of cloud cover over the subtropical and tropical oceans. In this case, the transition typically occurs as air masses move equatorward around the eastern side of subtropical oceanic high pressure systems. As they do so, the STBL, initially shallow due to the relatively strong subsidence associated with the high, deepens and warms due to increased surface fluxes (particularly latent heating) as the air mass moves over progressively warmer water (Krueger et al. 1995a; Wyant et al. 1997). This drives strong entrainment that leads to increasingly negative subcloud buoyancy fluxes, which decouple the layer (Bretherton and Wyant 1997), allowing cumulus clouds to form below the stratocumulus. This process of decoupling the STBL is termed the *deepening–warming* mechanism (Bretherton and Wyant 1997). The cumuli initially help to maintain extensive stratocumulus cloud cover by supplying moisture (Martin et al. 1995; Miller and Albrecht 1995; Wang and Lenschow 1995). As the cumuli become more vigorous they increase the entrainment of dry air from aloft (Wyant et al. 1997), which leads to dissipation of the stratocumulus layer (Xiao et al. 2010). As discussed above, the relative strength of the moisture and temperature inversion jumps appear to be important for determining the eventual loss of the stratocumulus (Lock 2009) after the STBL has already become decoupled.

4) Dissipation induced by precipitation

Although not a necessary condition for stratocumulus breakup, there is evidence and a theoretical basis for increased precipitation (section 4e) promoting decoupling and stratocumulus breakup (Nicholls 1984; Wang and Wang 1994; Miller and Albrecht 1995; Bretherton and Wyant 1997; Stevens et al. 1998; Mechem and Kogan 2003; Caldwell et al. 2005; Comstock et al. 2005). The relative importance of precipitation-induced decoupling compared with the deepening–warming mechanism for driving the stratocumulus to cumulus transition is currently not well understood.

In addition to there being regulating feedbacks associated with precipitation in the STBL (section 6a), under some circumstances precipitation can drive strong positive internal feedbacks. Figure 26 shows that increased precipitation can stabilize the STBL, reducing TKE and entrainment, and producing thicker clouds and more precipitation. Coalescence scavenging is also an important and efficient sink of CCN (Wood 2006), which reduces the cloud droplet concentration, favoring more precipitation. Both of these effects can work together under conditions favoring heavy precipitation, to produce catastrophic changes in the STBL system. There appear to be two distinct types of response of the marine STBL to heavy drizzle (rates of several millimeters per day). In some STBLs, drizzle appears to drive the transition from closed to open mesoscale cellular convection observed in regions of extensive marine stratocumulus (Savic-Jovcic and Stevens 2008; Wang and Feingold 2009). The nascent open cells are, in some cases, entirely surrounded by closed cells, in which case they have become known as pockets of open cells (POCs; Stevens et al. 2005a). Figure 27 shows an example of POCs, together with broader regions of open cells, over the southeastern Pacific Ocean. The few in situ case studies of POCs indicate that sharp cloud microphysical and aerosol transitions accompany the macroscale cloud transitions (vanZanten and Stevens 2005; Sharon et al. 2006; Petters et al. 2006; Wood et al. 2008, 2011a), and that the POCs contain stronger and larger drizzling cells that occur more intermittently (Comstock et al. 2007).

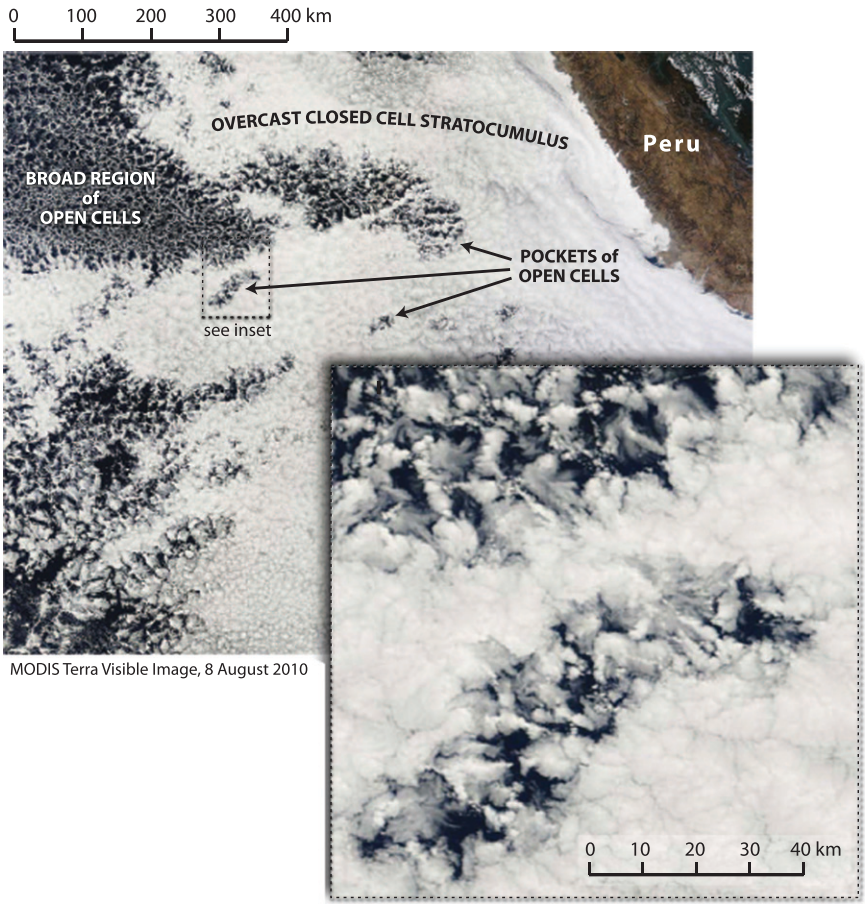

FIG. 27. Visible imagery from MODIS on the NASA *Terra* satellite showing pockets of open cells (POCs) embedded in overcast closed-cell marine stratocumulus over the tropical southeastern Pacific Ocean. The inset shows an enlarged region detailing the cellular structure within a POC.

The boundary between the open- and closed-cell regions has also been observed to drizzle strongly (Comstock et al. 2007; Wood et al. 2011a). Coalescence scavenging also takes place in the transition to open cells (Wood et al. 2011a), which may help explain the rapidity of these transitions.

In some cases, heavy drizzle causes the STBL to collapse to a much shallower boundary layer (typically 500 m or less) consisting of only a few patchy clouds or no clouds at all. In these cases, drizzle drives strong reductions in TKE and consequently cloud-top entrainment (Ackerman et al. 1993; Stevens et al. 1998). As in the transition to open cells, coalescence scavenging of CCN appears to be important for enhancing the precipitation efficiency and possibly for reducing the efficacy of longwave cooling in driving turbulence, both of which accelerate the collapse. It is interesting that the most spectacular ship tracks tend to form in collapsed boundary layers. These tracks are significantly elevated above the surrounding patchy clouds (Christensen and Stephens 2011), which suggests that increased colloidal stability can mitigate collapse and perhaps even regrow the boundary layer to a state that can support stratocumulus.

Why heavy drizzle promotes a transition to open cells in some cases and a collapsed boundary layer in others is unclear. Large eddy simulations show reduced cloud-top entrainment rate in POCs compared with the surrounding closed cells (Berner et al. 2011) and yet the rate of growth of the boundary layer has been observed to be quite even across the open-closed transition (Wood et al. 2011a). This suggests that secondary circulations above the inversion are important for reducing the subsidence above the open cells (Bretherton et al. 2010b; Berner et al. 2011), thereby mitigating STBL collapse. One hypothesis is that when the area susceptible to collapse is large enough, there is effectively no strongly entraining "surrounding" cloud to maintain the STBL depth against subsidence. Another possible factor affecting the outcome for heavily

drizzling STBLs is the initial depth of the STBL. Deeper STBLs may tend to evolve into an open-cell state while initially shallower ones may have a tendency to collapse (Bretherton et al. 2010b). Shallower STBLs tend not to support mesoscale cellular convection (Wood and Hartmann 2006), which may be required for the transition to open cells.

7. Summary

Stratocumulus clouds are Earth's most common cloud type and cover vast tracts of the globe and thus have a profound impact on Earth's radiation budget. Approximately four-fifths of all stratocumuli are located over ocean regions, which explains why much of the research has focused on the marine forms of these clouds.

Stratocumuli are susceptible to perturbations in atmospheric aerosol, through both microphysical and macrophysical mechanisms. Thus, a better understanding of their behavior is as pertinent for quantifying aerosol indirect effects on climate as well as for quantifying how clouds respond to increasing greenhouse gases. Despite a substantial research focus on stratocumuli, there are many aspects of their behavior and structure that remain poorly understood. On a basic level, this is because a stratocumulus cloud system is the product of a tight coupling between radiation, turbulence, and cloud microphysical processes occurring over a wide range of scales from millimeters to tens of kilometers.

Stratocumulus are convective clouds whose vertical development is constrained by an inversion atop the boundary layer. Most of the energy in the vertical motion field in stratocumulus cloud systems occurs on horizontal scales close to the depth of the boundary layer, and yet these clouds frequently organize into mesoscale cellular convection with characteristic horizontal scales of several kilometers to several tens of kilometers (the scale increases as the STBL depth increases). This organization, which is particularly prevalent in marine stratocumulus, is associated with an intermittency imposed on the vertical coupling, suppressing it in places and concentrating it locally. Precipitation, which new observations are revealing to be a key driver of stratocumulus behavior, further adds to the complexity of the organization through its combined effects of cloud layer latent heat release and subcloud layer evaporation. Indeed, the marine stratocumulus cloud system in general can be thought of as an organized and interconnected ensemble of marine boundary layer convective elements in which both radiation and precipitation provide the key energetic forcings.

Turbulence generated in stratocumulus clouds, together with evaporation of liquid water, increases the cloud-top entrainment rate. This in turn modulates the STBL moisture, temperature, and mass budgets, thereby influencing the liquid water content and ipso facto other processes (e.g., precipitation) that themselves influence turbulence production. Through these internal feedbacks, stratocumulus cloud thickness and liquid water path are strongly regulated. Nevertheless, stratocumuli are impacted by both the temperature and humidity of the free-tropospheric air being entrained, along with the rate at which this air is subsiding. Understanding stratocumulus responses to anthropogenic increases in greenhouse gases and aerosols will require an understanding of interaction with the free troposphere. Observational and modeling advances in the last decade show that the influence of precipitation on the moisture and energy budgets in marine STBLs is greater than was previously thought, and that cloud-top entrainment rates are lower than previously thought. Thus, our thinking about the STBL energy and moisture budgets, and the interactions between processes that control them, is still evolving.

Observational studies, mostly in subtropical stratocumulus regions, are revealing the rich mesoscale structure and dynamics in stratocumulus cloud systems, and allow greatly improved quantification of the effects of precipitation on this structure. Doppler radar and lidar shows that horizontal wind fluctuations in the STBL, unlike those in the vertical, are often dominated by motions with horizontal scales comparable with the mesoscale cells. Precipitating cells clearly show coherent inflows near cloud base and outflow near the top of the cloud layer that appear to supply moisture to the cell. Cold pools in the subcloud layer generated by the precipitation ultimately suppresses buoyant production in the cell, but can drive new cell formation at the confluence of the gravity currents the cold air produces (Feingold et al. 2010). Light precipitation of this type has recently become observable from space (Kubar et al. 2009; Lebsock et al. 2011), which opens up a new avenue for global mapping of the interactions between stratocumulus and the precipitation it produces.

Aerosol impacts on stratocumulus clouds include the purely microphysical (Twomey) impact of increased albedo due to increased droplet concentration and reduced droplet surface area, but also include impacts on macrophysical processes such as precipitation suppression, changes to evaporation/condensation rates due to decreased droplet integral radius, and the enhancement of cloud-top entrainment through cloud droplet sedimentation suppression. Many of these effects of these processes on stratocumulus dynamics and structure remain poorly understood and in urgent need of future exploration.

Challenges for future observations of stratocumulus include a need for more and better observations of midlatitude and high-latitude stratocumulus (particularly over the remote oceans, but also over land). New remote sensing developments, from aircraft, the surface, and from space, are providing new approaches to stratocumulus observation. Observation of turbulence structure in STBLs remains quite poor and new Doppler radar and lidar measurements from the surface and from aircraft should be used more routinely, and the measurement technologies improved. Improved observational approaches to cloud-top entrainment measurement are needed. Spaceborne millimeter radar, while providing unprecedented insights into drizzle processes, is currently unable to quantify the vertical structure of precipitation in and below cloud in shallow STBLs because returns become contaminated by ground clutter below ~800 m, but this can be overcome with currently available technology. Although it is possible to estimate column amounts of condensate using passive sensors (solar reflectance and microwave), there are no reliable spaceborne measurements of the vertical structure of condensate in stratocumulus. Wide field-of-view lidars, although currently underused, offer tantalizing possibilities for addressing this challenge.

Acknowledgments. The author appreciates the encouragement of David Schultz and Robert Houze who both stimulated this review article. Discussions with Chris Bretherton, Tom Ackerman, Paul Field, Dave Leon, Sally McFarlane, Dave Turner, Rhea George, Bruce Albrecht, Roberto Mechoso, Peter Blossey, and numerous others provided important insight and guidance. The author thanks Chris Bretherton, Bruce Albrecht, Bjorn Stevens, Grant Allen, David Schultz, and an anonymous reviewer for insightful and constructive reviews that improved the quality of the manuscript. Beth Tully helped with several of the figures. The author's work is supported by NSF Grant ATM-0745702, NASA Grant NNX10AN78G, NOAA Grant NA07OAR4310282, and DOE Grant DE-SC0002081.

REFERENCES

Abdul-Razzak, H., and S. J. Ghan, 2000: A parameterization of aerosol activation 2. Multiple aerosol types. *J. Geophys. Res.,* **105** (D5), 6837–6844.

——, ——, and C. Rivera-Carpio, 1998: A parameterization of aerosol activation. 1. Single aerosol type. *J. Geophys. Res.,* **103** (D6), 6123–6131.

Ackerman, A. S., O. B. Toon, and P. V. Hobbs, 1993: Dissipation of marine stratiform clouds and collapse of the marine boundary-layer due to the depletion of cloud condensation nuclei by clouds. *Science,* **262,** 226–229.

——, ——, and ——, 1995: Numerical modeling of ship tracks produced by injections of cloud condensation nuclei into marine stratiform clouds. *J. Geophys. Res.,* **100** (D4), 7121–7133.

——, ——, D. E. Stevens, A. J. Heymsfield, V. Ramanathan, and E. J. Welton, 2000: Reduction of tropical cloudiness by soot. *Science,* **288,** 1042–1047.

——, M. P. Kirkpatrick, D. E. Stevens, and O. B. Toon, 2004: The impact of humidity above stratiform clouds on indirect aerosol climate forcing. *Nature,* **432,** 1014–1017.

——, and Coauthors, 2009: Large-eddy simulations of a drizzling, stratocumulus-topped marine boundary layer. *Mon. Wea. Rev.,* **137,** 1083–1110.

Ackerman, T., and M. B. Baker, 1977: Shortwave radiative effects of unactivated aerosol-particles in clouds. *J. Appl. Meteor.,* **16,** 63–69.

Agee, E. M., 1987: Meso-scale cellular convection over the oceans. *Dyn. Atmos. Oceans,* **10,** 317–341.

——, T. S. Chen, and K. E. Dowell, 1973: A review of mesoscale cellular convection. *Bull. Amer. Meteor. Soc.,* **54,** 1004–1012.

Albrecht, B. A., C. W. Fairall, D. W. Thomson, A. B. White, J. B. Snider, and W. H. Schubert, 1990: Surface-based remote-sensing of the observed and the adiabatic liquid water content of stratocumulus clouds. *Geophys. Res. Lett.,* **17,** 89–92.

——, C. S. Bretherton, D. Johnson, W. H. Schubert, and A. S. Frisch, 1995a: The Atlantic Stratocumulus Transition Experiment—ASTEX. *Bull. Amer. Meteor. Soc.,* **76,** 889–904.

——, M. P. Jensen, and W. J. Syrett, 1995b: Marine boundary layer structure and fractional cloudiness. *J. Geophys. Res.,* **100** (D7), 14 209–14 222.

Arnason, G., and R. S. Greenfield, 1972: Micro- and macro-structures of numerically simulated convective clouds. *J. Atmos. Sci.,* **29,** 342–367.

Atkinson, B. W., and J. W. Zhang, 1996: Mesoscale shallow convection in the atmosphere. *Rev. Geophys.,* **34,** 403–431.

Austin, P., Y. Wang, R. Pincus, and V. Kujala, 1995: Precipitation in stratocumulus clouds: Observations and modelling results. *J. Atmos. Sci.,* **52,** 2329–2352.

Baker, M. B., 1993: Variability in concentrations of cloud condensation nuclei in the marine cloud-topped boundary layer. *Tellus,* **45B,** 458–472.

Barker, H. W., J. J. Morcrette, and G. D. Alexander, 1998: Broadband solar fluxes and heating rates for atmospheres with 3D broken clouds. *Quart. J. Roy. Meteor. Soc.,* **124,** 1245–1271.

Beesley, J. A., and R. E. Moritz, 1999: Toward an explanation of the annual cycle of cloudiness over the Arctic Ocean. *J. Climate,* **12,** 395–415.

Beheng, K. D., 1994: A parameterization of warm cloud microphysical conversion processes. *Atmos. Res.,* **33,** 193–206.

——, and G. Doms, 1986: A general formulation of collection rates of cloud and raindrops using the kinetic equation and comparison with parameterizations. *Beitr. Phys. Atmos.,* **59,** 66–84.

Bennartz, R., 2007: Global assessment of marine boundary layer cloud droplet number concentration from satellite. *J. Geophys. Res.,* **112,** D02201, doi:10.1029/2006JD007547.

Bergman, J. W., and M. L. Salby, 1996: Diurnal variations of cloud cover and their relationship to climatological conditions. *J. Climate,* **9,** 2802–2820.

Berner, A., C. S. Bretherton, and R. Wood, 2011: Large-eddy simulation of mesoscale dynamics and entrainment around a pocket of open cells observed in VOCALS RF06. *Atmos. Chem. Phys.,* **11,** 13 317–13 353.

Betts, A. K., and W. Ridgway, 1989: Climatic equilibrium of the atmospheric convective boundary layer over a tropical ocean. *J. Atmos. Sci.,* **46,** 2621–2641.

——, C. S. Bretherton, and E. Klinker, 1995: Relation between mean boundary-layer structure and cloudiness at the *R/V Valdivia* during ASTEX. *J. Atmos. Sci.,* **52,** 2752–2762.

Boers, R., and P. B. Krummel, 1998: Microphysical properties of boundary layer clouds over the Southern Ocean during ACE 1. *J. Geophys. Res.,* **103** (D13), 16 651–16 663.

——, G. P. Ayers, and J. L. Gras, 1994: Coherence between seasonal-variation in satellite-derived cloud optical depth and boundary-layer CCN concentrations at a midlatitude southern-hemisphere station. *Tellus,* **46B,** 123–131.

Bony, S., and J.-L. Dufresne, 2005: Marine boundary layer clouds at the heart of cloud feedback uncertainties in climate models. *Geophys. Res. Lett.,* **32,** L20806, doi:10.1029/2005GL023851.

Brenguier, J.-L., and R. Wood, 2009: Observational strategies from the micro to meso scale. *Clouds in the Perturbed Climate System: Their Relationship to Energy Balance, Atmospheric Dynamics, and Precipitation,* J. Heintzenberg and R. Charlson, Eds., MIT Press, 487–510.

Brenguier, J. L., H. Pawlowska, L. Schuller, R. Preusker, J. Fischer, and Y. Fouquart, 2000a: Radiative properties of boundary layer clouds: Droplet effective radius versus number concentration. *J. Atmos. Sci.,* **57,** 803–821.

——, and Coauthors, 2000b: An overview of the ACE-2 CLOUDYCOLUMN closure experiment. *Tellus,* **52B,** 815–827.

Bretherton, C. S., 1997: Convection in stratocumulus-capped atmospheric boundary layers. *The Physics and Parameterization of Moist Atmospheric Convection,* R. K. Smith, Ed., Kluwer Publishers, 127–142.

——, and R. Pincus, 1995: Cloudiness and marine boundary layer dynamics in the ASTEX Lagrangian experiments. Part I: Synoptic setting and vertical structure. *J. Atmos. Sci.,* **52,** 2707–2723.

——, and M. C. Wyant, 1997: Moisture transport, lower-tropospheric stability, and decoupling of cloud-topped boundary layers. *J. Atmos. Sci.,* **54,** 148–167.

——, and D. L. Hartmann, 2009: Large-scale controls on cloudiness. *Clouds in the Perturbed Climate System: Their Relationship to Energy Balance, Atmospheric Dynamics, and Precipitation,* J. Heintzenberg and R. Charlson, Eds., MIT Press, 217–234.

——, P. Austin, and S. T. Siems, 1995: Cloudiness and marine boundary layer dynamics in the ASTEX Lagrangian experiments. Part II: Cloudiness, drizzle, surface fluxes and entrainment. *J. Atmos. Sci.,* **52,** 2724–2735.

——, T. Uttal, C. W. Fairall, S. E. Yuter, R. A. Weller, D. Baumgardner, K. Comstock, and R. Wood, 2004: The EPIC 2001 stratocumulus study. *Bull. Amer. Meteor. Soc.,* **85,** 967–977.

——, P. Blossey, and J. Uchida, 2007: Cloud droplet sedimentation, entrainment efficiency, and subtropical stratocumulus albedo. *Geophys. Res. Lett.,* **34,** L03813, doi:10.1029/2006GL027648.

——, R. George, R. Wood, G. Allen, D. Leon, and B. Albrecht, 2010a: Southeast Pacific stratocumulus clouds, precipitation and boundary layer structure sampled along 20S during VOCALS-REx. *Atmos. Chem. Phys.,* **10,** 15 921–15 962.

——, J. Uchida, and P. Blossey, 2010b: Slow manifolds and multiple equilibria in stratocumulus-capped boundary layers. *J. Adv. Model. Earth Syst.,* **2,** doi:10.3894/JAMES.2010.2.14.

Brost, R. A., D. H. Lenschow, and J. C. Wyngaard, 1982a: Marine stratocumulus layers. Part I: Mean conditions. *J. Atmos. Sci.,* **39,** 800–817.

——, J. C. Wyngaard, and D. H. Lenschow, 1982b: Marine stratocumulus layers. Part II: Turbulence budgets. *J. Atmos. Sci.,* **39,** 818–836.

Cahalan, R. F., and J. B. Snider, 1989: Marine stratocumulus structure. *Remote Sens. Environ.,* **28,** 95–107.

——, W. Ridgway, W. J. Wiscombe, T. L. Bell, and J. B. Snider, 1994: The albedo of fractal stratocumulus clouds. *J. Atmos. Sci.,* **51,** 2434–2455.

Caldwell, P., and C. S. Bretherton, 2009: Response of a subtropical stratocumulus-capped mixed layer to climate and aerosol changes. *J. Climate,* **22,** 20–38.

——, R. Wood, and C. S. Bretherton, 2005: Mixed-layer budget analysis of the diurnal cycle of entrainment in southeast Pacific stratocumulus. *J. Atmos. Sci.,* **62,** 3775–3791.

Cantrell, W., and A. Heymsfield, 2005: Production of ice in tropospheric clouds: A review. *Bull. Amer. Meteor. Soc.,* **86,** 795–807.

Caughey, S. J., and M. Kitchen, 1984: Simultaneous measurements of the turbulent and microphysical structure of nocturnal stratocumulus cloud. *Quart. J. Roy. Meteor. Soc.,* **110,** 13–34.

——, B. A. Crease, and W. T. Roach, 1982: A field-study of nocturnal stratocumulus. 2. Turbulence structure and entrainment. *Quart. J. Roy. Meteor. Soc.,* **108,** 125–144.

Chen, T., W. B. Rossow, and Y. C. Zhang, 2000: Radiative effects of cloud-type variations. *J. Climate,* **13,** 264–286.

Chlond, A., 1992: Three-dimensional simulation of cloud street development during a cold air outbreak. *Bound.-Layer Meteor.,* **58,** 161–200.

Christensen, M. W., and G. L. Stephens, 2011: Microphysical and macrophysical responses of marine stratocumulus polluted by underlying ships: Evidence of cloud deepening. *J. Geophys. Res.,* **116,** D03201, doi:10.1029/2010JD014638.

Chylek, P., P. Damiano, and E. P. Shettle, 1992: Infrared emittance of water clouds. *J. Atmos. Sci.,* **49,** 1459–1472.

——, G. B. Lesins, G. Videen, J. G. D. Wong, R. G. Pinnick, D. Ngo, and J. D. Klett, 1996: Black carbon and absorption of solar radiation by clouds. *J. Geophys. Res.,* **101** (D18), 23 365–23 371.

Ciesielski, P. E., W. H. Schubert, and R. H. Johnson, 1999: Large-scale heat and moisture budgets over the ASTEX region. *J. Atmos. Sci.,* **56,** 3241–3261.

——, ——, and ——, 2001: Diurnal variability of the marine boundary layer during ASTEX. *J. Atmos. Sci.,* **58,** 2355–2376.

Coakley, J. A. J., and C. D. Walsh, 2002: Limits to the aerosol indirect radiative effect derived from observations of ship tracks. *J. Atmos. Sci.,* **59,** 668–680.

Cohard, J. M., and J. P. Pinty, 2000: A comprehensive two-moment warm microphysical bulk scheme. I: Description and tests. *Quart. J. Roy. Meteor. Soc.,* **126,** 1815–1842.

——, ——, and C. Bedos, 1998: Extending Twomey's analytical estimate of nucleated cloud droplet concentrations from CCN spectra. *J. Atmos. Sci.,* **55,** 3348–3357.

Comstock, K., R. Wood, S. Yuter, and C. S. Bretherton, 2004: Radar observations of precipitation in and below stratocumulus clouds. *Quart. J. Roy. Meteor. Soc.,* **130,** 2891–2918.

——, C. S. Bretherton, and S. Yuter, 2005: Mesoscale variability and drizzle in southeast Pacific stratocumulus. *J. Atmos. Sci.,* **62,** 3792–3807.

——, S. E. Yuter, R. Wood, and C. S. Bretherton, 2007: The three dimensional structure and kinematics of drizzling stratocumulus. *Mon. Wea. Rev.,* **135,** 3767–3784.

Conant, W. C., and Coauthors, 2004: Aerosol–cloud drop concentration closure in warm cumulus. *J. Geophys. Res.,* **109,** D13204, doi:10.1029/2003JD004324.

Curry, J. A., W. B. Rossow, D. Randall, and J. L. Schramm, 1996: Overview of Arctic cloud and radiation characteristics. *J. Climate,* **9,** 1731–1764.

Dai, A., 2001: Global precipitation and thunderstorm frequencies. Part II: Diurnal variations. *J. Climate,* **14,** 1112–1128.

——, T. R. Karl, B. M. Sun, and K. E. Trenberth, 2006: Recent trends in cloudiness over the United States—A tale of monitoring inadequacies. *Bull. Amer. Meteor. Soc.,* **87,** 597–606.

Danielson, R. E., D. R. Moore, and H. Van de Hulst, 1969: Transfer of visible radiation through clouds. *J. Atmos. Sci.,* **26,** 1078–1087.

Davis, A., A. Marshak, W. Wiscombe, and R. Cahahlan, 1996: Scale invariance of liquid water distributions in marine stratocumulus. Part I: Spectral properties and stratonarity issues. *J. Atmos. Sci.,* **53,** 1538–1558.

——, ——, H. Gerber, and W. J. Wiscombe, 1999: Horizontal structure of marine boundary layer clouds from centimeter to kilometer scales. *J. Geophys. Res.,* **104** (D6), 6123–6144.

de Roode, S. R., and P. G. Duynkerke, 1996: Dynamics of cumulus rising into stratocumulus as observed during the first 'Lagrangian' experiment of ASTEX. *Quart. J. Roy. Meteor. Soc.,* **122,** 1597–1623.

——, and ——, 1997: Observed Lagrangian transition of stratocumulus into cumulus during ASTEX: Mean state and turbulence structure. *J. Atmos. Sci.,* **54,** 2157–2173.

——, and Q. Wang, 2007: Do stratocumulus clouds detrain? FIRE I data revisited. *Bound.-Layer Meteor.,* **122,** 479–491.

——, P. G. Duynkerke, and H. J. Jonker, 2004: Large eddy simulation: How large is large enough? *J. Atmos. Sci.,* **61,** 403–421.

Deardorff, J. W., 1976: Entrainment rate of stratocumulus topped mixed layer. *Quart. J. Roy. Meteor. Soc.,* **102,** 563–582.

——, 1980a: Cloud top entrainment instability. *J. Atmos. Sci.,* **37,** 561–563.

——, 1980b: Stratocumulus-capped mixed layers derived from a 3-dimensional model. *Bound.-Layer Meteor.,* **18,** 495–527.

——, 1981: On the distribution of mean radiative cooling at the top of a stratocumulus-capped mixed layer. *Quart. J. Roy. Meteor. Soc.,* **107,** 191–202.

Driedonks, A. G. M., 1982: Models and observations of the growth of the atmospheric boundary-layer. *Bound.-Layer Meteor.,* **23,** 283–306.

——, and P. G. Duynkerke, 1989: Current problems in the stratocumulus-topped atmospheric boundary-layer–(survey paper). *Bound.-Layer Meteor.,* **46,** 275–303.

Dusek, U., and Coauthors, 2006: Size matters more than chemistry for cloud-nucleating ability of aerosol particles. *Science,* **312,** 1375–1378.

Duynkerke, P. G., 1993: The stability of cloud top with regard to entrainment: Amendment of the theory of cloud-top entrainment instability. *J. Atmos. Sci.,* **50,** 495–502.

——, and P. Hignett, 1993: Simulation of a diurnal variation in a stratocumulus-capped marine boundary layer during FIRE. *Mon. Wea. Rev.,* **121,** 3291–3300.

——, and J. Teixeira, 2001: Comparison of the ECMWF reanalysis with FIRE I observations: Diurnal variation of marine stratocumulus. *J. Climate,* **14,** 1466–1478.

——, H. Q. Zhang, and P. J. Jonker, 1995: Microphysical and turbulent structure of nocturnal stratocumulus as observed during ASTEX. *J. Atmos. Sci.,* **52,** 2763–2777.

Eastman, R., S. G. Warren, and C. J. Hahn, 2011: Variations in cloud cover and cloud types over the ocean from surface observations, 1954–2008. *J. Climate,* **24,** 5914–5934.

Erlick, C., and D. Schlesinger, 2008: Another look at the influence of absorbing aerosols in drops on cloud absorption: Large aerosols. *J. Atmos. Sci.,* **65,** 661–669.

Evan, A. T., A. K. Heidinger, and D. J. Vimont, 2007: Arguments against a physical long-term trend in global ISCCP cloud amounts. *Geophys. Res. Lett.,* **34,** L04701, doi:10.1029/2006GL028083.

Facchini, M. C., M. Mircea, S. Fuzzi, and R. J. Charlson, 1999: Cloud albedo enhancement by surface-active organic solutes in growing droplets. *Nature,* **401,** 257–259.

Faloona, I., and Coauthors, 2005: Observations of entrainment in eastern Pacific marine stratocumulus using three conserved scalars. *J. Atmos. Sci.,* **62,** 3268–3285.

Feingold, G., 2003: Modeling of the first indirect effect: Analysis of measurement requirements. *Geophys. Res. Lett.,* **30,** 1997, doi:10.1029/2003GL017967.

——, and P. Y. Chuang, 2002: Analysis of the influence of film-forming compounds on droplet growth: Implications for cloud microphysical processes and climate. *J. Atmos. Sci.,* **59,** 2006–2018.

——, and H. Siebert, 2009: Cloud-aerosol interactions from the micro to the cloud scale. *Clouds in the Perturbed Climate System: Their Relationship to Energy Balance, Atmospheric Dynamics, and Precipitation,* J. Heintzenberg and R. Charlson, Eds., MIT Press, 319–338.

——, W. Cotton, B. Stevens, and A. S. Frisch, 1996: The relationship between drop in-cloud residence time and drizzle production in numerically simulated stratocumulus clouds. *J. Atmos. Sci.,* **53,** 1108–1122.

——, I. Koren, H. Wang, H. Xue, and W. Brewer, 2010: Precipitation-generated oscillations in open cellular cloud fields. *Nature,* **466,** 849–852.

Ferek, R. J., and Coauthors, 2000: Drizzle suppression in ship tracks. *J. Atmos. Sci.,* **57,** 2707–2728.

Field, P. R., and R. Wood, 2007: Precipitation and cloud structure in midlatitude cyclones. *J. Climate,* **20,** 233–254.

Fountoukis, C., and Coauthors, 2007: Aerosol-cloud drop concentration closure for clouds sampled during the International Consortium for Atmospheric Research on Transport and Transformation 2004 campaign. *J. Geophys. Res.,* **112,** D10S30, doi:10.1029/2006JD007272.

Fridlind, A. M., A. S. Ackerman, G. McFarquhar, G. Zhang, M. R. Poellot, P. J. DeMott, A. J. Prenni, and A. J. Heymsfield, 2007: Ice properties of single-layer stratocumulus during the Mixed-Phase Arctic Cloud Experiment: 2. Model results. *J. Geophys. Res.,* **112,** D24202, doi:10.1029/2007JD008646.

Garay, M., R. Davies, C. Averill, and J. Westphal, 2004: Actinoform clouds: Overlooked examples of cloud self-organization at the mesoscale. *Bull. Amer. Meteor. Soc.,* **85,** 1585–1594.

Garratt, J. R., 1992: *The Atmospheric Boundary Layer*. 1st ed. Cambridge University Press, 316 pp.

——, and R. A. Brost, 1981: Radiative cooling effects within and above the nocturnal boundary-layer. *J. Atmos. Sci.,* **38,** 2730–2746.

Garreaud, R. D., and J. Rutllant, 2003: Coastal lows along the subtropical west coast of South America: Numerical simulation of a typical case. *Mon. Wea. Rev.,* **131,** 891–908.

——, and R. Muñoz, 2004: The diurnal cycle in circulation and cloudiness over the subtropical southeast Pacific: A modeling study. *J. Climate,* **17,** 1699–1710.

——, J. Rutllant, J. Quintana, J. Carrasco, and P. Minnis, 2001: CIMAR-5: A snapshot of the lower troposphere over the

subtropical southeast Pacific. *Bull. Amer. Meteor. Soc.,* **82,** 2193–2207.

——, ——, and H. Fuenzalida, 2002: Coastal lows along the subtropical west coast of South America: Mean structure and evolution. *Mon. Wea. Rev.,* **130,** 75–88.

Garrett, T. J., L. F. Radke, and P. V. Hobbs, 2002: Aerosol effects on cloud emissivity and surface longwave heating in the Arctic. *J. Atmos. Sci.,* **59,** 769–778.

Geoffroy, O., J. L. Brenguier, and I. Sandu, 2008: Relationship between drizzle rate, liquid water path and droplet concentration at the scale of a stratocumulus cloud system. *Atmos. Chem. Phys.,* **8,** 4641–4654.

George, R. C., and R. Wood, 2010: Subseasonal variability of low cloud properties over the southeast Pacific Ocean. *Atmos. Chem. Phys.,* **10,** 4047–4063.

Gerber, H., 1996: Microphysics of marine stratocumulus with two drizzle modes. *J. Atmos. Sci.,* **53,** 1649–1662.

——, G. Frick, S. P. Malinowski, J. L. Brenguier, and F. Burnet, 2005: Holes and entrainment in stratocumulus. *J. Atmos. Sci.,* **62,** 443–459.

Ghan, S. J., G. Guzman, and H. Abdul-Razzak, 1998: Competition between sea salt and sulfate particles as cloud condensation nuclei. *J. Atmos. Sci.,* **55,** 3340–3347.

Glantz, P., K. J. Noone, and S. R. Osborne, 2003: Scavenging efficiencies of aerosol particles in marine stratocumulus and cumulus clouds. *Quart. J. Roy. Meteor. Soc.,* **129,** 1329–1350.

Greenwald, T. J., G. L. Stephens, S. A. Christopher, and T. H. VonderHaar, 1995: Observations of the global characteristics and regional radiative effects of marine cloud liquid water. *J. Climate,* **8,** 2928–2946.

Gultepe, I., and G. A. Isaac, 2004: Aircraft observations of cloud droplet number concentration: Implications for climate studies. *Quart. J. Roy. Meteor. Soc.,* **130,** 2377–2390.

Hahn, C. J., and S. G. Warren, 2007: A gridded climatology of clouds over land (1971–96) and ocean (1954–97) from surface observations worldwide. Numeric Data Package NDP-026E ORNL/CDIAC-153, CDIAC, Department of Energy, Oak Ridge, TN.

——, W. B. Rossow, and S. G. Warren, 2001: ISCCP cloud properties associated with standard cloud types identified in individual surface observations. *J. Climate,* **14,** 11–28.

Hakim, G. J., 2003: Developing wave packets in the North Pacific storm track. *Mon. Wea. Rev.,* **131,** 342–355.

Hall, W. D., 1980: A detailed microphysical model within a two-dimensional dynamic framework: Model description and preliminary results. *J. Atmos. Sci.,* **37,** 2486–2507.

Haman, K. E., S. P. Malinowski, M. J. Kurowski, H. Gerber, and J. L. Brenguier, 2007: Small scale mixing processes at the top of a marine stratocumulus—A case study. *Quart. J. Roy. Meteor. Soc.,* **133,** 213–226.

Hansen, J. E., and L. D. Travis, 1974: Light scattering in planetary atmospheres. *Space Sci. Rev.,* **16,** 527–610.

Hanson, H. P., 1991: Marine stratocumulus climatologies. *Int. J. Climatol.,* **11,** 147–164.

Hartmann, D. L., 1994: *Global Physical Climatology*. Academic Press, 408 pp.

——, and D. Short, 1980: On the use of earth radiation budget statistics for studies of clouds and climate. *J. Atmos. Sci.,* **37,** 1233–1250.

——, M. E. Ockert-Bell, and M. L. Michelsen, 1992: The effect of cloud type on earth's energy balance—Global analysis. *J. Climate,* **5,** 1281–1304.

Haywood, J. M., and K. P. Shine, 1997: Multi-spectral calculations of the direct radiative forcing of tropospheric sulphate and soot aerosols using a column model. *Quart. J. Roy. Meteor. Soc.,* **123,** 1907–1930.

Henrion, X., H. Sauvageot, and D. Ramond, 1978: Finestructure of precipitation and temperature in a stratocumulus cloud. *J. Atmos. Sci.,* **35,** 2315–2324.

Hermann, G., and R. Goody, 1976: Formation and persistence of summertime arctic stratus clouds. *J. Atmos. Sci.,* **33,** 1537–1553.

Hignett, P., 1991: Observations of diurnal variation in a cloud-capped marine boundary layer. *J. Atmos. Sci.,* **48,** 1474–1482.

Hobbs, P. V., and A. L. Rangno, 1998: Microstructures of low and middle-level clouds over the Beaufort Sea. *Quart. J. Roy. Meteor. Soc.,* **124,** 2035–2071.

Hogan, R. J., A. L. M. Grant, A. J. Illingworth, G. N. Pearson, and E. J. O'Connor, 2009: Vertical velocity variance and skewness in clear and cloud-topped boundary layers as revealed by Doppler lidar. *Quart. J. Roy. Meteor. Soc.,* **135,** 635–643.

Howell, W. E., 1949: The growth of cloud drops in uniformly cooled air. *J. Meteor.,* **6,** 134–149.

Hu, Y. X., and K. Stamnes, 1993: An accurate parameterization of the radiative properties of water clouds suitable for use in climate models. *J. Climate,* **6,** 728–742.

Hudson, J. G., 2007: Variability of the relationship between particle size and cloud-nucleating ability. *Geophys. Res. Lett.,* **34,** L08801, doi:10.1029/2006GL028850.

Huffman, G. J., and G. A. Norman, 1988: The supercooled warm rain process and the specification of freezing precipitation. *Mon. Wea. Rev.,* **116,** 2172–2182.

Isaksen, I. S. A., and Coauthors, 2009: Atmospheric composition change: Climate–chemistry interactions. *Atmos. Environ.,* **43,** 5138–5192.

Jensen, J. B., S. Lee, P. B. Krummel, J. Katzfey, and D. Gogoasa, 2000: Precipitation in marine cumulus and stratocumulus. Part I: Thermodynamic and dynamic observations of closed cell circulations and cumulus bands. *Atmos. Res.,* **54,** 117–155.

Jiang, H., G. Feingold, and W. R. Cotton, 2002: Simulations of aerosol-cloud-dynamical feedbacks resulting from entrainment of aerosol into the marine boundary layer during the Atlantic Stratocumulus Transition Experiment. *J. Geophys. Res.,* **107,** 4813, doi:10.1029/2001JD001502.

——, ——, and A. Sorooshian, 2010: Effect of aerosol on the susceptibility and efficiency of precipitation in warm trade cumulus clouds. *J. Atmos. Sci.,* **67,** 3525–3540.

Jonas, P. R., 1996: Turbulence and cloud microphysics. *Atmos. Res.,* **40,** 283–306.

Jones, C., C. Bretherton, and D. Leon, 2011: Coupled vs. decoupled boundary layers in VOCALS-REx. *Atmos. Chem. Phys.,* **11,** 7143–7153.

Jonker, H., P. Duynkerke, and J. Cuijpers, 1999: Mesoscale fluctuations in scalars generated by boundary layer convection. *J. Atmos. Sci.,* **56,** 801–808.

Junge, C., and E. McLaren, 1971: Relationship of cloud nuclei spectra to aerosol size distribution and composition. *J. Atmos. Sci.,* **28,** 382–390.

Kajikawa, M., K. Kikuchi, Y. Asuma, Y. Inoue, and N. Sato, 2000: Supercooled drizzle formed by condensation-coalescence in the mid-winter season of the Canadian Arctic. *Atmos. Res.,* **52,** 293–301.

Kawa, S. R., and R. Pearson Jr., 1989: An observational study of stratocumulus entrainment and thermodynamics. *J. Atmos. Sci.,* **46,** 2649–2661.

Kessler, E., 1969: *On the Distribution and Continuity of Water Substance in Atmospheric Circulation. Meteor. Monogr.,* No. 10, Amer. Meteor. Soc., 84 pp.

Khain, A., M. Ovchinnikov, M. Pinsky, A. Pokrovsky, and H. Krugliak, 2000: Notes on the state-of-the-art numerical modeling of cloud microphysics. *Atmos. Res.,* **55,** 159–224.

Khairoutdinov, M., and Y. Kogan, 2000: A new cloud physics parameterization in a large-eddy simulation model of marine stratocumulus. *J. Atmos. Sci.,* **57,** 229–243.

Kim, B. G., S. A. Klein, and J. R. Norris, 2005: Continental liquid water cloud variability and its parameterization using Atmospheric Radiation Measurement data. *J. Geophys. Res.,* **110,** D15S08, doi:10.1029/2004JD005122.

King, M. D., and Harshvardhan, 1986: Comparative accuracy of selected multiple scattering approximations. *J. Atmos. Sci.,* **43,** 784–801.

——, S.-C. Tsay, S. E. Platnick, M. Wang, and K.-N. Liou, 1997: Cloud retrieval algorithms for MODIS: Optical thickness, effective particle radius, and thermodynamic phase. MODIS Algorithm Theoretical Basis Document ATBD-MOD-05, NASA, 78 pp.

Klein, S. A., 1997: Synoptic variability of low-cloud properties and meteorological parameters in the subtropical trade wind boundary layer. *J. Climate,* **10,** 2018–2039.

——, and D. L. Hartmann, 1993: The seasonal cycle of low stratiform clouds. *J. Climate,* **6,** 1588–1606.

——, and C. Jakob, 1999: Validation and sensitivities of frontal clouds simulated by the ECMWF model. *Mon. Wea. Rev.,* **127,** 2514–2531.

——, D. L. Hartmann, and J. R. Norris, 1995: On the relationships among low-cloud structure, sea surface temperature, and atmospheric circulation in the summertime northeast Pacific. *J. Climate,* **8,** 1140–1155.

Kloesel, K. A., 1992: A 70-year history of marine stratocumulus cloud field experiments off the coast of California. *Bull. Amer. Meteor. Soc.,* **73,** 1581–1585.

Kogan, Y. L., and W. J. Martin, 1994: Parameterization of bulk condensation in numerical models. *J. Atmos. Sci.,* **51,** 1728–1739.

——, M. P. Khairoutdinov, D. K. Lilly, Z. N. Kogan, and Q. Liu, 1995: The simulation of a convective cloud in a 3-D model with explicit microphysics. Part I: Model description and sensitivity experiments. *J. Atmos. Sci.,* **52,** 2923–2940.

Kollias, P., and B. Albrecht, 2000: The turbulence structure in a continental stratocumulus cloud from millimeter-wavelength radar observations. *J. Atmos. Sci.,* **57,** 2417–2434.

——, G. Tselioudis, and B. A. Albrecht, 2007: Cloud climatology at the Southern Great Plains and the layer structure, drizzle, and atmospheric modes of continental stratus. *J. Geophys. Res.,* **112,** D09116, doi:10.1029/2006JD007307.

Koponen, I. K., A. Virkkula, R. Hillamo, V. M. Kerminen, and M. Kulmala, 2003: Number size distributions and concentrations of the continental summer aerosols in Queen Maud Land, Antarctica. *J. Geophys. Res.,* **108,** 4587, doi:10.1029/2003JD003614.

Kraus, E., 1963: The diurnal precipitation change over the sea. *J. Atmos. Sci.,* **20,** 551–556.

Krueger, S. K., G. T. McLean, and Q. Fu, 1995a: Numerical simulation of the stratus-to-cumulus transition in the subtropical marine boundary layer. Part I: Boundary-layer structure. *J. Atmos. Sci.,* **52,** 2839–2850.

——, ——, and ——, 1995b: Numerical simulation of the stratus-to-cumulus transition in the subtropical marine boundary layer. Part II: Boundary layer circulation. *J. Atmos. Sci.,* **52,** 2851–2868.

Kubar, T. L., D. L. Hartmann, and R. Wood, 2009: On the importance of macrophysics and microphysics for precipitation in warm clouds. Part I: Satellite observations. *J. Atmos. Sci.,* **66,** 2953–2972.

Kulmala, M., A. Laaksonen, P. Korhonen, T. Vesala, T. Ahonen, and J. C. Barrett, 1993: The effect of atmospheric nitric-acid vapor on cloud condensation nucleus activation. *J. Geophys. Res.,* **98** (D12), 22 949–22 958.

Kuo, H.-C., and W. H. Schubert, 1988: Stability of cloud-topped boundary layers. *Quart. J. Roy. Meteor. Soc.,* **114,** 887–916.

Larson, V. E., K. E. Kotenberg, and N. B. Wood, 2007: An analytic longwave radiation formula for liquid layer clouds. *Mon. Wea. Rev.,* **135,** 689–699.

Lau, N. C., and M. W. Crane, 1997: Comparing satellite and surface observations of cloud patterns in synoptic-scale circulation systems. *Mon. Wea. Rev.,* **125,** 3172–3189.

Lawson, R. P., B. A. Baker, C. G. Schmitt, and T. L. Jensen, 2001: An overview of microphysical properties of Arctic clouds observed in May and July 1998 during FIRE ACE. *J. Geophys. Res.,* **106** (D14), 14 989–15 014.

Leaitch, W. R., and Coauthors, 1996: Physical and chemical observations in marine stratus during the 1993 North Atlantic Regional Experiment: Factors controlling cloud droplet number concentrations. *J. Geophys. Res.,* **101** (D22), 29 123–29 135.

Lebsock, M. D., T. S. L'Ecuyer, and G. L. Stephens, 2011: Detecting the ratio of rain and cloud water in low-latitude shallow marine clouds. *J. Appl. Meteor. Climatol.,* **50,** 419–432.

L'Ecuyer, T. S., W. Berg, J. Haynes, M. Lebsock, and T. Takemura, 2009: Global observations of aerosol impacts on precipitation occurrence in warm maritime clouds. *J. Geophys. Res.,* **114,** D09211, doi:10.1029/2008JD011273.

Lee, S. S., J. E. Penner, and S. M. Saleeby, 2009: Aerosol effects on liquid-water path of thin stratocumulus clouds. *J. Geophys. Res.,* **114,** D07204, doi:10.1029/2008JD010513.

Lenderink, G., and A. P. Siebesma, 2004: On the role of drizzle in stratocumulus and its implications for large-eddy simulation. *Quart. J. Roy. Meteor. Soc.,* **130,** 3429–3434.

Lenschow, D. H., and B. B. Stankov, 1986: Length scales in the convective boundary layer. *J. Atmos. Sci.,* **43,** 1190–1209.

——, M. Y. Zhou, X. B. Zeng, L. S. Chen, and X. D. Xu, 2000: Measurements of fine-scale structure at the top of marine stratocumulus. *Bound.-Layer Meteor.,* **97,** 331–357.

Leon, D. C., Z. Wang, and D. Liu, 2008: Climatology of drizzle in marine boundary layer clouds based on 1 year of data from CloudSat and Cloud-Aerosol Lidar and Infrared Pathfinder Satellite Observations (CALIPSO). *J. Geophys. Res.,* **113,** D00A14, doi:10.1029/2008JD009835.

Lewellen, D. C., and W. S. Lewellen, 1998: Large-eddy boundary layer entrainment. *J. Atmos. Sci.,* **55,** 2645–2665.

——, and ——, 2002: Entrainment and decoupling relations for cloudy boundary layers. *J. Atmos. Sci.,* **59,** 2966–2986.

Li, J., J. W. Geldart, and P. Chylek, 1994: Solar radiative-transfer in clouds with vertical internal inhomogeneity. *J. Atmos. Sci.,* **51,** 2542–2552.

Lilly, D. K., 1968: Models of cloud-topped mixed layers under a strong inversion. *Quart. J. Roy. Meteor. Soc.,* **94,** 292–309.

——, 2002: Entrainment into mixed layers. Part II: A new closure. *J. Atmos. Sci.,* **59,** 3353–3361.

——, and B. Stevens, 2008: Validation of a mixed-layer closure. I: Theoretical tests. *Quart. J. Roy. Meteor. Soc.,* **134,** 47–55.

Liou, K.-N., 1992: *Radiation and Cloud Processes in the Atmosphere: Theory, Observation and Modeling.* Oxford University Press, 504 pp.

Liu, Y., and P. H. Daum, 2004: On the parameterization of the autoconversion process. Part I: Analytical formulation of the Kessler-type parameterizations. *J. Atmos. Sci.,* **61,** 1539–1548.

Locatelli, J. D., P. V. Hobbs, and K. R. Biswas, 1983: Precipitation from stratocumulus clouds affected by fallstreaks and artificial seeding. *J. Climate Appl. Meteor.,* **22,** 1393–1403.

Lock, A. P., 1998: The parametrization of entrainment in cloudy boundary layers. *Quart. J. Roy. Meteor. Soc.,* **124,** 2729–2754.

——, 2009: Factors influencing cloud area at the capping inversion for shallow cumulus clouds. *Quart. J. Roy. Meteor. Soc.,* **135,** 941–952.

Lohmann, U., and J. Feichter, 2005: Global indirect aerosol effects: A review. *Atmos. Chem. Phys.,* **5,** 715–737.

Long, A. B., 1974: Solutions to the droplet collection equation for polynomial kernels. *J. Atmos. Sci.,* **31,** 1040–1052.

Lu, M. L., W. C. Conant, H. H. Jonsson, V. Varutbangkul, R. C. Flagan, and J. H. Seinfeld, 2007: The Marine Stratus/Stratocumulus Experiment (MASE): Aerosol-cloud relationships in marine stratocumulus. *J. Geophys. Res.,* **112,** D10209, doi:10.1029/2006JD007985.

——, A. Sorooshian, H. H. Jonsson, G. Feingold, R. C. Flagan, and J. H. Seinfeld, 2009: Marine stratocumulus aerosol-cloud relationships in the MASE-II experiment: Precipitation susceptibility in eastern Pacific marine stratocumulus. *J. Geophys. Res.,* **114,** D24203, doi:10.1029/2009JD012774.

MacVean, M. K., 1993: A numerical investigation of the criterion for cloud-top entrainment instability. *J. Atmos. Sci.,* **50,** 2481–2495.

——, and P. J. Mason, 1990: Cloud-top entrainment instability through small-scale mixing and its parameterization in numerical models. *J. Atmos. Sci.,* **47,** 1012–1030.

Martin, G. M., D. W. Johnson, and A. Spice, 1994: The measurement and parameterization of effective radius of droplets in warm stratocumulus clouds. *J. Atmos. Sci.,* **51,** 1823–1842.

——, ——, D. P. Rogers, P. R. Jonas, P. Minnis, and D. A. Hegg, 1995: Observations of the interaction between cumulus clouds and warm stratocumulus clouds in the marine boundary layer during ASTEX. *J. Atmos. Sci.,* **52,** 2902–2922.

McFarquhar, G. M., G. Zhang, M. R. Poellot, G. L. Kok, R. McCoy, T. Tooman, A. Fridlind, and A. J. Heymsfield, 2007: Ice properties of single-layer stratocumulus during the Mixed-Phase Arctic Cloud Experiment: 1. Observations. *J. Geophys. Res.,* **112,** D24201, doi:10.1029/2007JD008633.

McFiggans, G., and Coauthors, 2006: The effect of physical and chemical aerosol properties on warm cloud droplet activation. *Atmos. Chem. Phys.,* **6,** 2593–2649.

Mechem, D. B., and Y. Kogan, 2003: Simulating the transition from drizzling marine stratocumulus to boundary layer cumulus with a mesoscale model. *Mon. Wea. Rev.,* **131,** 2342–2360.

——, ——, and D. M. Schultz, 2010: Large-eddy observation of post-cold-frontal continental stratocumulus. *J. Atmos. Sci.,* **67,** 3368–3383.

Mellado, B., 2010: The evaporatively driven cloud-top mixing layer. *J. Fluid Mech.,* **660,** 5–36.

Miles, N. L., J. Verlinde, and E. E. Clothiaux, 2000: Cloud droplet size distributions in low-level stratiform clouds. *J. Atmos. Sci.,* **57,** 295–311.

Miller, M. A., and B. A. Albrecht, 1995: Surface-based observations of mesoscale cumulus-stratocumulus interaction during ASTEX. *J. Atmos. Sci.,* **52,** 2809–2826.

——, M. P. Jensen, and E. E. Clothiaux, 1998: Diurnal cloud and thermodynamic variations in the stratocumulus transition regime: A case study using in situ and remote sensors. *J. Atmos. Sci.,* **55,** 2294–2310.

Mitchell, T. P., and J. M. Wallace, 1992: The annual cycle in equatorial convection and sea surface temperature. *J. Climate,* **5,** 1140–1156.

Moeng, C. H., S. H. Shen, and D. A. Randall, 1992: Physical processes within the nocturnal stratus-topped boundary layer. *J. Atmos. Sci.,* **49,** 2384–2401.

——, and Coauthors, 1996: Simulation of a stratocumulus-topped planetary boundary layer: Intercomparison among different numerical codes. *Bull. Amer. Meteor. Soc.,* **77,** 261–278.

——, B. Stevens, and P. P. Sullivan, 2005: Where is the interface of the stratocumulus-topped PBL? *J. Atmos. Sci.,* **62,** 2626–2631.

Mordy, W., 1959: Computations of the growth by condensation of a population of cloud droplets. *Tellus,* **11,** 16–44.

Moyer, K. A., and G. S. Young, 1994: Observations of mesoscale cellular convection from the marine stratocumulus phase of fire. *Bound.-Layer Meteor.,* **71,** 109–134.

Nakajima, T., M. D. King, J. D. Spinhirne, and L. F. Radke, 1991: Determination of the optical thickness and effective particle radius of clouds from reflected solar radiation measurements: 2. Marine stratocumulus observations. *J. Atmos. Sci.,* **48,** 728–750.

Nastrom, G., and K. Gage, 1985: A climatology of atmospheric wavenumber spectra of wind and temperature observed by commercial aircraft. *J. Atmos. Sci.,* **42,** 950–960.

Neiburger, M., D. S. Johnson, and C. W. Chien, 1961: Studies of the structure of the atmosphere over the eastern Pacific Ocean in summer: Part 1. The inversion over the eastern North Pacific Ocean. University of California Publ. in Meteorology, Vol. 1, University of California Press, 94 pp.

Nenes, A., and J. H. Seinfeld, 2003: Parameterization of cloud droplet formation in global climate models. *J. Geophys. Res.,* **108,** 4415, doi:10.1029/2002JD002911.

——, R. J. Charlson, M. C. Facchini, M. Kulmala, A. Laaksonen, and J. H. Seinfeld, 2002: Can chemical effects on cloud droplet number rival the first indirect effect? *Geophys. Res. Lett.,* **29,** 1848, doi:10.1029/2002GL015295.

Nicholls, S., 1984: The dynamics of stratocumulus: Aircraft observations and comparisons with a mixed layer model. *Quart. J. Roy. Meteor. Soc.,* **110,** 783–820.

——, 1987: A model of drizzle growth in warm, turbulent, stratiform clouds. *Quart. J. Roy. Meteor. Soc.,* **113,** 1141–1170.

——, 1989: The structure of radiatively driven convection in stratocumulus. *Quart. J. Roy. Meteor. Soc.,* **115,** 487–511.

——, and J. Leighton, 1986: An observational study of the structure of stratiform cloud sheets: Part I. Structure. *Quart. J. Roy. Meteor. Soc.,* **112,** 431–460.

——, and J. D. Turton, 1986: An observational study of the structure of stratiform cloud sheets: Part II. Entrainment. *Quart. J. Roy. Meteor. Soc.,* **112,** 461–480.

Nieuwstadt, F. T. M., and J. A. Businger, 1984: Radiative cooling near the top of a cloudy mixed layer. *Quart. J. Roy. Meteor. Soc.,* **110,** 1073–1078.

——, and P. G. Duynkerke, 1996: Turbulence in the atmospheric boundary layer. *Atmos. Res.,* **40,** 111–142.

Norris, J. R., 1998: Low cloud type over the ocean from surface observations. Part I: Relationship to surface meteorology and the vertical distribution of temperature and moisture. *J. Climate,* **11,** 369–382.

——, and C. B. Leovy, 1994: Interannual variability in stratiform cloudiness and sea surface temperature. *J. Climate,* **7,** 1915–1925.

——, and S. A. Klein, 2000: Low cloud type over the ocean from surface observations. Part III: Relationship to vertical motion and the regional synoptic environment. *J. Climate,* **13,** 245–256.

——, and A. Slingo, 2009: Trends in observed cloudiness and Earth's radiation budget: What do we not know and what do we need to know? *Clouds in the Perturbed Climate System: Their Relationship to Energy Balance, Atmospheric Dynamics, and Precipitation,* J. Heintzenberg and R. Charlson, Eds., MIT Press, 17–36.

——, Y. Zhang, and J. M. Wallace, 1998: Role of low clouds in summertime atmosphere–ocean interactions over the North Pacific. *J. Climate,* **11,** 2482–2490.

Nucciarone, J. J., and G. S. Young, 1991: Aircraft measurements of turbulence spectra in the marine stratocumulus-topped boundary layer. *J. Atmos. Sci.,* **48,** 2382–2392.

O'Dell, C. W., F. J. Wentz, and R. Bennartz, 2008: Cloud liquid water path from satellite-based passive microwave observations: A new climatology over the global oceans. *J. Climate,* **21,** 1721–1738.

O'Dowd, C. D., J. A. Lowe, M. H. Smith, B. Davison, C. N. Hewitt, and R. M. Harrison, 1997: Biogenic sulphur emissions and inferred non-sea-salt-sulphate cloud condensation nuclei in and around Antarctica. *J. Geophys. Res.,* **102** (D11), 12 839–12 854.

——, ——, ——, and A. D. Kaye, 1999a: The relative importance of non-sea-salt sulphate and sea-salt aerosol to the marine cloud condensation nuclei population: An improved multi-component aerosol-cloud droplet parametrization. *Quart. J. Roy. Meteor. Soc.,* **125,** 1295–1313.

——, ——, and —— , 1999b: Coupling sea-salt and sulphate interactions and its impact on cloud droplet concentration predictions. *Geophys. Res. Lett.,* **26,** 1311–1314.

O'Hirok, W., and C. Gautier, 1998: A three-dimensional radiative transfer model to investigate the solar radiation within a cloudy atmosphere. Part II: Spectral effects. *J. Atmos. Sci.,* **55,** 3065–3076.

Ohtake, T., 1963: Hemispheric investigations of warm rain by radiosonde data. *J. Appl. Meteor.,* **2,** 594–607.

Paltridge, G. W., 1974: Infrared emissivity, shortwave albedo, and the microphysics of stratiform water clouds. *J. Geophys. Res.,* **79,** 4053–4058.

Paluch, I. R., and D. H. Lenschow, 1991: Stratiform cloud formation in the marine boundary layer. *J. Atmos. Sci.,* **48,** 2141–2158.

——, ——, S. Siems, S. McKeen, G. L. Kok, and R. D. Schillawski, 1994: Evolution of the subtropical marine boundary-layer–comparison of soundings over the eastern Pacific from FIRE and HARP. *J. Atmos. Sci.,* **51,** 1465–1479.

Park, S., C. B. Leovy, and M. A. Rozendaal, 2004: A new heuristic marine boundary layer cloud model. *J. Atmos. Sci.,* **61,** 3002–3024.

——, C. Deser, and M. Alexander, 2005: Estimation of the surface heat flux response to sea surface temperature anomalies over the global oceans. *J. Climate,* **18,** 4582–4599.

Pawlowska, H., and J. L. Brenguier, 2003: An observational study of drizzle formation in stratocumulus clouds for general circulation model (GCM) parameterizations. *J. Geophys. Res.,* **108,** 8630, doi:10.1029/2002JD002679.

Petters, M. D., J. R. Snider, B. Stevens, G. Vali, I. Faloona, and L. Russell, 2006: Accumulation mode aerosol, pockets of open cells, and particle nucleation in the remote subtropical Pacific marine boundary layer. *J. Geophys. Res.,* **111,** D02206, doi:10.1029/2004JD005694.

Petty, G. W., 1995: Frequencies and characteristics of global oceanic precipitation from shipboard present-weather reports. *Bull. Amer. Meteor. Soc.,* **76,** 1593–1616.

Pinnick, R. G., S. G. Jennings, P. Chylek, and H. J. Auvermann, 1979: Verification of a linear relation between IR extinction, absorption and liquid water-content of fogs. *J. Atmos. Sci.,* **36,** 1577–1586.

Pinsky, M. B., and A. P. Khain, 1997: Turbulence effects on droplet growth and size distribution in clouds–a review. *J. Aerosol Sci.,* **28,** 1177–1214.

——, ——, and M. Shapiro, 2001: Collision efficiency of drops in a wide range of Reynolds numbers: Effects of pressure on spectrum evolution. *J. Atmos. Sci.,* **58,** 742–764.

Platnick, S., and S. Twomey, 1994: Determining the susceptibility of cloud albedo to changes in droplet concentration with the Advanced Very High Resolution Radiometer. *J. Appl. Meteor.,* **33,** 334–347.

Platt, C. M. R., 1976: Infrared absorption and liquid water content in stratocumulus clouds. *Quart. J. Roy. Meteor. Soc.,* **102,** 553–556.

Pruppacher, H. R., and J. D. Klett, 1997: *Microphysics of Clouds and Precipitation.* Kluwer Academic Publishers, 976 pp.

Ramaswamy, V., and S. M. Freidenreich, 1991: Solar radiative line-by-line determination of water vapor absorption and water cloud extinction in inhomogeneous atmospheres. *J. Geophys. Res.,* **96** (D5), 9133–9157.

Randall, D. A., 1980: Conditional instability of the first kind upside down. *J. Atmos. Sci.,* **37,** 125–130.

——, 1984: Stratocumulus cloud deepening through entrainment. *Tellus,* **36A,** 446–457.

——, and M. J. Suarez, 1984: On the dynamics of stratocumulus formation and dissipation. *J. Atmos. Sci.,* **41,** 3052–3057.

——, J. A. Coakley, C. W. Fairall, R. A. Knopfli, and D. H. Lenschow, 1984: Outlook for research on marine subtropical stratocumulus clouds. *Bull. Amer. Meteor. Soc.,* **65,** 1290–1301.

Rangno, A. L., and P. V. Hobbs, 1991: Ice particle concentrations and precipitation development in small polar maritime cumuliform clouds. *Quart. J. Roy. Meteor. Soc.,* **117,** 207–241.

Rasmussen, R. M., I. Geresdi, G. Thompson, K. Manning, and E. Karplus, 2002: Freezing drizzle formation in stably stratified layer clouds: The role of radiative cooling of cloud droplets, cloud condensation nuclei, and ice initiation. *J. Atmos. Sci.,* **59,** 837–860.

Richter, I., and C. R. Mechoso, 2004: Orographic influences on the annual cycle of Namibian stratocumulus clouds. *Geophys. Res. Lett.,* **31,** L24108, doi:10.1029/2004GL020814.

——, and ——, 2006: Orographic influences on subtropical stratocumulus. *J. Atmos. Sci.,* **63,** 2585–2601.

Riehl, H., and J. S. Malkus, 1957: On the heat balance and maintenance of circulation in the trades. *Quart. J. Roy. Meteor. Soc.,* **83,** 21–29.

——, T. C. Yeh, J. S. Malkus, and N. E. LaSeur, 1951: The northeast trade of the Pacific Ocean. *Quart. J. Roy. Meteor. Soc.,* **77,** 598–626.

Roach, W. T., 1961: Some aircraft observations of fluxes of solar radiation in the atmosphere. *Quart. J. Roy. Meteor. Soc.,* **87,** 346–363.

——, and A. Slingo, 1979: A high resolution infrared radiative transfer scheme to study the interaction of radiation with cloud. *Quart. J. Roy. Meteor. Soc.,* **105,** 603–614.

——, R. Brown, S. J. Caughey, B. A. Crease, and A. Slingo, 1982: A field-study of nocturnal stratocumulus: 1. Mean structure and budgets. *Quart. J. Roy. Meteor. Soc.,* **108,** 103–123.

Rogers, D. P., and D. Koracin, 1992: Radiative transfer and turbulence in the cloud-topped marine atmospheric boundary layer. *J. Atmos. Sci.,* **49,** 1473–1486.

Rossow, W. B., and W. B. Garder, 1993: Cloud detection using satellite measurements of infrared and visible radiances for ISCCP. *J. Climate,* **6,** 2341–2369.

——, C. Delo, and B. Cairns, 2002: Implications of the observed mesoscale variations of clouds for earth's radiation budget. *J. Climate,* **15,** 557–585.

Rothermel, J., and E. M. Agee, 1980: Aircraft investigation of mesoscale cellular convection during AMTEX75. *J. Atmos. Sci.,* **37,** 1027–1040.

Rozendaal, M. A., C. B. Leovy, and S. A. Klein, 1995: An observational study of the diurnal cycle of marine stratiform cloud. *J. Climate,* **8,** 1795–1809.

Rutledge, S. A., and P. V. Hobbs, 1983: The mesoscale and microscale structure and organization of clouds and precipitation in midlatitude cyclones. VIII: A model for the ''seeder-feeder'' process in warm-frontal rainbands. *J. Atmos. Sci.,* **40,** 1185–1206.

Sandu, I., B. Stevens, and R. Pincus, 2010: On the transitions in marine boundary layer cloudiness. *Atmos. Chem. Phys. Discuss.,* **10,** 2377–2391.

Savic-Jovcic, V., and B. Stevens, 2008: The structure and mesoscale organization of precipitating stratocumulus. *J. Atmos. Sci.,* **65,** 1587–1605.

Schubert, W. H., 1976: Experiments with Lilly's cloud-topped mixed layer model. *J. Atmos. Sci.,* **33,** 436–446.

——, J. S. Wakefield, E. J. Steiner, and S. K. Cox, 1979a: Marine stratocumulus convection. Part I: Governing equations and horizontally homogeneous solutions. *J. Atmos. Sci.,* **36,** 1286–1307.

——, ——, ——, and ——, 1979b: Marine stratocumulus convection. Part II: Horizontally inhomogeneous solutions. *J. Atmos. Sci.,* **36,** 1308–1324.

Schultz, D., D. Arndt, D. Stensrud, and J. Hanna, 2004: Snowbands during the cold-air outbreak of 23 January 2003. *Mon. Wea. Rev.,* **132,** 827–842.

Sears-Collins, A. L., D. M. Schultz, and R. H. Johns, 2006: Spatial and temporal variability of nonfreezing drizzle in the United States and Canada. *J. Climate,* **19,** 3629–3639; Corrigendum, **21,** 1447–1448.

Seifert, A., L. Nuijens, and B. Stevens, 2010: Turbulence effects on warm-rain autoconversion in precipitating shallow convection. *Quart. J. Roy. Meteor. Soc.,* **136,** 1753–1762.

Seinfeld, J. H., and S. N. Pandis, 1997: *Atmospheric Chemistry and Physics: From Air Pollution to Climate Change.* Wiley-Interscience, 1326 pp.

Serpetzoglou, E., B. A. Albrecht, P. Kollias, and C. W. Fairall, 2008: Boundary layer, cloud, and drizzle variability in the southeast Pacific stratocumulus regime. *J. Climate,* **21,** 6191–6214.

Shao, Q., and D. A. Randall, 1996: Closed mesoscale cellular convection driven by cloud-top radiative cooling. *J. Atmos. Sci.,* **53,** 2144–2165.

Sharon, T. M., B. A. Albrecht, H. Jonsson, P. Minnis, M. M. Khaiyer, T. M. VanReken, J. Seinfeld, and R. Flagan, 2006: Aerosol and cloud microphysical characteristics of rifts and gradients in maritime stratocumulus clouds. *J. Atmos. Sci.,* **63,** 983–997.

Siebert, H., H. Franke, K. Lehmann, R. Maser, E. Saw, D. Schell, R. A. Shaw, and M. Wendisch, 2006a: Probing finescale dynamics and microphysics of clouds with helicopter-borne measurements. *Bull. Amer. Meteor. Soc.,* **87,** 1727–1738.

——, K. Lehmann, and M. Wendisch, 2006b: Observations of small-scale turbulence and energy dissipation rates in the cloudy boundary layer. *J. Atmos. Sci.,* **63,** 1451–1466.

Siebesma, A., and Coauthors, 2004: Cloud representation in general-circulation models over the northern Pacific Ocean: A EUROCS intercomparison study. *Quart. J. Roy. Meteor. Soc.,* **130,** 3245–3267.

Siems, S. T., C. Bretherton, M. Baker, S. Shy, and R. Breidenthal, 1990: Buoyancy reversal and cloud-top entrainment instability. *Quart. J. Roy. Meteor. Soc.,* **116,** 705–739.

——, D. H. Lenschow, and C. S. Bretherton, 1993: A numerical study of the interaction between stratocumulus and the air ovserlying it. *J. Atmos. Sci.,* **50,** 3663–3676.

Slingo, A., 1989: A GCM parameterization for the shortwave properties of water clouds. *J. Atmos. Sci.,* **46,** 1419–1427.

——, 1990: Sensitivity of the Earth's radiation budget to changes is low clouds. *Nature,* **343,** 49–51.

——, and H. M. Schrecker, 1982: On the shortwave radiative properties of stratiform water clouds. *Quart. J. Roy. Meteor. Soc.,* **108,** 407–426.

——, R. Brown, and C. L. Wrench, 1982a: A field-study of nocturnal stratocumulus. 3. High-resolution radiative and microphysical observations. *Quart. J. Roy. Meteor. Soc.,* **108,** 145–165.

——, S. Nicholls, and J. Schmetz, 1982b: Aircraft observations of marine stratocumulus during JASIN. *Quart. J. Roy. Meteor. Soc.,* **108,** 833–856.

Slingo, J. M., 1987: The development and verification of a cloud prediction scheme for the ECMWF model. *Quart. J. Roy. Meteor. Soc.,* **113,** 899–927.

Snider, J. R., S. Guibert, J. L. Brenguier, and J. P. Putaud, 2003: Aerosol activation in marine stratocumulus clouds: 2. Kohler and parcel theory closure studies. *J. Geophys. Res.,* **108,** 8629, doi:10.1029/2002JD002692.

Soden, B. J., and G. A. Vecchi, 2011: The vertical distribution of cloud feedback in coupled ocean-atmosphere models. *Geophys. Res. Lett.,* **38,** L12704, doi:10.1029/2011GL047632.

Solomon, A., M. D. Shupe, P. O. G. Persson, and H. Morrison, 2011: Moisture and dynamical interactions maintaining decoupled arctic mixed-phase stratocumulus in the presence of a humidity inversion. *Atmos. Chem. Phys. Discuss.,* **11,** 13 469–13 524.

Sorooshian, A., G. Feingold, M. Lebsock, H. Jiang, and G. Stephens, 2009: On the precipitation susceptibility of clouds to aerosol perturbations. *Geophys. Res. Lett.,* **36,** L13803, doi:10.1029/2009GL038993.

Squires, P., 1952: The growth of cloud drops by condensation. 1: General characteristics. *Aust. J. Sci. Res.,* **5,** 59–86.

Stage, S. A., and J. A. Businger, 1981: A model for entrainment into a cloud-topped marine boundary-layer. 1. Model description and application to a cold-air outbreak episode. *J. Atmos. Sci.,* **38,** 2213–2229.

Stephens, G. L., 1978a: Radiation profiles in extended water clouds: 1. Theory. *J. Atmos. Sci.,* **35,** 2111–2122.

——, 1978b: Radiation profiles in extended water clouds: 2. Parameterization schemes. *J. Atmos. Sci.,* **35,** 2123–2132.

——, and T. J. Greenwald, 1991: Observations of the Earth's radiation budget in relation to atmospheric hydrology. Part II: Cloud effects and cloud feedback. *J. Geophys. Res.,* **96,** 15 325–15 340.

——, G. W. Paltridge, and C. M. R. Platt, 1978: Radiation profiles in extended water clouds: 3. Observations. *J. Atmos. Sci.,* **35,** 2133–2141.

——, S. Ackerman, and E. A. Smith, 1984: A shortwave parameterization revised to improve cloud absorption. *J. Atmos. Sci.,* **41,** 687–690.

Stevens, B., 2000: Cloud-transitions and decoupling in shear-free stratocumulus-topped boundary layers. *Geophys. Res. Lett.,* **27** (16), 2557–2560.

——, 2002: Entrainment in stratocumulus topped mixed layers. *Quart. J. Roy. Meteor. Soc.,* **128,** 2663–2690.

——, 2005: Atmospheric moist convection. *Annu. Rev. Earth Planet. Sci.,* **32,** 605–643.

——, 2006: Bulk boundary-layer concepts for simplified models of tropical dynamics. *Theor. Comput. Fluid Dyn.,* **20,** 279–304.

——, 2010: Cloud top entrainment instability? *J. Fluid Mech.,* **660,** 1–4.

——, and G. Feingold, 2009: Untangling aerosol effects on clouds and precipitation in a buffered system. *Nature,* **461** (7264), 607–613.

——, W. R. Cotton, G. Feingold, and C.-H. Moeng, 1998: Large-eddy simulations of strongly precipitating, shallow, stratocumulus-topped boundary layers. *J. Atmos. Sci.,* **55,** 3616–3638.

——, C.-H. Moeng, and P. P. Sullivan, 1999: Large-eddy simulations of radiatively driven convection: Sensitivities to the representation of small scales. *J. Atmos. Sci.,* **56,** 3963–3984.

——, and Coauthors, 2001: Simulations of trade wind cumuli under a strong inversion. *J. Atmos. Sci.,* **58,** 1870–1891.

——, J. J. Duan, J. C. McWilliams, M. Munnich, and J. D. Neelin, 2002: Entrainment, Rayleigh friction, and boundary layer winds over the tropical Pacific. *J. Climate,* **15,** 30–44.

——, and Coauthors, 2003a: Dynamics and Chemistry of Marine Stratocumulus—DYCOMS II. *Bull. Amer. Meteor. Soc.,* **84,** 579–593.

——, and Coauthors, 2003b: On entrainment rates in nocturnal marine stratocumulus. *Quart. J. Roy. Meteor. Soc.,* **129,** 3469–3493.

——, G. Vali, K. Comstock, R. Wood, M. VanZanten, P. H. Austin, C. S. Bretherton, and D. H. Lenschow, 2005a: Pockets of open cells (POCs) and drizzle in marine stratocumulus. *Bull. Amer. Meteor. Soc.,* **86,** 51–57.

——, and Coauthors, 2005b: Evaluation of large-eddy simulations via observations of nocturnal marine stratocumulus. *Mon. Wea. Rev.,* **133,** 1443–1462.

——, A. Beljaars, S. Bordoni, C. Holloway, M. Kohler, S. Krueger, V. Savic-Jovcic, and Y. Y. Zhang, 2007: On the structure of the lower troposphere in the summertime stratocumulus regime of the northeast Pacific. *Mon. Wea. Rev.,* **135,** 985–1005.

Stewart, D. A., and O. M. Essenwanger, 1982: A survey of fog and related optical propagation characteristics. *Rev. Geophys.,* **20,** 481–495.

Sundararajan, R., and M. Tjernstrom, 2000: Observations and simulations of a non-stationary coastal atmospheric boundary layer. *Quart. J. Roy. Meteor. Soc.,* **126,** 445–476.

Szczodrak, M., P. H. Austin, and P. B. Krummel, 2001: Variability of optical depth and effective radius in marine stratocumulus clouds. *J. Atmos. Sci.,* **58,** 2912–2926.

Taylor, J. P., J. M. Edwards, M. D. Glew, P. Hignett, and A. Slingo, 1996: Studies with a flexible new radiation code. 2. Comparisons with aircraft short-wave observations. *Quart. J. Roy. Meteor. Soc.,* **122,** 839–861.

Tennekes, H., and J. L. Lumley, 1972: *A First Course in Turbulence.* MIT Press, 293 pp.

Thompson, W., S. Burk, and J. Lewis, 2005: Fog and low clouds in a coastally trapped disturbance. *J. Geophys. Res.,* **110,** D18213, doi:10.1029/2004JD005522.

Tjemkes, S. A., and P. G. Duynkerke, 1989: The nocturnal boundary layer: Model calculations compared with observations. *J. Appl. Meteor.,* **28,** 161–175.

Tjernstrom, M., and A. Rune, 2003: The structure of gradually transforming marine stratocumulus during the ASTEX first Lagrangian experiment. *Quart. J. Roy. Meteor. Soc.,* **129,** 1071–1100.

Toniazzo, T., S. J. Abel, R. Wood, C. R. Mechoso, G. Allen, and L. C. Shaffrey, 2011: Large-scale and synoptic meteorology in the south-east Pacific during the observations campaign VOCALS-REx in austral Spring 2008. *Atmos. Chem. Phys.,* **11,** 4977–5009, doi:10.5194/acp-11-4977-2011.

Tripoli, G. J., and W. R. Cotton, 1980: A numerical investigation of several factors contributing to the observed variable density of deep convection over South Florida. *J. Appl. Meteor.,* **19,** 1037–1063.

Turton, J. D., and S. Nicholls, 1987: A study of the diurnal variation of stratocumulus using a multiple mixed layer model. *Quart. J. Roy. Meteor. Soc.,* **113,** 969–1009.

Twohy, C. H., M. D. Petters, J. R. Snider, B. Stevens, W. Tahnk, M. Wetzel, L. Russell, and F. Burnet, 2005: Evaluation of the aerosol indirect effect in marine stratocumulus clouds: Droplet number, size, liquid water path, and radiative impact. *J. Geophys. Res.,* **110,** D08203, doi:10.1029/2004JD005116.

Twomey, S., 1959: The nuclei of natural cloud formation. Part II: The supersaturation in natural clouds and the variation of cloud droplet concentration. *Geofis. Pura Appl.,* **43,** 243–249.

——, 1974: Pollution and the planetary albedo. *Atmos. Environ.,* **8,** 1251–1256.

——, 1977: The influence of pollution on the shortwave albedo of clouds. *J. Atmos. Sci.,* **34,** 1149–1152.

——, and C. F. Bohren, 1980: Simple approximations for calculations of absorption in clouds. *J. Atmos. Sci.,* **37,** 2086–2094.

Vaillancourt, P. A., and M. K. Yau, 2000: Review of particle–turbulence interactions and consequences for cloud physics. *Bull. Amer. Meteor. Soc.,* **81,** 285–298.

Vali, G., R. D. Kelly, J. French, H. S. D. Leon, A. McIntosh, and R. E. Pazmany, 1998: Finescale structure and microphysics of coastal stratus. *J. Atmos. Sci.,* **55,** 3540–3564.

Vallis, G., 2006: *Atmospheric and Oceanic Fluid Dynamics.* Cambridge University Press, 745 pp.

vanZanten, M. C., and P. G. Duynkerke, 2002: Radiative and evaporative cooling in the entrainment zone of stratocumulus—The role of longwave radiative cooling above cloud top. *Bound.-Layer Meteor.,* **102,** 253–280.

——, and B. Stevens, 2005: Observations of the structure of heavily precipitating marine stratocumulus. *J. Atmos. Sci.,* **62,** 4327–4342.

——, P. G. Duynkerke, and J. W. M. Cuijpers, 1999: Entrainment parameterization in convective boundary layers. *J. Atmos. Sci.,* **56,** 813–828.

——, B. Stevens, G. Vali, and D. Lenschow, 2005: Observations of drizzle in nocturnal marine stratocumulus. *J. Atmos. Sci.,* **62,** 88–106.

Vohl, O., S. K. Mitra, S. Wurzler, K. Diehl, and H. R. Pruppacher, 2007: Collision efficiencies empirically determined from

laboratory investigations of collisional growth of small raindrops in a laminar flow field. *Atmos. Res.,* **85,** 120–125.

Walter, B. A., 1980: Wintertime observations of roll clouds over the Bering Sea. *Mon. Wea. Rev.,* **108,** 2024–2031.

Wang, H., and G. Feingold, 2009: Modeling mesoscale cellular structures and drizzle in marine stratocumulus. Part I: Impact of drizzle on the formation and evolution of open cells. *J. Atmos. Sci.,* **66,** 3237–3255.

Wang, J. H., W. B. Rossow, T. Uttal, and M. Rozendaal, 1999: Variability of cloud vertical structure during ASTEX observed from a combination of rawinsonde, radar, ceilometer, and satellite. *Mon. Wea. Rev.,* **127,** 2484–2502.

Wang, Q., and B. A. Albrecht, 1994: Observations of cloud-top entrainment in marine stratocumulus clouds. *J. Atmos. Sci.,* **51,** 1530–1547.

——, and D. H. Lenschow, 1995: An observational study of the role of penetrating cumulus in a marine stratocumulus-topped boundary layer. *J. Atmos. Sci.,* **52,** 2902–2922.

Wang, S., and B. A. Albrecht, 1986: A stratocumulus model with an internal circulation. *J. Atmos. Sci.,* **43,** 2374–2391.

——, and Q. Wang, 1994: Roles of drizzle in a one-dimensional third-order turbulence closure model of the nocturnal stratus-topped marine boundary layer. *J. Atmos. Sci.,* **51,** 1559–1576.

——, ——, and G. Feingold, 2003: Turbulence, condensation, and liquid water transport in numerically simulated nonprecipitating stratocumulus clouds. *J. Atmos. Sci.,* **60,** 262–278.

——, J. C. Golaz, and Q. Wang, 2008: Effect of intense wind shear across the inversion on stratocumulus clouds. *Geophys. Res. Lett.,* **35,** L15814, doi:10.1029/2008GL033865.

Warren, S. G., C. J. Hahn, J. London, R. M. Chervin, and R. L. Jenne, 1986: Global distribution of total cloud cover and cloud types over land. NCAR Tech. Note NCAR/TN-273+STR, National Center for Atmospheric Research, Boulder, CO, 29 pp. + 200 maps.

——, ——, ——, ——, and R. L. Jenne, 1988: Global distribution of total cloud cover and cloud types over ocean. NCAR Tech. Note NCAR/TN-317+STR, National Center for Atmospheric Research, Boulder, CO, 42 pp. + 170 maps.

Weaver, C. J., and R. Pearson, 1990: Entrainment instability and vertical motion as causes of stratocumulus breakup. *Quart. J. Roy. Meteor. Soc.,* **116,** 1359–1388.

Weaver, C. P., and V. Ramanathan, 1997: Relationships between large-scale vertical velocity, static stability, and cloud radiative forcing over Northern Hemisphere extratropical oceans. *J. Climate,* **10,** 2871–2887.

Weng, F. Z., and N. C. Grody, 1994: Retrieval of cloud liquid water using the Special Sensor Microwave Imager (SSM/I). *J. Geophys. Res.,* **99** (D12), 25 535–25 551.

——, ——, R. Ferraro, A. Basist, and D. Forsyth, 1997: Cloud liquid water climatology from the Special Sensor Microwave/Imager. *J. Climate,* **10,** 1086–1098.

Wood, R., 2005a: Drizzle in stratiform boundary layer clouds. Part I: Vertical and horizontal structure. *J. Atmos. Sci.,* **62,** 3011–3033.

——, 2005b: Drizzle in stratiform boundary layer clouds. Part II: Microphysical aspects. *J. Atmos. Sci.,* **62,** 3034–3050.

——, 2006: Rate of loss of cloud droplets by coalescence in warm clouds. *J. Geophys. Res.,* **111,** D21205, doi:10.1029/2006JD007553.

——, 2007: Cancellation of aerosol indirect effects in marine stratocumulus through cloud thinning. *J. Atmos. Sci.,* **64,** 2657–2669.

——, and J. P. Taylor, 2001: Liquid water path variability in unbroken marine stratocumulus. *Quart. J. Roy. Meteor. Soc.,* **127,** 2635–2662.

——, and C. S. Bretherton, 2004: Boundary layer depth, entrainment, and decoupling in the cloud-capped subtropical and tropical marine boundary layer. *J. Climate,* **17,** 3576–3588.

——, and P. N. Blossey, 2005: Comments on ''Parameterization of the autoconversion process. Part I: Analytical formation of the Kessler-type parameterizations.'' *J. Atmos. Sci.,* **62,** 3003–3006.

——, and C. S. Bretherton, 2006: On the relationship between stratiform low cloud cover and lower-tropospheric stability. *J. Climate,* **19,** 6425–6432.

——, and D. L. Hartmann, 2006: Spatial variability of liquid water path in marine boundary layer clouds: The importance of mesoscale cellular convection. *J. Climate,* **19,** 1748–1764.

——, C. S. Bretherton, and D. L. Hartmann, 2002a: Diurnal cycle of liquid water path over the subtropical and tropical oceans. *Geophys. Res. Lett.,* **29,** 2092, doi:10.1029/2002GL015371.

——, P. R. Field, and W. R. Cotton, 2002b: Autoconversion rate bias in boundary layer cloud parameterizations. *Atmos. Res.,* **65,** 109–128.

——, K. K. Comstock, C. S. Bretherton, C. Cornish, J. Tomlinson, D. R. Collins, and C. Fairall, 2008: Open cellular structure in marine stratocumulus sheets. *J. Geophys. Res.,* **113,** D12207, doi:10.1029/2007JD009371.

——, M. Köhler, R. Bennartz, and C. O'Dell, 2009a: The diurnal cycle of surface divergence over the global oceans. *Quart. J. Roy. Meteor. Soc.,* **135,** 1484–1493.

——, T. Kubar, and D. L. Hartmann, 2009b: Understanding the importance of microphysics and macrophysics for warm rain in marine low clouds. Part II: Heuristic models of rain formation. *J. Atmos. Sci.,* **66,** 2973–2990.

——, C. Bretherton, D. Leon, A. Clarke, P. Zuidema, G. Allen, and H. Coe, 2011a: An aircraft case study of the spatial transition from closed to open mesoscale cellular convection over the southeast Pacific. *Atmos. Chem. Phys.,* **11,** 2341–2370.

——, and Coauthors, 2011b: The VAMOS Ocean-Cloud-Atmosphere-Land Study Regional Experiment (VOCALS-REx): Goals, platforms, and field operations. *Atmos. Chem. Phys.,* **11,** 627–654.

Wyant, M. C., C. S. Bretherton, H. A. Rand, and D. E. Stevens, 1997: Numerical simulations and a conceptual model of the stratocumulus to trade cumulus transition. *J. Atmos. Sci.,* **54,** 168–192.

——, ——, J. T. Bacmeister, J. T. Kiehl, I. M. Held, M. Zhao, S. A. Klein, and B. A. Soden, 2006: A comparison of tropical cloud properties and their response to climate change in three AGCMs sorted into regimes using mid-tropospheric vertical velocity. *Climate Dyn.,* **27,** 261–279.

Wyngaard, J. C., and R. A. Brost, 1984: Top-down and bottom-up diffusion of a scalar in the convective boundary layer. *J. Atmos. Sci.,* **41,** 102–112.

Xiao, H., C.-M. Wu, and C. R. Mechoso, 2010: Buoyancy reversal, decoupling and the transition from stratocumulus-topped to trade-wind cumulus-topped marine boundary layer. *Climate Dyn.,* **37,** 971–984.

Xu, H., Y. Wang, and S. P. Xie, 2004: Effects of the Andes on eastern Pacific climate: A regional atmospheric model study. *J. Climate,* **17,** 589–602.

Xue, H., G. Feingold, and B. Stevens, 2008a: Aerosol effects on clouds, precipitation, and the organization of shallow cumulus convection. *J. Atmos. Sci.,* **65,** 392–406.

Xue, Y., L. P. Wang, and W. W. Grabowski, 2008b: Growth of cloud droplets by turbulent collision-coalescence. *J. Atmos. Sci.,* **65,** 331–356.

Yamaguchi, T., and D. A. Randall, 2008: Large-eddy simulation of evaporatively driven entrainment in cloud-topped mixed layers. *J. Atmos. Sci.,* **65,** 1481–1504.

Yang, S., and E. A. Smith, 2006: Mechanisms for diurnal variability of global tropical rainfall observed from TRMM. *J. Climate,* **19,** 5190–5226.

Young, G. S., and T. D. Sikora, 2003: Mesoscale stratocumulus bands caused by Gulf Stream meanders. *Mon. Wea. Rev.,* **131,** 2177–2191.

Yum, S. S., and J. G. Hudson, 2002: Maritime/continental microphysical contrasts in stratus. *Tellus,* **54B,** 61–73.

——, and ——, 2004: Wintertime/summertime contrasts of cloud condensation nuclei and cloud microphysics over the Southern Ocean. *J. Geophys. Res.,* **109,** D06204, doi:10.1029/2003JD003864.

Zhang, M. H., and Coauthors, 2005: Comparing clouds and their seasonal variations in 10 atmospheric general circulation models with satellite measurements. *J. Geophys. Res.,* **110,** D15S02, doi:10.1029/2004JD005021.

Zhang, Y., B. Stevens, B. Medeiros, and M. Ghil, 2009: Low-cloud fraction, lower-tropospheric stability, and large-scale divergence. *J. Climate,* **22,** 4827–4844.

Zhu, P., B. Albrecht, and J. Gottschalck, 2001: Formation and development of nocturnal boundary layer clouds over the Southern Great Plains. *J. Atmos. Sci.,* **58,** 1409–1426.

——, and Coauthors, 2005: Intercomparison and interpretation of single-column model simulations of a nocturnal stratocumulus-topped marine boundary layer. *Mon. Wea. Rev.,* **133,** 2741–2758.

Zuidema, P., and D. L. Hartmann, 1995: Satellite determination of stratus cloud microphysical properties. *J. Climate,* **8,** 1638–1656.

——, E. R. Westwater, C. Fairall, and D. Hazen, 2005: Ship-based liquid water path estimates in marine stratocumulus. *J. Geophys. Res.,* **110,** D20206, doi:10.1029/2005JD005833.